



University of HUDDERSFIELD

University of Huddersfield Repository

Shahzad, Atif

Transient Flow Features in the Vicinity of a Vertical Axis Wind Turbine

Original Citation

Shahzad, Atif (2015) Transient Flow Features in the Vicinity of a Vertical Axis Wind Turbine. Masters thesis, University of Huddersfield.

This version is available at <http://eprints.hud.ac.uk/id/eprint/28695/>

The University Repository is a digital collection of the research output of the University, available on Open Access. Copyright and Moral Rights for the items on this site are retained by the individual author and/or other copyright owners. Users may access full items free of charge; copies of full text items generally can be reproduced, displayed or performed and given to third parties in any format or medium for personal research or study, educational or not-for-profit purposes without prior permission or charge, provided:

- The authors, title and full bibliographic details is credited in any copy;
- A hyperlink and/or URL is included for the original metadata page; and
- The content is not changed in any way.

For more information, including our policy and submission procedure, please contact the Repository Team at: E.mailbox@hud.ac.uk.

<http://eprints.hud.ac.uk/>

**TRANSIENT FLOW FEATURES IN THE VICINITY OF A
VERTICAL AXIS WIND TURBINE**

Atif Shahzad

Master of Science by Research

2015

University of Huddersfield

School of Computing and Engineering

DECLARATION

- The author of this thesis (including any appendices and/or schedules to this thesis) owns any copyright in it (the “Copyright”) and he has given The University of Huddersfield the right to use such copyright for any administrative, promotional, educational and/or teaching purposes.
- Copies of this thesis, either in full or in extracts, may be made only in accordance with the regulations of the University Library. Details of these regulations may be obtained from the Librarian. This page must form part of any such copies made.
- The ownership of any patents, designs, trademarks and any and all other intellectual property rights except for the Copyright (the “Intellectual Property Rights”) and any reproductions of copyright works, for example graphs and tables (“Reproductions”), which may be described in this thesis, may not be owned by the author and may be owned by third parties. Such Intellectual Property Rights and Reproductions cannot and must not be made available for use without the prior written permission of the owner(s) of the relevant Intellectual Property Rights and/or Reproductions.

The University of Huddersfield

ACKNOWLEDGEMENTS

First and foremost, I would like to thank Allah. I would like to gratefully acknowledge the enthusiastic supervision team, Dr. Taimoor Asim and Prof. Rakesh Mishra, for the guidance and constant support, as well as for providing me with the necessary information regarding the project, and also supporting me in completing this project.

Special thanks go to my colleagues Mr. Noukhez Ahmed and Mr. Sree Kaysthaqir. Thanks to the Engineering Research School Office at the University of Huddersfield for their advice and support.

Last, but by no means least, I wish to express my special thanks to my mother, brothers and my sisters for their on-going spiritual support, love and help during this long and challenging project.

ABSTRACT

The increasing demand of energy in the world is driving the search for more renewable and sustainable energy sources. Renewable sources of energy are being explored globally to overcome the depletion of fossil fuels and the resulting energy crisis. Moreover, use of fossil fuels has significant negative effects on the environment. Therefore, the focus is currently on both to ensure long-term energy supply, as well as to monitor and minimise the negative effects of these sources on the environment. In order to meet renewable energy targets, harnessing energy from all available resources such as wind, (through wind turbine), is necessary. Wind energy is one of the important sources of renewable energy. Wind turbine technology has been developed continuously, but the maintenance of wind turbines is still a topic of interest. Horizontal axis wind turbines (HAWT) have dominated the wind energy market due to their large size and high power generation characteristics. However, vertical axis wind turbines (VAWT) are also gaining wide acceptance owing to being capable of producing power even at low speeds.

The present study focuses on the quantification of the effect of steady wind flow conditions on the performance of Savonius type vertical axis wind turbine. The Savonius vertical axis wind turbine considered in this study comprises of multi-blade rotor and stationary inlet guide vanes, with the arrangement most suitable for a low wind speed application. Advanced numerical modeling tools within ANSYS–Fluent have been used in the present work to simulate the flow in and around the Savonius vertical wind turbine in order to quantify the flow behavior. Sliding mesh technique has been incorporated to simulate the rotation of the rotor blade, which capture the flow phenomenon caused by the stator and the rotor interaction, and hence providing more accurate results. A critical analysis of the flow across vertical axis wind turbine has been conducted through investigating the static pressure and velocity magnitude variations in the vicinity of the wind turbine.

Furthermore, the present study has also focused on the performance of a vertical axis wind turbine under unsteady flow conditions whereby the flow is accelerated and decelerated as characterised by the change in the wind velocity. The torque and power generation capabilities of the turbine have been characterised and in particular the rotor contribution has been quantified. The effect of transient phenomena under varying torque outputs during accelerating and decelerating flows has also been highlighted. Overall performance of the turbine has also been quantified.

CONTENTS

Chapter 1	1
Introduction.....	1
1.1. Wind Energy Evolution and Energy Crises	2
1.2. Wind Turbines	6
1.2.1. Horizontal Axis Wind Turbine	7
1.2.2. Vertical Axis Wind Turbine.....	8
1.3. Types of Vertical Axis Wind Turbine.....	9
1.3.1. Darrieus Type Vertical Axis Wind Turbine.....	9
1.3.2. Savonius Type Vertical Axis Wind Turbine	10
1.4. Performance Characteristics of VAWTs.....	11
1.5. Motivation.....	12
1.6. Research Aims	13
1.7. Organisation of Thesis	13
Chapter 2.....	15
Literature Review.....	15
2.1. Introduction.....	16
2.2. Performance Output of Vertical Axis Wind Turbines under steady flow conditions	17
2.3. Performance Output of Vertical Axis Wind Turbines under transient flow conditions.....	20
2.4. Research Objectives.....	25
Chapter 3.....	26
Numerical Modelling of Vertical Axis Wind Turbine.....	26
3.1. Introduction to Computational Fluid Dynamics	27
3.2. Working of CFD Codes	27
3.3. Numerical Formulation of the Fluid Flow	29
3.3.1. Conservation of Mass.....	30
3.3.2. Conservation of Momentum	30
3.3.3. Navier – Stokes Equation.....	31
3.4. Pre-Processing.....	31
3.4.1. Geometry of VAWT	32
3.4.2. Meshing of the Flow Domain	33

3.5.	Solver Execution	34
3.5.1.	Boundary Conditions	35
3.5.2.	Sliding Mesh	35
3.6.	Solver Settings	36
3.7.	Convergence Criteria	37
3.8.	Scope of Work	38
Chapter 4.....		39
Performance Analysis of a Vertical Axis Wind Turbine operating under Constant Wind Velocity ..		39
4.1.	Grid Sensitivity Analysis	40
4.2.	Time Step Independence Testing	40
4.3.	Verification of Numerical Results	41
4.4.	Performance Analysis of the VAWT	43
4.4.1.	General Performance Characteristics of the VAWT	45
4.4.2.	Effect of Tip Speed Ratio on the Performance Characteristics of the VAWT.....	51
4.4.3.	Summary	57
Chapter 5.....		58
Performance Analysis of a Vertical Axis Wind Turbine operating under Varying Wind Velocity ...		58
5.1.	Introduction.....	59
5.2.	Performance Evaluation of the VAWT operating under Transient Flow Conditions with constant Rotating Speed.....	59
5.3.	Performance Evaluation of the VAWT operating under Transient Flow Conditions with variable Rotating Speed	72
Chapter 6.....		78
Conclusions.....		78
6.1.	Research Problem Synopsis	79
6.2.	Research Aims and Major Achievements	79
6.3.	Thesis Conclusions	80
6.4.	Recommendations for Future Work.....	81

LIST OF FIGURES

FIGURE 1.1 THE IMPROVEMENTS IN THE WIND TURBINES FROM THE EARLY STAGES OF WIND ENERGY TO THE OUTBREAK OF CALIFORNIA, USA [2].....	2
FIGURE 1.2 A TREND OF AN HISTORICAL DEVELOPMENT OF WIND TURBINES [5]	3
FIGURE 1.3 CONTRIBUTION OF CO ₂ EMISSIONS REDUCTIONS IN VARIOUS POWER SECTORS [7]	4
FIGURE 1.4 COUNTRY DISTRIBUTION OF WIND POWER CAPACITY INSTALLED IN 2014.....	5
FIGURE 1.5 REGIONAL DISTRIBUTION OF WIND POWER CAPACITY INSTALLED IN 2014 [12]	5
FIGURE 1.6 COMPARISON BETWEEN THE TWO DIFFERENT CONCEPTS OF WIND TURBINES [11, 14].....	6
FIGURE 1.7 GROWTH SIZE OF THE COMMERCIAL HAWTs [17]	8
FIGURE 1.8 DARRIEUS TYPE VERTICAL AXIS WIND TURBINE	10
FIGURE 1.9 SAVONIUS TYPE VERTICAL AXIS WIND TURBINE	11
FIGURE 2.1 AVERAGE TORQUE TO POWER OUTPUT AGAINST TIP SPEED RATIO [39]	17
FIGURE 2.2 EFFECT OF GUIDE VANES ON THE PERFORMANCE OUTPUT OF A VAWT [44].....	19
FIGURE 2.3 C _p VARIATION WITH ROTATIONAL VELOCITY FOR TURBINE MODEL WITH TWO BLADES, FOR SMOOTH AND ROUGH BLADE SURFACES [45].....	19
FIGURE 2.4 CONTOUR PLOT OF THE PERCENTAGE POWER REDUCTION DUE TO THE EFFECTS OF WIND DIRECTION FLUCTUATIONS ($\Sigma\phi$) AND THE NORMALIZED VELOCITY FLUCTUATIONS (I_v) ON THE AERODYNAMIC PERFORMANCE OF THE VAWT [47]	21
FIGURE 2.5 VTM-PREDICTED VARIATION OF THE POWER COEFFICIENTS FOR THE STRAIGHT-BLADED AND CURVED-BLADED AND THE HELICALLY TWISTED BLADES TURBINES WHEN THE ROTORS ARE OPERATED IN UNSTEADY WIND CONDITIONS WITH $\Delta V/V_\infty = \pm 0.3$ AND $R_G = 1.5$ (WHICH CORRESPONDS TO $K_G = 0.74$ AT $\lambda = 3:5$). ERROR BARS DENOTE THE VARIATION OF THE POWER COEFFICIENT DURING ONE ROTOR REVOLUTION IN STEADY WIND CONDITIONS [16]	22
FIGURE 2.6 VTM-PREDICTED AERODYNAMIC ANGLE OF ATTACK AND SECTIONAL FORCES IN STEADY AND UNSTEADY WIND CONDITIONS [16]	23
FIGURE 3.1 CFD SOLVER	28
FIGURE 3.2 OVERVIEW OF CFD MODELLING [54].....	29
FIGURE 3.3 GEOMETRY OF THE VAWT.....	32
FIGURE 3.4 FLOW DOMAIN OF THE VAWT	32
FIGURE 3.5 MESH IN (A) VAWT (B) FLOW DOMAIN	33
FIGURE 3.6 INTERFACES BETWEEN DIFFERENT ZONES	36
FIGURE 4.1 TIME STEP INDEPENDENCE TESTING OF THE VAWT	41
FIGURE 4.2 VERIFICATION OF THE NUMERICAL RESULTS (A) VARIATIONS IN PRESSURE COEFFICIENT (B) VARIATIONS IN NORMALISED FLOW VELOCITY	43
FIGURE 4.3 INSTANTANEOUS EVALUATION OF THE VAWT'S PERFORMANCE AT (A) 0° (B) 3° (C) 15° (D) 27°	44
FIGURE 4.4 STATIC GAUGE PRESSURE (PA) VARIATIONS IN THE VICINITY OF THE VAWT AT (A) 0° (B) 3° (C) 15° (D) 27°.....	47
FIGURE 4.5 VELOCITY MAGNITUDE (M/S) VARIATIONS IN THE VICINITY OF THE VAWT AT (A) 0° (B) 3° (C) 15° (D) 27°	50
FIGURE 4.6 INSTANTANEOUS TORQUE COEFFICIENT OF THE VAWT AT $\lambda = 0.1$	50
FIGURE 4.7 INSTANTANEOUS POWER COEFFICIENT OF THE VAWT AT $\lambda = 0.1$	51
FIGURE 4.8 DIFFERENCE CONTOUR OF STATIC GAUGE PRESSURE BETWEEN TSRs OF 0.1 AND 0.2.....	52
FIGURE 4.9 DIFFERENCE CONTOUR OF VELOCITY MAGNITUDE BETWEEN TSRs OF 0.1 AND 0.2	52
FIGURE 4.10 DIFFERENCE CONTOUR OF STATIC GAUGE PRESSURE BETWEEN TSRs OF 0.1 AND 0.4.....	53

FIGURE 4.11 DIFFERENCE CONTOUR OF VELOCITY MAGNITUDE BETWEEN TSRs OF 0.1 AND 0.4	53
FIGURE 4.12 DIFFERENCE IN INSTANTANEOUS C_t BETWEEN TSRs OF (A) 0.1 AND 0.2 (B) 0.1 AND 0.4.....	54
FIGURE 4.13 DIFFERENCE IN INSTANTANEOUS C_p BETWEEN TSRs OF (A) 0.1 AND 0.2 (B) 0.1 AND 0.4.....	55
FIGURE 4.14 VARIATION OF (A) INSTANTANEOUS TORQUE COEFFICIENT, AND (B) THE MEAN INSTANTANEOUS TORQUE COEFFICIENT FOR THE VAWT DURING ONE REVOLUTION	56
FIGURE 4.15 VARIATION OF (A) INSTANTANEOUS TORQUE COEFFICIENT, AND (B) THE MEAN INSTANTANEOUS TORQUE COEFFICIENT FOR THE VAWT DURING ONE REVOLUTION	57
FIGURE 5.1 STATIC GAUGE PRESSURE (PA) VARIATIONS IN THE VICINITY OF THE VAWT AT (A) 0° (B) 3° (C) 15° (D) 27° ORIENTATION AT WIND VELOCITIES OF 6.75M/S, 6.80M/S, 7.00M/S AND 7.20M/S RESPECTIVELY AND A CONSTANT ROTATING SPEED OF 1.143RAD/S.....	61
FIGURE 5.2 VELOCITY MAGNITUDE (M/S) VARIATIONS IN THE VICINITY OF THE VAWT AT (A) 0° (B) 3° (C) 15° (D) 27° ORIENTATION AT WIND VELOCITIES OF 6.75M/S, 6.80M/S, 7.00M/S AND 7.20M/S RESPECTIVELY AND A CONSTANT ROTATING SPEED OF 1.143RAD/S	63
FIGURE 5.3 STATIC GAUGE PRESSURE (PA) VARIATIONS IN THE VICINITY OF THE VAWT AT (A) 0° (B) 3° (C) 15° (D) 27° ORIENTATION AT WIND VELOCITIES OF 9.75M/S, 9.80M/S, 10.00M/S AND 9.20M/S RESPECTIVELY AND A CONSTANT ROTATING SPEED OF 1.143RAD/S	65
FIGURE 5.4 VELOCITY MAGNITUDE (M/S) VARIATIONS IN THE VICINITY OF THE VAWT AT (A) 0° (B) 3° (C) 15° (D) 27° ORIENTATION AT WIND VELOCITIES OF 9.75M/S, 9.80M/S, 10.00M/S AND 9.20M/S RESPECTIVELY AND A CONSTANT ROTATING SPEED OF 1.143RAD/S	67
FIGURE 5.5 STATIC GAUGE PRESSURE (PA) VARIATIONS IN THE VICINITY OF THE VAWT AT (A) 0° (B) 3° (C) 15° (D) 27° ORIENTATION AT WIND VELOCITIES OF 7.25M/S, 7.20M/S, 7.00M/S AND 6.80M/S RESPECTIVELY AND A CONSTANT ROTATING SPEED OF 1.143RAD/SEC.....	69
FIGURE 5.6 VELOCITY MAGNITUDE (M/S) VARIATIONS IN THE VICINITY OF THE VAWT AT (A) 0° (B) 3° (C) 15° (D) 27° ORIENTATION AT WIND VELOCITIES OF 7.25M/S, 7.20M/S, 7.00M/S AND 6.80M/S RESPECTIVELY AND A CONSTANT ROTATING SPEED OF 1.143RAD/S	70
FIGURE 5.7 INSTANTANEOUS TORQUE COEFFICIENT OF THE VAWT UNDER VARIABLE WIND VELOCITY AT A CONSTANT ROTATING SPEED OF 1.143RAD/S	71
FIGURE 5.8 INSTANTANEOUS POWER COEFFICIENT OF THE VAWT UNDER VARIABLE WIND VELOCITY AT A CONSTANT ROTATING SPEED OF 1.143RAD/S	72
FIGURE 5.9 DIFFERENCE CONTOUR OF STATIC GAUGE PRESSURE BETWEEN ACCELERATED WIND VELOCITY OF 7M/S AND STEADY WIND VELOCITY OF 4M/S	73
FIGURE 5.10 DIFFERENCE CONTOUR OF VELOCITY MAGNITUDE BETWEEN ACCELERATED WIND VELOCITY OF 7M/S AND STEADY WIND VELOCITY OF 4M/S	73
FIGURE 5.11 DIFFERENCE CONTOUR OF STATIC GAUGE PRESSURE BETWEEN THE WIND VELOCITY AT THE PEAK OF 10M/S AND ACCELERATED WIND VELOCITY OF 7M/S	74
FIGURE 5.12 DIFFERENCE CONTOUR OF VELOCITY MAGNITUDE BETWEEN THE WIND VELOCITY AT THE PEAK OF 10M/S AND ACCELERATED WIND VELOCITY OF 7M/S	74
FIGURE 5.13 DIFFERENCE CONTOUR OF STATIC GAUGE PRESSURE BETWEEN THE DECELERATED WIND VELOCITY OF 7M/S AND THE WIND VELOCITY AT THE PEAK OF 10M/S.....	75
FIGURE 5.14 DIFFERENCE CONTOUR OF VELOCITY MAGNITUDE BETWEEN THE DECELERATED WIND VELOCITY OF 7M/S AND THE WIND VELOCITY AT THE PEAK OF 10M/S.....	75
FIGURE 5.15 INSTANTANEOUS TORQUE COEFFICIENT OF THE VAWT UNDER VARIABLE FLOW CONDITIONS	77
FIGURE 5.16 INSTANTANEOUS POWER COEFFICIENT OF THE VAWT UNDER VARIABLE FLOW CONDITIONS	77

LIST OF TABLES

TABLE 3.1 BOUNDARY TYPES AND CONDITIONS.....	35
TABLE 3.2 SCOPE OF WORK	38
TABLE 4.1 GRID SENSITIVITY TESTING OF THE VAWT.....	40
TABLE 4.2 TIME STEP INDEPENDENCE TESTING OF THE VAWT.....	40
TABLE 4.3 GEOMETRIC DIMENSIONS OF THE VAWT.....	41
TABLE 5.1 DIFFERENCE IN INSTANTANEOUS TORQUE COEFFICIENTS AND INSTANTANEOUS POWER COEFFICIENTS AT ACCELERATED, PEAK AND DECELERATED WIND VELOCITIES RESPECTIVELY.....	76

NOMENCLATURE

A	Frontal area of the VAWT (m^2)
a	Acceleration (m^2/s)
C_p	Power coefficient (-)
C_t	Torque coefficient (-)
d	Diameter (m)
P	Local static gauge pressure (Pa)
r	Radius of the rotor (m)
Re	Reynolds number (-)
T	Torque output (Nm)
t	Time (s)
V	Linear velocity (m/s)

GREEK SYMBOLS

θ	Azimuthal angle ($^\circ$)
λ	Tip Speed Ratio (-)
μ	Dynamic Viscosity (kg/m-s)
ρ	Density (kg/m^3)
ω	Angular Velocity (rad/s)

CHAPTER 1

INTRODUCTION

In recent years, the wind turbines have become an acceptable alternative for electrical energy generation by fossil or nuclear power plants. This is primarily due to the environmental and economic benefits. Wind is a renewable energy source that plays a key role in meeting the increased energy demand. It can be harnessed through various types of wind turbines. The wind turbines are classified into two categories, namely the Vertical Axis Wind Turbines (VAWT) and the Horizontal Axis Wind Turbines (HAWT). The present study focuses on the issues associated with VAWTs. This chapter focuses on the historic development of the wind turbines and provides an overview of wind energy as a source for electric power generation.

1.1. Wind Energy Evolution and Energy Crises

The depletion of fossil fuel and the pollution due to the use of these fuel to extract useful energy has become a bigger economical and environment concern recently. One of the significant developments in meeting energy in the 20th century onwards is the development of wind turbines to harness wind energy more efficiently to substitute the fossil fuels. Various studies have concluded that the wind energy is an alternative sustainable energy source that is capable of generating enough electricity to meet the demands of business, industrial and residential sectors with or without subsidies. The evolution of wind turbine technology can be traced back to 200 BC, with the discovery of a vertical axis wind turbine found at the Persian-Afghan borders dating back to 200 BC. Since then the technology has evolved in different parts of the world. The horizontal axis wind turbine has been built later in Netherlands and the Mediterranean [1]. These types of turbines underwent various stages of upgradations as depicted in figure 1 in the USA during the 19th century [2]. Furthermore, around 6 million of small turbines were used for water pumping between 1850 and 1970 in USA. The first large wind turbine used to generate electricity was built in Cleveland, Ohio, in 1888, which worked at very low speed and with high solidity ratio and had a maximum power generation capacity of 12kW.

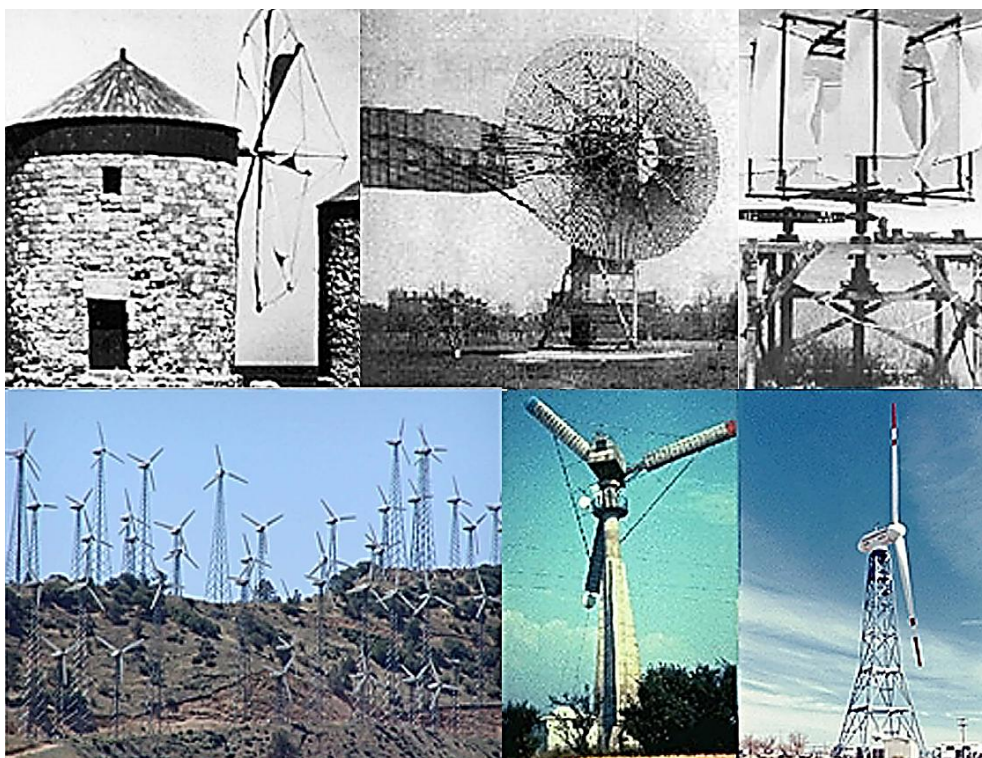


Figure 1.1 The improvements in the wind turbines from the early stages of wind energy to the outbreak of California, USA [2]

On the other hand, during 1917 and 1918 Denmark built the wind turbines that were capable of generating 25kW of power. Also, large-scale wind turbines were constructed in France, Germany, Denmark and the UK during 1935 to 1970.

Gedser mill wind turbine was designed in Denmark in the early 1960s which had a power production of 200kW. This wind turbine consisted of three-bladed upwind rotor [3]. In the late 1970s, Danish government has established a programme, which has led to commercial development of Danish wind turbines having power ratings of around 20kW. The progress in the wind turbines designs evolved further during the oil crises of 1973 and US government supported the research and development (R&D) program in wind turbines [4]. This was a major milestone in the wind energy history.

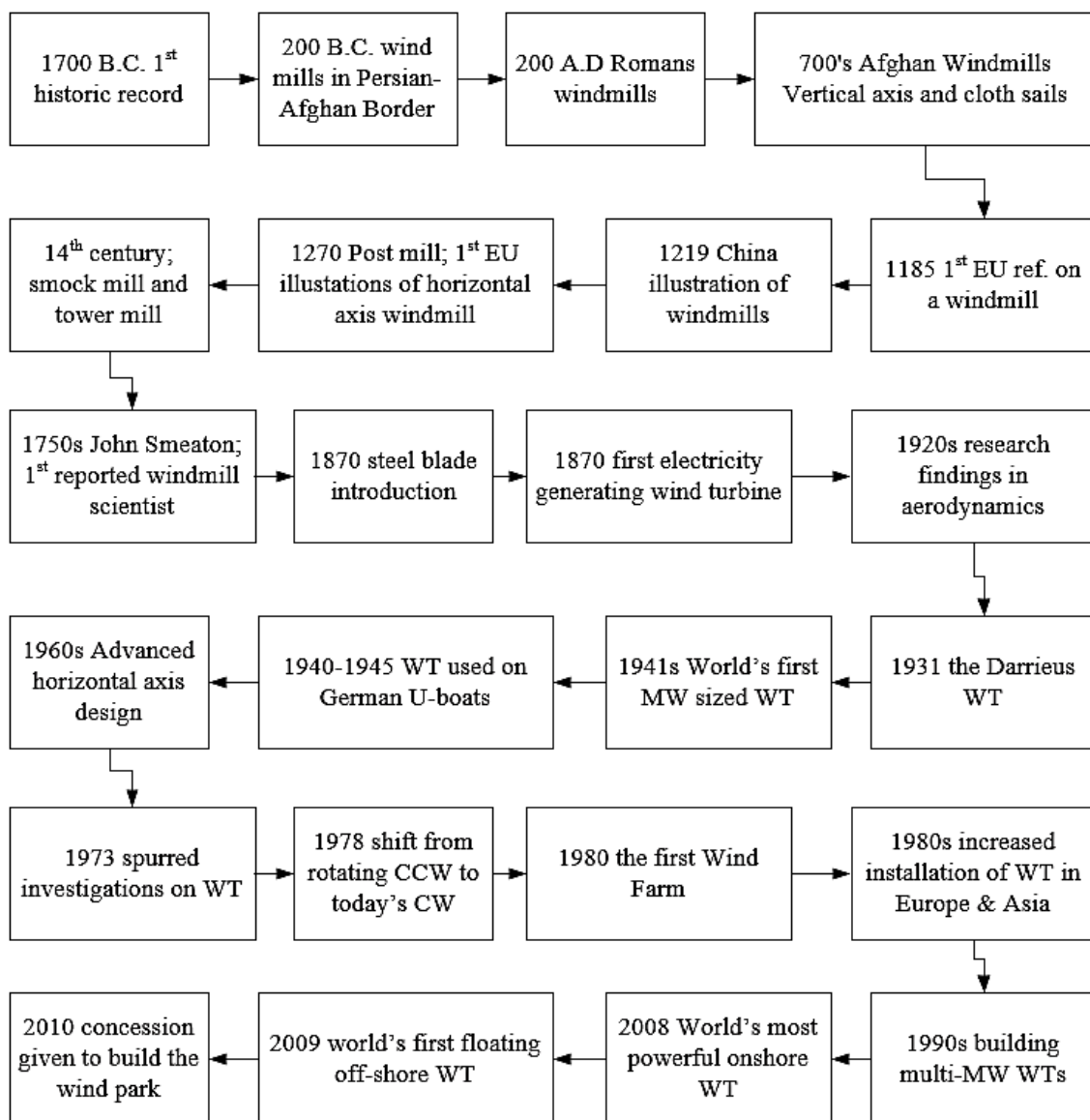


Figure 1.2 A trend of an historical development of wind turbines [5]

The history of wind power shows a general evolution from the use of simple and light devices driven by aerodynamic drag forces, to very heavy-material drag devices. However, in the modern era, increased use of light material with efficient aerodynamic lift devices has resulted in very efficient turbines. The historical development of wind turbines from 1700 B.C. to 2010 has been depicted in figure 1.2.

The International Energy Agency (IEA) has carried out an investigation to discover the effects of greenhouse gases that are released by the power sector. The IEA’s Energy Technology perspective (ETP) has estimated that the emission of greenhouse gases from the power sectors will rise by 130% from 2005 to 2050, without the intervention of new technologies [6]. An energy technology evolution is needed to wipe out these greenhouse gas emissions. The energy technology evolution could be renewable energy, nuclear energy, larger energy productivity and the power generation based upon decarbonisation of fossil fuel. According to Energy Technology Association BLUE map scenario, the wind power could contribute towards 12% of the necessary reduction in the greenhouse gases released by the power sector [7]. Figure 1.3 depicts the contribution in CO₂ reductions that can be achieved from the different energy sectors. In addition to the CO₂ reduction benefit of wind power, the emissions of pollutants like oxides of sulphur and nitrogen can also be reduced by wind energy technologies [8]. Due to the modern technological developments, the wind power has achieved remarkable advances in energy efficiency. Since 1980s, advancement in aerodynamics, structural dynamics and micro-metrology has contributed to a 5% annual increase in the energy production of the turbines [9].

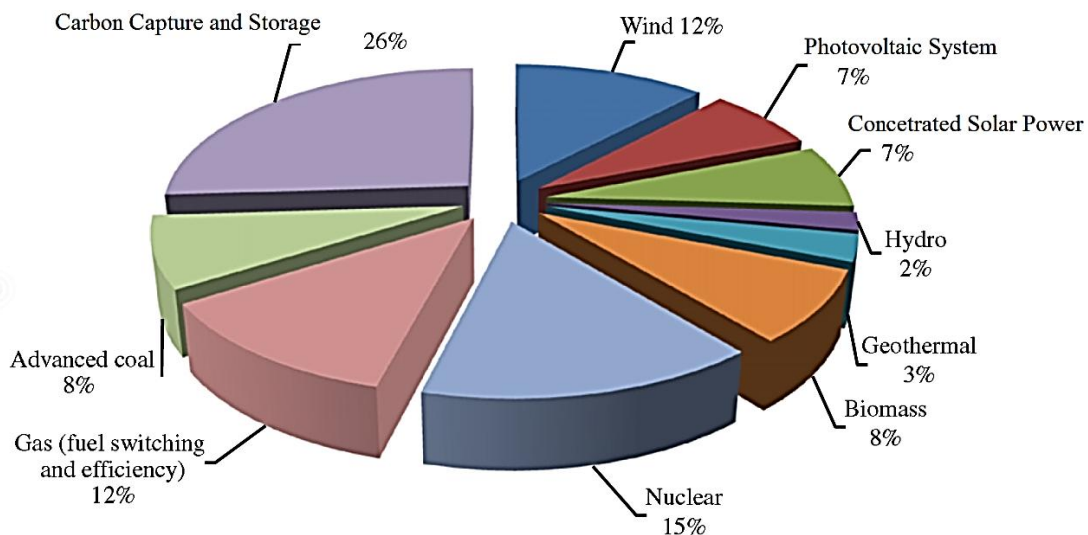


Figure 1.3 Contribution of CO₂ emissions reductions in various power sectors [7]

Concerning the present status of wind power capacities as depicted in figure 1.4, the China managed to add new 25% over its cumulative capacity during 2014. At the same time the USA achieved to install almost 5GW which is almost equal to the installed capacity by Germany and 30% of the Chinese cumulative capacity. As a result China has reached the

first place in the world ranking table and Germany and the USA have reached the second and third place in the world ranking table for the installed wind turbine capacity.

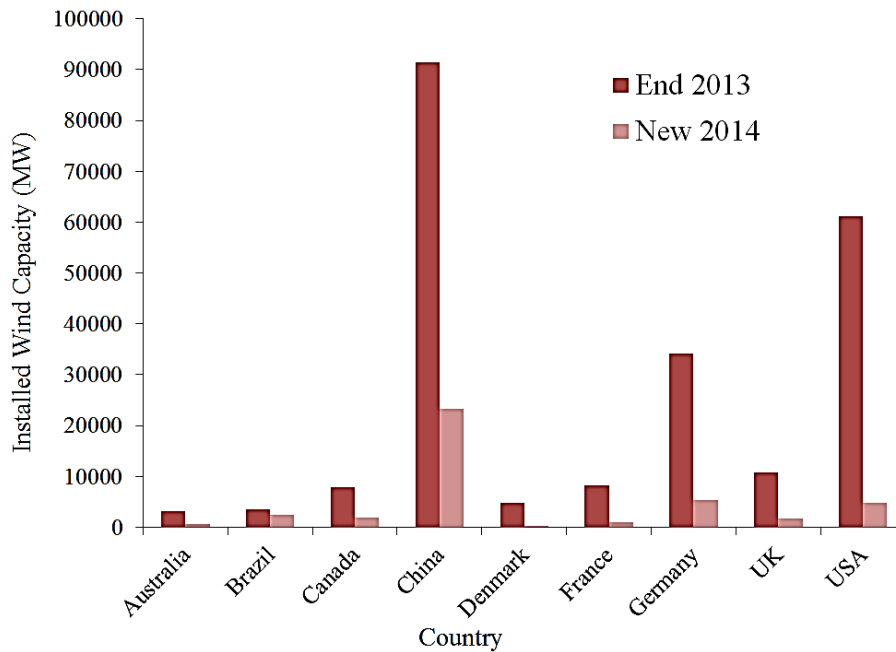


Figure 1.4 Country distribution of wind power capacity installed in 2014

Furthermore, based upon the regional distribution of wind power capacity installed in 2014 EU has generated the most wind energy of 38% of the total capacity installed as shown in figure 1.5. Asia has reached second position in producing wind energy with 36% although this has a maximum contribution from China. The above discussion has indicated that the installed wind turbine capacity is increasing exponentially and it is expected that in future this trend will continue. Efforts will, therefore, be needed to make these systems more efficient, reliable and maintainable.

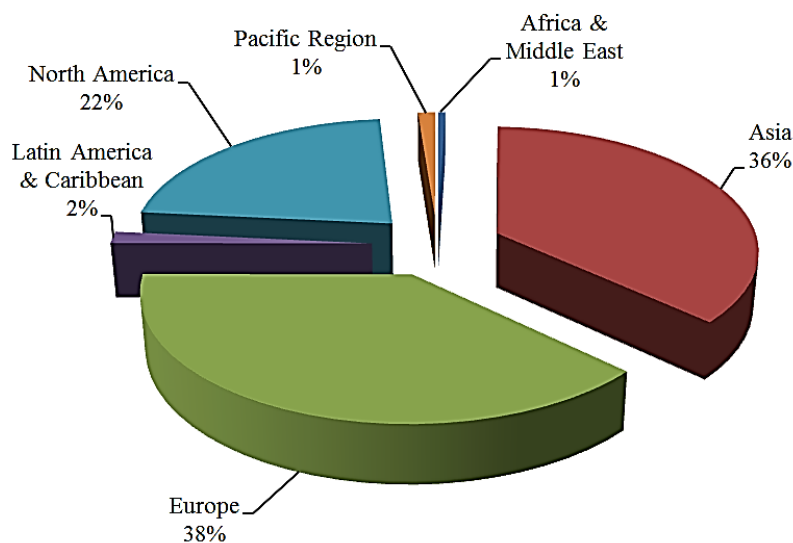


Figure 1.5 Regional distribution of wind power capacity installed in 2014 [12]

1.2. Wind Turbines

A wind turbine is a mechanical device that converts the kinetic energy of the wind into useful forms such as mechanical work and electrical energy. According to Eriksson et al. [10], the turbines are differentiated into two categories based upon their axis of rotation. Furthermore, Erich Hau [11] carried out the classification of wind energy converters according to their aerodynamic functions and conceptual designs. A vertical axis wind turbine (VAWT) has a vertical axis of rotation, which is perpendicular to the ground and horizontal axis wind turbine (HAWT) has horizontal axis of rotation, which is parallel to the ground. Figure 1.6 shows the comparison between the two different concepts of wind turbines.

The operation of wind turbine is based upon the fundamental facts [13]. Wind turbines use the basic aerodynamic forces to generate a net positive torque on a rotating shaft. This results in the production of mechanical power and its transformation into electricity generation. Wind turbines produce energy only in response to the resource that is immediately available. The direct storage of the wind power is not possible [13]. The output of a wind turbine is thus inherently fluctuating. The energy production from a large wind farm consisting of many wind turbines may be enough to reduce the total electrical load of certain area. The generated power from a small wind turbine networks can be stored using backup generators and some specialised control systems.

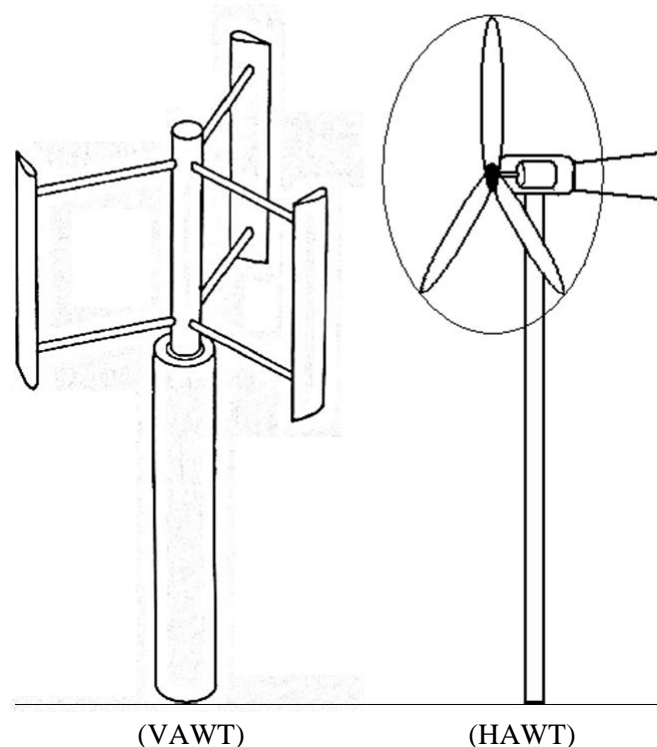


Figure 1.6 Comparison between the two different concepts of wind turbines [11, 14]

Many developments have been carried out since the large scale commercialisation of the wind turbine technology in the early 1980s but the engineering principles of the turbine design have changed very little. The major challenge for the modern wind industry is to design the efficient wind turbines to harness the wind energy and maximise the power generation [15, 16].

1.2.1. Horizontal Axis Wind Turbine

Wind energy converters with their axis of rotation in a horizontal position parallel to the ground are designed almost on the basis of propeller or turbine-like concepts. In HAWTs the rotating axis of the wind turbine remains horizontal, or parallel with the ground. The wind energy is extracted by means of a rotor on vertical plane, upwind of the tower, which has a number of the blades that can be pitched to control the rotational speed of linked shaft in the modern HAWTs. These turbines have the ability to produce more electricity from a given amount of wind. These turbines are mostly suitable for larger applications. HAWTs are generally heavier and hence have severe problems in high wind velocity applications because of excessive turbulence.

There are several [parameters that affect operational behaviours of wind turbines. Schaffarczyk [17] has described the following important indicators that are associated with the standard horizontal axis wind turbine:

- Horizontal axis of rotation
- Mainly three bladed
- Lift force is used to drive the wind turbine
- Upwind arrangement of the rotor; tower downwind
- Variable speed with constant tip speed ratio operation
- Pitch control after rated power is reached.

HAWTs design improvement was a major challenge for the researchers/industries in the last few decades. Researchers have attempted increased HAWT size with a view to extract more power from the wind turbines. Figure 1.7 depicts the history of the growth in the size of the HAWTs and anticipated size for the future wind turbines. For the past many years, the size of the HAWT has been increased dramatically [17]. A survey in 2005 showed that most of the wind turbine has installed capacity of about 750kW and, only 21.5% of the newly installed wind turbine had the capacity to produce MW power. Subsequently, companies like Dong Fang and Gold Wind started to develop MW-level wind turbine, which increased the capacity from 600kW to 1MW or above and by 2010, 86.8% of the market share is occupied by the MW-level wind turbines [5].

HAWTs do have few drawbacks such as their orientation is dependent on the specific direction of wind. Furthermore, they are not suitable for generating electricity at wind

velocity lower than 6m/s. Moreover, the HAWTs do not have the capability to withstand severe weather conditions due to freezing rain, frost or heavy snow. These turbines cannot bear heavy winds in excess of 50m/s. Another major drawback of the HAWTs is their limitation in self-starting feature. They are also difficult to transport and install at various locations due to their heavy and big components.

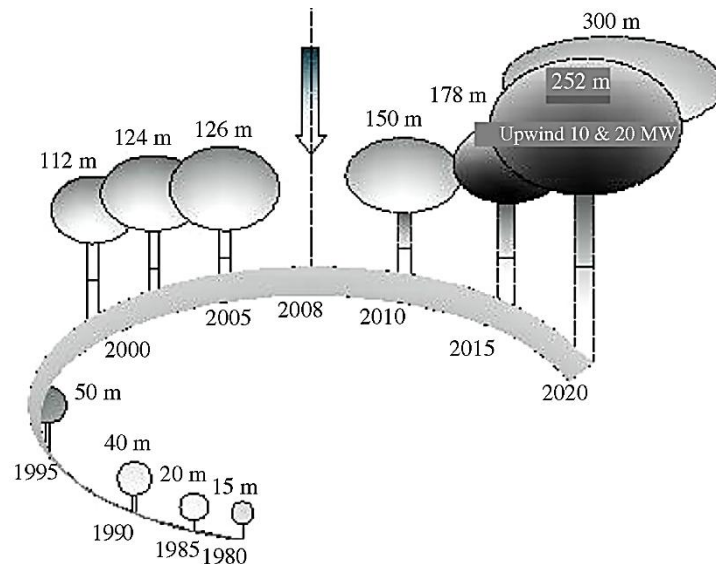


Figure 1.7 Growth size of the commercial HAWTs [17]

1.2.2. Vertical Axis Wind Turbine

The vertical axis wind turbines (VAWT) have a shaft mounted along the vertical axis, perpendicular to the ground, as shown in the figure 1.5. VAWTs are always aligned with any wind direction. Vertical axis wind-mills and subsequently the VAWTs are older in evolution clock than HAWT as it was first built in 200 B.C. by Persians. They used vertical axis rotating device to grind the grains as described by Mittal [19]. The design of the wind turbines are based upon the required operational characteristics of the wind energy conversion system. Moreover, it also depends upon the aerodynamic drag and lift generated. The current wind turbines are aerodynamic lift dependent [20]. Particularly, the design proposed in 1925 by French engineer, Darrieus [5] in which the rotation of the blades follows a troposkien (spinning rope) pattern, with a vertical axis of rotation. This system uses aerodynamic lift to rotate the rotor blades. However, this design has made the geometric shape of the rotor blades more complicated and thus difficult to manufacture.

Vertical axis technologies have the advantage of producing up to 50% more electricity on an annual basis versus conventional turbines with the same swept area. This system is mostly suitable for small wind projects and residential applications. These turbines are very light weight and hence, functions well in severe wind conditions. The major advantage of with the vertical axis of rotation is that the performance of wind turbine is not affected the wind direction. Furthermore, VAWTs can generate electrical energy with the wind velocity as

low as 2m/s and as high as 65m/s depending upon the design of the VAWT. These turbines have the ability to withstand at extreme weather conditions unlike HAWTs and can resist very high wind conditions in excess of 60m/s. Furthermore, these systems have a low starting torque and require a small amount of energy to start turning. Moreover, it has lower construction and transportation costs.

Furthermore, these turbines can be installed closer to the ground. The largest VAWT manufactured so far was the so-called EO1e-C made in Canada. Its height was about 100m, the rotating mass was 880 metric tons, and the rated power was supposed to be 4MW. Unfortunately, due to severe vibration problems, the rotational speed was limited to such low values that only 2MW was reached [17].

1.3. Types of Vertical Axis Wind Turbine

The vertical axis wind turbines are categorised into two different types, based on their aerodynamic design. The first VAWT type uses aerodynamic lift to rotate the rotor blade known as Darrieus and the second VAWT type uses aerodynamic drag to rotate the blade called as Savonius Rotor. The detailed discussions on both types of VAWT are included in the following sections.

1.3.1. Darrieus Type Vertical Axis Wind Turbine

The Darrieus type vertical axis wind turbine is named after a French engineer Darrieus G, who patented his turbine design in 1931 [21]. The wind turbine was manufactured by a company from US known as FloWind. In Darrieus type VAWT, the energy is taken from the wind through the lift force working in the direction of rotation. Lift force is perpendicular to the resultant of two velocity components of wind velocity and relative velocity of airfoil to the shaft. These types of turbines have the highest values of efficiency among VAWTs. The tip speed ratios for these turbines can be much higher resulting in a much higher rotating speed. However, these wind turbines suffer critical problems such as low starting torque or poor integration of assembly. A schematic of Darrieus type VAWT is depicted in the figure 1.8.

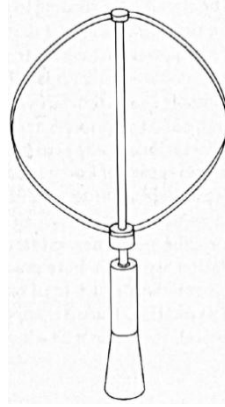


Figure 1.8 Darrieus type Vertical Axis Wind Turbine

The Darrieus type VAWT consists of set of vertically oriented airfoils connecting to a rotating shaft [22]. Unlike the common horizontal-axis wind turbine (HAWT), the direction of incoming flow is perpendicular to the axis of rotation instead of parallel. This allows the device to capture energy from the wind coming from any direction. However, the design encounters several problems, including its inability to self-start, cyclic loads and poor response to high wind speeds. The aerodynamic behaviour of this wind turbine is considered to be very complex, which makes accurate performance predictions very difficult. According to Hameed et al. [23], the long blades of the Darrieus type VAWT, with high aspect ratios, are subjected to large values of bending moments due to the centrifugal forces that may result in the failure of the blades. Furthermore, Castelli et al. [24] noted that the modifications to the basic Darrieus type VAWT can be made to suit different tip speed ratios (TSR).

1.3.2. Savonius Type Vertical Axis Wind Turbine

The Savonius type VAWT has blades with S-shaped cross section when viewed from the axial direction of the rotor blades [25]. A schematic of Savonius type VAWT is depicted in the figure 1.9. The Savonius type VAWT is invented by the Finnish engineer Savonius S. in 1922. The Savonius type VAWT capture power from wind through the action of drag force. Therefore, there is a difference in the drag coefficients along the convex and concave side of the blades. Furthermore, according to D'Ambrosio et al. [26], Savonius rotor being a drag type VAWT, whereby the rotor cannot rotate faster than the speed of wind. The maximum tip speed ratio is equal to one or less. This report will focus on the Savonius rotor due to its suitability for low speed environments.

Previous studies were mostly conducted on the optimization of design parameters such as blade number, blade shape and overlap distances. Experimental studies carried out by Sheldahl et al. [27], Sivasegaram [28], Clayton [29] and Fujisawa et al. [30] all report varying power coefficients for Savonius rotors ranging from 0.14 to 0.33 within a TSR range of 0.8 to 1.0. Given the high solidity of this type of rotor, significant torque output

was observed during static and rotational modes of operation making start-ability consistent at low wind speeds. Due to this high solidity to low speed ratio design, the acoustic emission from this machine during normal operation is considerably less than the traditional HAWT. With current UK planning legislation in view, this type of machine lends itself to installation in the built urban environment where noise restrictions are of primary concern [31].

The Savonius type VAWTs are simple and cheap to design. They can withstand high wind speeds due to its low rotational speed, unlike HAWTs, which are stopped in severe weather conditions as described earlier. These turbines generate high starting torque, which enables them to operate at low wind speeds. On the other hand, low rotational speed limits the power generation. Moreover, the Savonius VAWTs have low efficiency with the power coefficients of around 10% [32].

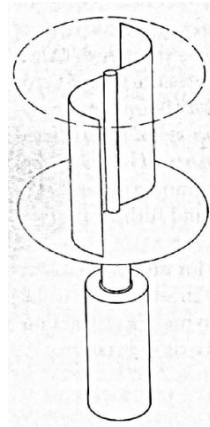


Figure 1.9 Savonius type Vertical Axis Wind Turbine

One problem that was present in some of these machines was the large variation in rotor torque output due to the fixed two blade design. Upon detailed investigations into the flow fields across the machine it was found that blade interaction effects were present on the non-torque generating blade. It was identified that unfavourable pressure gradients were the primary cause which resulted in a counter-rotating torque which significantly reduced the efficiency of the rotor. These blade interaction effects have become one of the major limitations of this type of turbine given torque generation is only provided by one bucket each rotor cycle. Such limitations provide strong justification for exploring alternative reaction type devices which maintain similar high levels of starting torque and provide a more consistent power delivery.

1.4. Performance Characteristics of VAWTs

According to Colley et al. [33], the important performance parameters for wind turbines are the torque output and the tip speed ratio (TSR, λ). The tip speed ratio of a VAWT has been defined as:

$$\lambda = \frac{\omega r}{v} \quad (1.1)$$

Where r is the radius of the rotor blades, ω is the rotational speed of the rotors and v is the wind velocity. Furthermore, the torque coefficient of the VAWT can be expressed as:

$$C_t = \frac{T}{\frac{1}{2} \rho v^2 A r} \quad (1.2)$$

Where T is the torque output of the VAWT, ρ is the density of air and A is the frontal area of the VAWT. Once the torque coefficient for the VAWT is known, the torque output can be calculated as follows:

$$T = \frac{1}{2} \rho v^2 A r C_T \quad (1.3)$$

Moreover, based on the torque and rotating speed of the rotor, the power generated by the vertical axis wind turbine can be calculated as:

$$P = \omega T \quad (1.4)$$

Where P is the power generated by the VAWT. Once the power of the VAWT is obtained, the power coefficient can be calculated as:

$$C_p = \frac{P}{\frac{1}{2} \rho v^3 A} \quad (1.5)$$

1.5. Motivation

Although the working principle of the Savonius type VAWT is reasonably well understood, the detailed aerodynamic flow features and the mechanical behaviour are too difficult to predict reasonably well, especially when the VAWT is experiencing variable wind speeds. The major issue with inconsistent behaviour of wind is that, it may be difficult to estimate the power output of the VAWT under such conditions. Furthermore, it has been noted that the instantaneous torque output from the VAWT varies significantly when a gust of wind is acting on the turbine. Due to fluctuation in the instantaneous torque values acting on the turbine, the transient load increases on the turbine structure and hence, it may induce heavy stresses on the turbine structure. This phenomenon introduces fatigue on the turbine structure and may reduce its life cycle.

The present research attempts to provide a deeper understanding into the physics of Savonius type VAWT behaviour under accelerating and decelerating wind velocity across

the VAWT. The present study employs a CFD approach, in order to allow the VAWT designer to extract several aerodynamic performance parameters such as pressure fluctuations, velocity variations and instantaneous performance characteristics of the VAWT. The performance of the Savonius type VAWT has been investigated numerically for a wide range of operating and flow conditions. In this investigation, accurate numerical models have been developed for accelerating and decelerating wind speeds across the VAWT.

1.6. Research Aims

The primary aim of this study is to investigate the effects of tip speed ratio on the unsteady fluid flow phenomena in and around the Savonius type VAWT. The study is designed to carry out numerical investigation using a commercial CFD code ANSYS. Both local and global flow parameters will be computed and a detailed investigation into qualitative and quantitative parameters of interests will be carried out. A novel prediction model will be developed for the performance analysis of the VAWT under a range of flow conditions. The research aims for this investigation are to:

1. Analyse the performance characteristics of a Vertical Axis Wind Turbine operating at a constant velocity.
2. Analyse the performance characteristics of a Vertical Axis Wind Turbine with accelerating and decelerating flow conditions.

1.7. Organisation of Thesis

Chapter 1 provides an overview of wind energy crisis and its evolution. Types of wind turbines have been discussed in detail, focusing on the Savonius type VAWTs. Advantages of VAWTs over HAWTs have been summarised. The operating principle of VAWTs has been discussed. The performance characteristics of VAWTs have also been introduced. Furthermore, the motivation to carry out this study has been stated.

Chapter 2 consists of an in-depth review of the research that has been carried out on steady and transient fluid flow conditions in the vicinity of the Savonius type VAWT. A critical review of the literature available for the unsteady flow around VAWTs has been carried out. Details of the scope of research are provided in the form of specific research objectives.

Chapter 3 documents the fundamental principles of Computational Fluid Dynamics. It includes the CFD modelling of the VAWTs, including the solver settings and the appropriate boundary conditions that have been specified to resolve the flow domain. The meshing technique that has been used for the flow domain has been discussed. A detailed discussion on the sliding mesh technique used for the rotation of the rotor blades has been presented.

Chapter 4 includes the mesh independence testing, time step size independence testing and the verification of the numerical results. Furthermore, transient and instantaneous performance of a Savonius type VAWT has been evaluated under steady flow conditions. Moreover, this chapter sheds light on the flow structure in the vicinity of the VAWT through analysing and investigating the pressure and velocity fields. Semi-empirical prediction tools have been developed for torque and power coefficients as functions of tip speed ratios.

Chapter 5 focuses on the performance characteristics of the Savonius type VAWT under transient flow conditions, where two types of investigations have been carried out. The first investigation corresponds to a constant rotational speed of the rotor, while the second investigation focuses on variable rotational speed of the rotor, while the operating wind velocity remains variable in both these cases.

Chapter 6 concludes the findings of this study, clearly mentioning the goals achieved and additions to the existing knowledge about VAWTs performance under transient conditions, whereby it can perform efficiently over a wide range of wind velocities. Recommendations for future work have also been included.

CHAPTER 2

LITERATURE REVIEW

The following chapter provides a detailed review of the available literature in the field of wind engineering with emphasis on the performance characteristics of Savonius type Vertical Axis Wind Turbines operating in various environmental conditions. The main areas addressed in this chapter are associated with the flow diagnostics of VAWTs that form the basis of this thesis. Within each of these areas, specific limitations have been identified which have been used to define the scope of the research. From the scope, specific research objectives of this thesis are provided such that efforts are made to provide novel contributions in each of the areas investigated.

2.1. Introduction

Energy being part of our everyday life plays an important role in our day to day activities. With the development of the technology, the demand of the energy is increasing exponentially. Therefore, energy security became one of the most important concerns of the government and in the world. Although, it is known that, the developed countries are the major consumers of global energy, the energy consumption is increasing demands in developing countries, where populations, economic activities and improvements in quality of life are growing most rapidly [34]. In addition because of the limited resources of fossil fuels and increased pollution from exploitation of these fuels, the world is focusing on the renewable energy sources. There are many on-going researches focussed to find suitable renewable and enviro-friendly sources such as solar, wind, hydro energy etc. Renewable energy resources are undergoing rapid development process and wind power technology is one of those where extensive efforts are directed. Wind power is widely recognized by various researchers including Mohammed et al. [35] as the one capable of providing a cost-effective, clean, renewable and sustainable source of energy.

Wind power involves converting the kinetic wind energy into electric energy using wind turbine. Since 200BC, people have been using wind power via wind mill for various domestic applications. However, the development of the wind energy as an alternative energy sources started after the energy-crisis of 1973-1974 [36]. Since wind turbines are recognised as a viable alternative source of energy, wind farms are being developed extensively and employed in various environmental conditions and setup. Hameed et al. [37] has mentioned that lots of effort has been made on the development of Horizontal axis turbine compare to vertical axis wind turbine.

Since, wind turbine use the kinetic energy of wind, the most important precondition for successful application of wind turbine is a good wind regime [Hau [38]]. It is very rare to have constant steady wind velocity all the time. The velocity of wind fluctuates according to the geometric location and its surroundings. The velocity of the wind and the components of the velocity acting on the blade differs and this affects the blade performance and hence the performance of the wind turbine. The vast majority of research published has been with the steady wind flows and very limited amount of work has been published investigating the VAWT performance under unsteady wind condition.

This chapter presents an examination of the effects of steady and unsteady wind velocities on blades and performance of the wind turbines based upon a review of relevant literature.

2.2. Performance Output of Vertical Axis Wind Turbines under steady flow conditions

As it is mentioned earlier blades are a critical component of wind turbines and the geometry of the blades is considered as one of the most critical parameters that affect the performance of turbine. Many researches have conducted numerical and experimental analyses to investigate the effect of the geometrical parameters on the turbine performance. Most of these researches have been conducted assuming a steady operating wind condition. This chapter focuses on some of the literature available in the area of the performance evaluation of wind turbine under steady wind condition.

Although a lot of research work has been carried out in this research area, only those research papers have been reviewed in this chapter that are directly relevant to the proposed work in this thesis. Park et al. [39] conducted a numerical study on the performance of savonius type vertical axis turbines by modifying their geometric features. The results indicates that, the optimum operating condition to achieve maximum power output from the vertical axis turbine used in the study occurs at a tip speed ratio of 0.17. Figure 2.1 depicts change in the average torque and power output of a vertical axis turbine with respect to TSR (Tip Speed Ratio) for one complete revolution of the turbine.

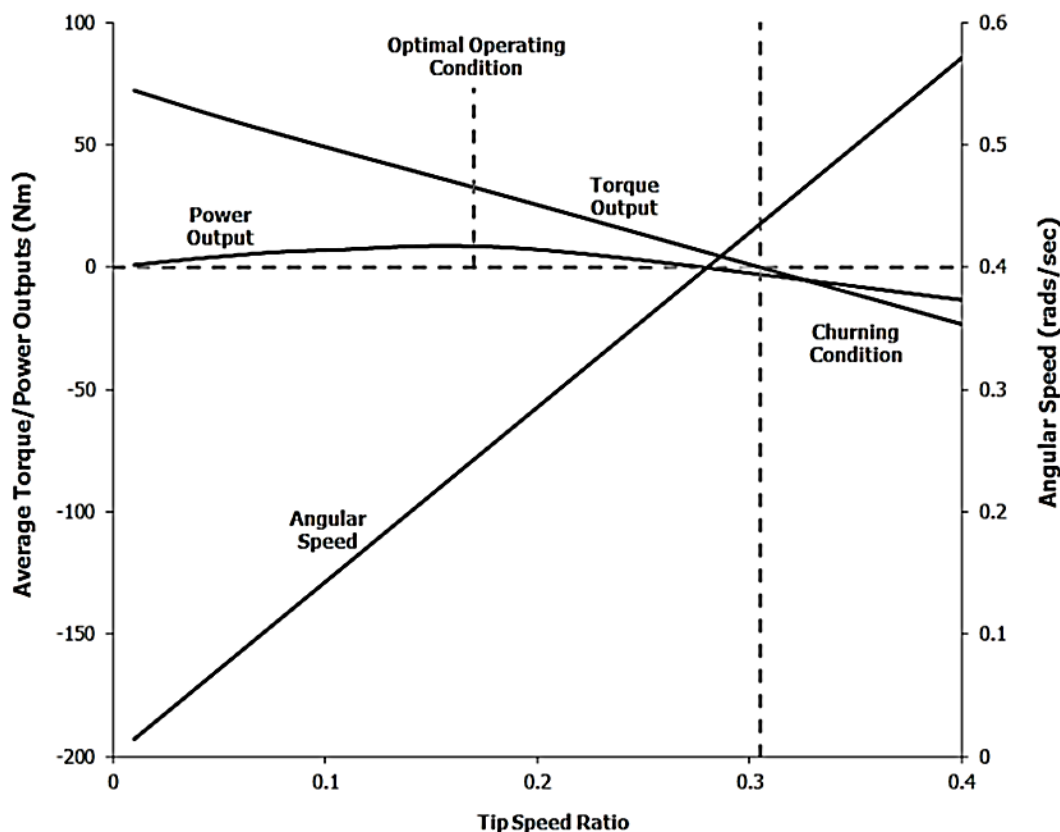


Figure 2.1 Average torque to power output against tip speed ratio [39]

It shows that the torque output decreases with increase of TSR, whereas, the average power output initially increase up to a certain value (optimal operating condition). After the optimum point, the power output starts to decrease as the value of TSR keeps on increasing along with the reduction of torque output.

Colley et al. [40] have tried to determine the operation characterises of Savonius type VAWT and carried out detailed investigation of the design, operation and the diagnostics of vertical axis wind turbines adopting both numerical and experimental methods. In this study, the overall performance of Savonius -type VAWTs has been quantified and the maximum torque coefficient and power coefficient were found to be 1.7, and 0.24 respectively. It is also been mentioned that the number of stator blades has a great impact on the torque and power output of the VAWTS.

Sabaeifard et al [41] conducted both experimental and CFD based numerical studies to analyse the performance output of a small scale Savonius VAWT and hence to optimise the design of the VAWT. Multiple Reference Frame technique has been used to rotate the blades of a two dimensional model of the VAWT. It has been reported that increase in number of blades increases the power output of the VAWT

Asim et al. [42] examined the effects of the shape of stator blades on the performance output of a Savonius type Vertical Axis Marine Turbine, demonstrating that curved stator blade performances in these turbines exhibit superior performance when compared to straight stator blades. While the study focused on marine current turbines in particular, it suggests that blade shape may be a significant influence on turbine performance.

A numerical investigation on the effect of rotor blade position on the VAWT performance was conducted by Colley et al. [43], for three Savonius type VAWT configurations. The investigation was conducted using the wind velocity of 4m/s and varying the tip speed ratio from zero to 0.6. The results indicate that within a typical rotor blade passage, maximum torque is obtained at a unique rotor angle. In addition, the torque output of the VAWT decreases with the increment of tip speed ratio for all rotor blade positions.

The experimental study by Takao, et al. [44], analyse the effects of directed guide vanes on the performance output of a VAWT (figure 2.2). A detail investigation was conducted on the effects of setting angle and gap between rotor blade and guide vane on power coefficient and starting characteristic. A significant increment on the peak coefficient was achieved with implication of guided vanes. Furthermore, it has also been noticed that, increase in the setting angle increase the performance output of the VAWT.

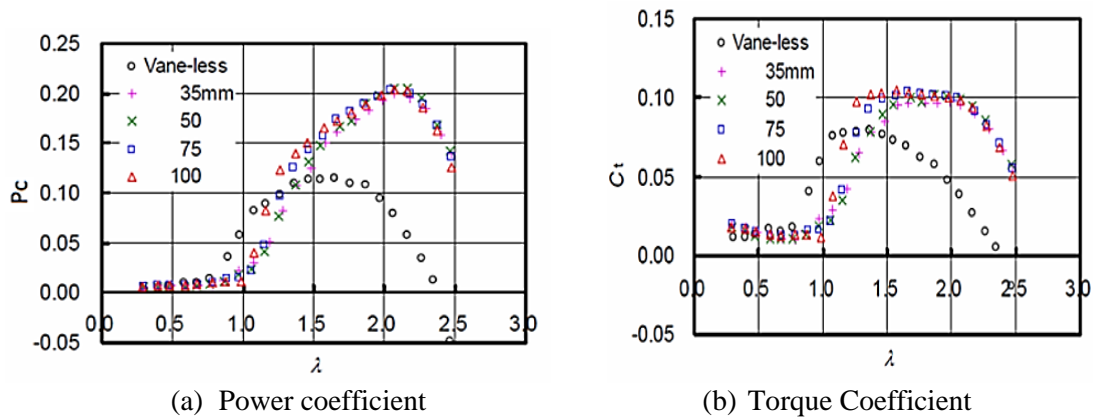


Figure 2.2 Effect of Guide Vanes on the performance output of a VAWT [44]

Howell [45] carried out a combined experimental and computational study into the aerodynamics and performance of a small scale vertical axis wind turbine (VAWT). The overall performance of the turbine is determined by a wind tunnel tests, whereas two- and three-dimensional unsteady computational fluid dynamics (CFD) models were generated to understand the aerodynamics of this performance. Wind tunnel test was conducted by varying the wind velocity, tip speed ratio and rotor blade surface finish. The experimental data depicts that the rotor blade surface finish has great impact on the turbine performance. The turbine performance degrades up to a certain wind speed known as critical wind speed. After the critical point, smooth surface finish enhances the turbine performance.

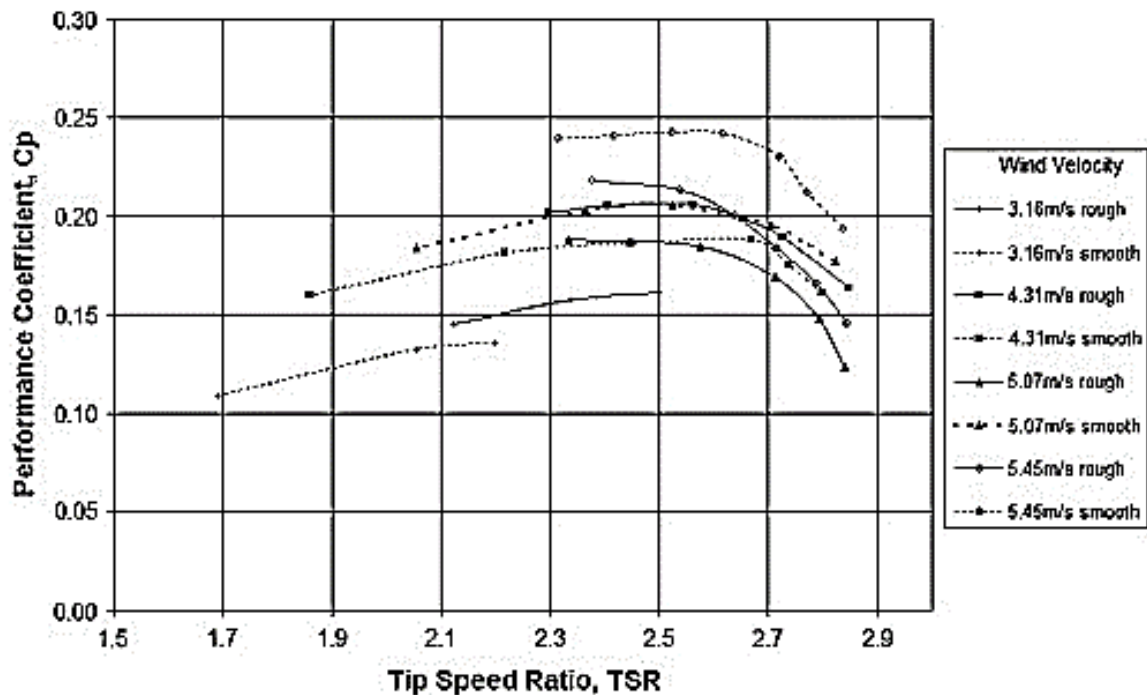


Figure 2. 3 C_p variation with rotational velocity for turbine model with two blades, for smooth and rough blade surfaces [45]

The above discussion indicates highlights that there is a scope for development of wind turbines that have directed entry through a well-designed stator configuration and this configuration can be optimised in conjunction with rotor blades for better performance output and reliable operation.

2.3. Performance Output of Vertical Axis Wind Turbines under transient flow conditions

Wind environment and the flow field around the rotor are directly related to its torque generating capabilities. However wind continuously changes its magnitude and direction. The transient effect of the approaching wind on the performance output of the wind turbine is an important measure in the design of the wind turbines and plays a major role in reducing turbine structure life because of fatigue effects.

Under transient conditions of the operating velocity, the excitation forces experienced by the blades vary considerably resulting in complex vibratory responses. Furthermore increased levels of accelerated velocity of air may result in amplified mechanical stresses. Hence it is necessary for the designers to include within load calculations for wind turbines the fatigue loads as well as occasional extreme loads. VAWT would behave differently under different wind conditions and the flow field around the rotor is directly related to its torque generating capabilities. It can be argued that, due to the location, different sizes and weights of turbines, small turbines experience different impact of wider range of transient wind conditions as compared to the large turbines.

Mcintosh et al. [46] conducted numerical investigation on the VAWT performance, when operating at a constant rotating speed under unsteady wind condition and quantified it using unsteady performance coefficient, which is similar to the power coefficient. The VAWT was operating at a constant rotation speed while encountering a fluctuating free stream of sinusoidal nature. The results indicate that the VAWT, at the tip speed ratio greater than the steady state maximum, shows a significant increment in the energy production. Moreover, implementation of over-speed control techniques increases the energy output by 42% and 245% for constant rotation speed and tip speed ratio feedback models respectively.

Kooiman et al. [47] carried out an experimental analysis on the effects of unsteady wind conditions on the aerodynamic performance of vertical axis wind turbine within the urban environment. Variations in the wind speed fluctuations and direction was quantified and compared to a reference case wind tunnel performance. The findings of the experiment confirmed that, the directional fluctuations have comparatively less impact on the turbine performance. Furthermore, the impact of the wind speed fluctuations on the turbine performance was quantified.

Figure 2.4 illustrates percentage power reduction contours with respect to wind direction fluctuations and the normalized wind velocity fluctuations. A dominant positive gradient for percentage power reduction vs. normalized velocity fluctuation is detected representing increment of normalised wind velocity fluctuation increases the percentage power reduction and hence reduces the power output and the aerodynamic performance of VAWT. On the other hand, the wind direction fluctuation shows a negative gradient signifying the increment of wind direction fluctuation decrease the percentage power reduction and hence, increases the power output and enhances the aerodynamic performance of VAWT.

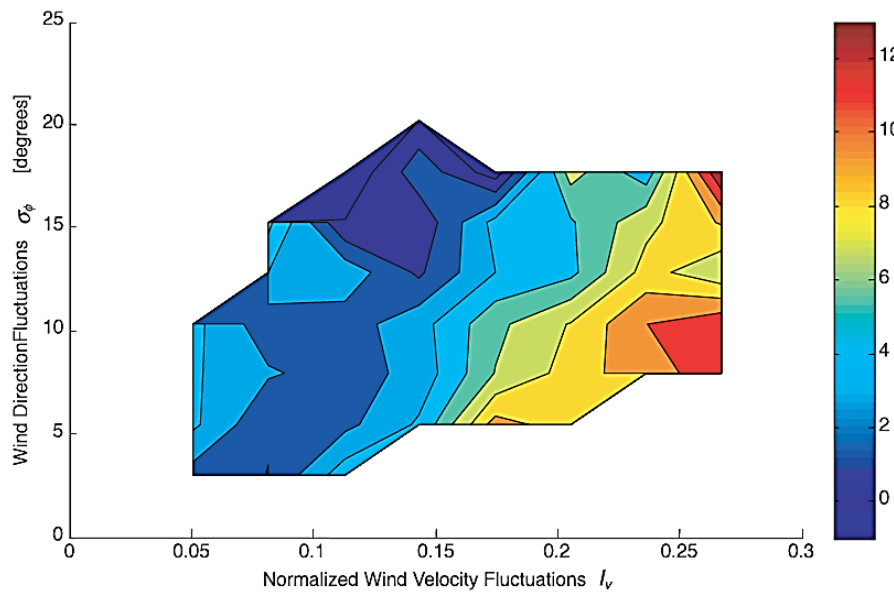


Figure 2.4 Contour plot of the percentage power reduction due to the effects of wind direction fluctuations (σ_ϕ) and the normalized velocity fluctuations (I_v) on the aerodynamic performance of the VAWT [47]

It is been noted that, for low velocity fluctuations with normalized velocity fluctuation below 0.15, the turbine performance shows minimal reduction. However, at high velocity fluctuations with Normalized velocity fluctuations above 0.15, the performance decreases with a roughly linear relationship with increasing normalized velocity fluctuations.

Hara et al. [48] conducted experimental and numerical investigations on the changes in the rotational speed of a small VAWT in pulsating wind, by varying the wind frequency and amplitude parameters. The experimental results suggest a relation between the rotational speed width and pulsating wind amplitude showing that the rate of change in the rotational speed divided by the wind cycle was inversely proportional to the moment of inertia and was independent of the wind cycle. Moreover, the energy efficiency of the VAWT in a pulsating wind with constant amplitude stayed almost constant under both changes in the moment of inertia and in the wind cycle, indicating the independence of energy efficiency of VAWT on the change of rotor moment of inertia and the wind fluctuation frequency

However, the energy efficiency of VAWT decreased with large wind amplitude. The numerical simulation of larger size VWAT showed similar trend for the effect of moment of inertia and wind cycle under constant load torque. Conversely, a long wind cycle and small moment of inertia may affect the energy efficiency depending on the torque curve.

Scheurich et al.[49] implemented the Vorticity Transport Model (VTM) to investigate the aerodynamic performance and wake dynamics, both in steady and unsteady wind conditions, of three different (with straight, curved and helically twisted blade) vertical-axis wind turbines.

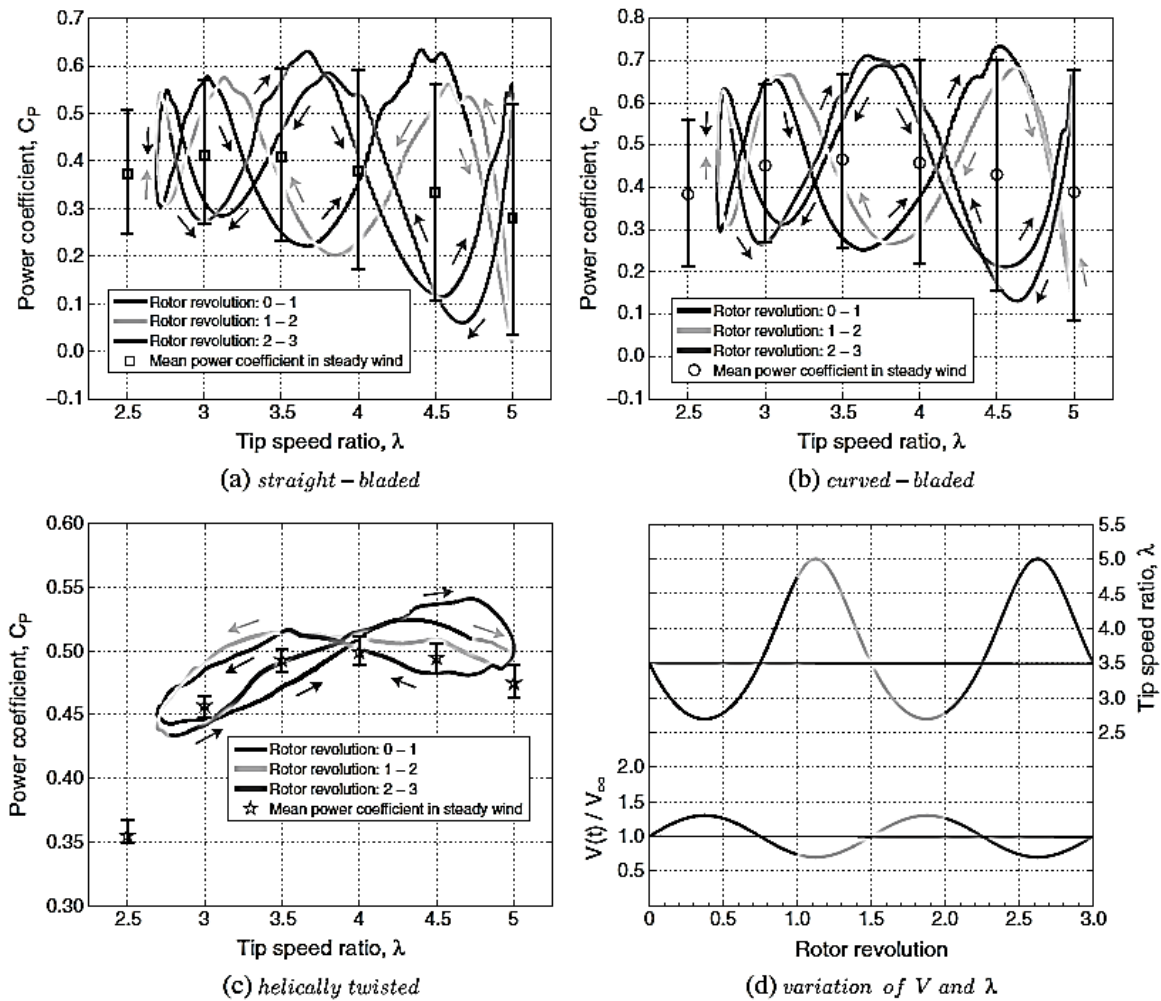


Figure 2.5 VTM-predicted variation of the power coefficients for the straight-bladed and curved-bladed and the helically twisted blades turbines when the rotors are operated in unsteady wind conditions with $\Delta V/V_\infty = \pm 0.3$ and $R_g = 1.5$ (which corresponds to $k_g = 0.74$ at $\lambda = 3.5$). Error bars denote the variation of the power coefficient during one rotor revolution in steady wind conditions [16]

Figure 2.5 depicts the variation of the power coefficient of each rotor operating in an unsteady wind conditions with R_g (number of rotor revolutions per gust) = 1:5 and for (the

sinusoidal variation of the free stream velocity) $\Delta V/V_\infty = \pm 0.3$ along with the variation of the wind speed. In figure 2.5 the power coefficients behaviour under unsteady wind conditions is characterised by a hysteresis loop, indicated by the arrows, along with the three dominant peaks per rotor revolution that characterise the variation of the power coefficients in unsteady wind conditions. The amplitude of the variation of the power coefficient produced by the helically twisted configuration in unsteady wind conditions is much smaller, than that produced by either the straight-bladed or the curved-bladed turbines. In addition, the power coefficient vs tip speed ratio graph for the straight-bladed and curved-bladed turbines exhibits a steeper gradient in mid-operating range than the turbine with helically twisted blades, referring; the turbines with non-twisted blades are less efficient than the turbine with helically twisted blades at constant rotational speed in unsteady wind conditions.

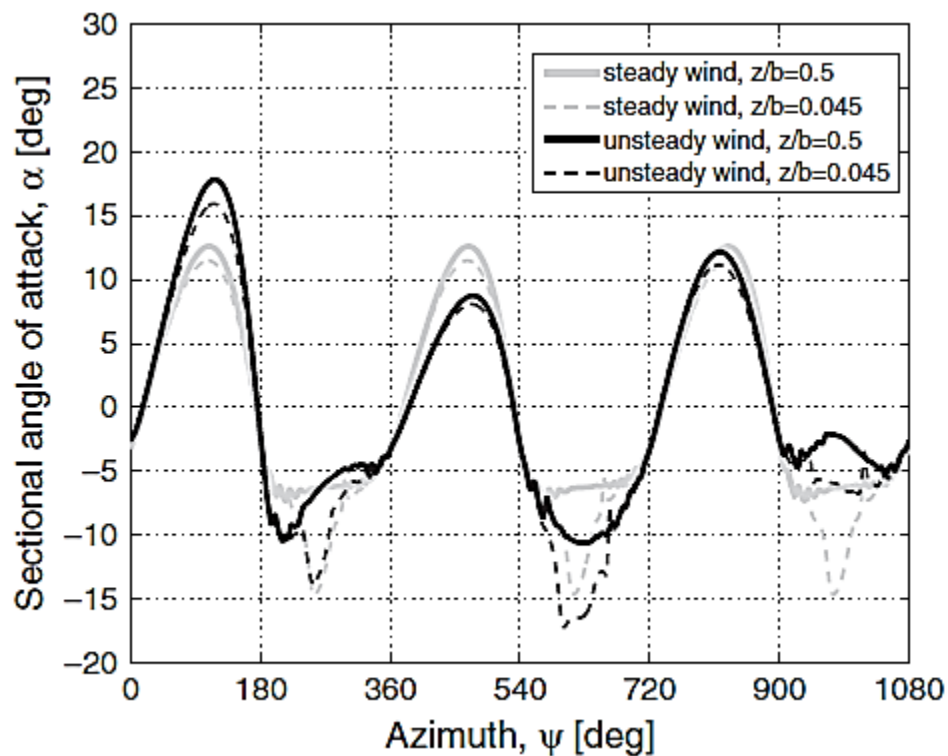


Figure 2. 6 VTM-predicted aerodynamic angle of attack and sectional forces in steady and unsteady wind conditions [16]

It has been observed from this analysis that the instantaneous tip speed ratio of a rotor changes according to the varying free stream velocity and deviates from the tip speed ratio at which the highest aerodynamic efficiency is obtained. The associated power loss becomes significant only when the amplitude of the oscillations in wind speed is high. In steady wind condition, the power coefficients developed by the straight-bladed and curved-bladed turbines varies considerably within one rotor revolution due to the continuous variation of the angle of attack on the blades and hence induce unsteadiness in the blade aerodynamic loading..

Scheurich et al. [50] simulated two straight blades using Brown's Vorticity Transport Model to study the aerodynamic performance and wake dynamics of a Darrieus-type vertical-axis wind turbine. The findings of the simulation showed good agreement with experimental measurements. The Vorticity Transport model (VTM) was able to capture the emergence of strong three-dimensional effects in the flow near the rotor that are mediated by the dynamics of the vorticity due to the blade-vortex interactions on the rotor that is shed and trailed into the wake behind the turbine.

Danao et al. [51] conducted CFD simulations on a micro scale VAWT operating at a constant rotating speed under steady and unsteady wind inflow condition to analyse VAWT performance under unsteady wind condition and to define the principles behind the performance phenomenon. A wide range of incoming unsteady wind frequency (1.16 Hz, 2.91 Hz and 11.6 Hz) were used for this purpose, where, the maximum frequency (11.6 Hz) was equal to the VAWT rotational frequency. The findings show that the VAWT performance reduces in unsteady incoming wind conditions compared to steady wind condition. The worst condition had 75% power coefficient drop compared to the steady condition.

Further investigation on 2.91 Hz fluctuation rate depicts a large hysteresis in the unsteady C_p of the VAWT within one wind cycle. Danao et al. [52] experimentally measured the wind turbine performance at a wind speed of 7 m/s with 7% and 12% fluctuations in wind velocity at a frequency of 0.5 Hz. The results show the unsteady power coefficient (C_p) fluctuates following the changes in wind speed. The time average of the unsteady C_p with a 7% fluctuation in wind velocity showed a good agreement to that with steady wind conditions. However, with 12% fluctuations in wind speed the time average of the unsteady C_p deviates from the steady wind condition with a drop in the mean C_p . This phenomenon refers that, unsteady winds of such amplitudes are detrimental to the energy yields from these wind turbines. In addition, there were no significant hysteresis observed at mean tip speed ratios (λ) beyond peak C_p , for both 7% and 12% fluctuations, whereas, for mean λ below peak C_p showed substantial hysteresis.

Numerical investigation by Danao et al. [52] aimed to study the effects of steady and unsteady wind on the performance of a wind tunnel scale VAWT. Authors found that when VAWT operates in periodically fluctuating wind conditions, there will be slight improvement of overall performance under certain operating condition. One of them is the mean tip speed ratio should be just above the λ of the steady performance maximum. Operating VAWT at a mean λ that is lower than λ for peak performance coefficient will cause the VAWT to run in the λ band with deep stall and vortex shedding and hence lead to the VAWT performance coefficient reduction. Other conditions to achieve better overall performance from VAWT under unsteady conditions are that, the amplitude of fluctuation is small (<10%), and the frequency of fluctuation is high (>1 Hz). Operation at Large

fluctuations in wind speed causes the VAWT to run in λ conditions that are drag dominated, thus reducing the performance of the wind turbine. Within realistic conditions, higher frequencies of fluctuation marginally improve the performance of the VAWT.

2.4. Research Objectives

Based on the research aims presented in the previous chapter it can be seen that although a number of investigations have been carried out on fluctuating wind velocities, there is limited information available regarding the effects of sustained acceleration and deceleration in wind velocity on the performance characteristics of the vertical axis wind turbines. Keeping this in view, the following objectives have been formulated which will address the gaps in the existing knowledge:

1. Investigation of the flow parameters and evaluation of performance characteristics of the VAWT operating under steady flow conditions.
2. Analyzing the effects of Tip Speed Ratio on the performance characteristics of the VAWT under steady flow conditions
3. Development of novel semi-empirical torque coefficient and power coefficient prediction tools accounting a range of varying flow conditions for the VAWT.
4. Investigation of the flow parameters and evaluation of performance characteristics of the VAWT operating under unsteady flow conditions with accelerating and decelerating wind velocities at a constant rotational speed
5. Investigation of the flow parameters and evaluation of performance characteristics of the VAWT operating under unsteady flow conditions with accelerating and decelerating wind velocities under variable rotational speeds

CHAPTER 3

NUMERICAL MODELLING OF VERTICAL AXIS WIND TURBINE

Based on the research objectives of this study that have been identified in the previous chapter, advanced CFD techniques have been used to computationally simulate the transient flow of air in the vicinity of a Savonius type VAWT. Sliding mesh technique has been used in order to rotate the rotor blades of the VAWT with respect to the stator blades. For this purpose, appropriate solver settings and boundary conditions need to be specified, that are discussed in this chapter.

3.1. Introduction to Computational Fluid Dynamics

Computational Fluid Dynamics or CFD is the analysis of systems involving fluid flow, heat transfer and associated phenomena such as chemical reactions by means of computer-based simulation. The technique is very powerful and spans a wide range of industrial and non – industrial application areas. From the 1960s onwards, the aerospace industry has integrated CFD techniques into the design, R&D and manufacture of aircraft and jet engines. More recently, the method has been applied to the design of internal combustion engines, combustion chambers of gas turbines and furnaces. Furthermore, motor vehicle manufacturers now routinely predict drag forces, under – bonnet air flows and the in – car environment with CFD. CFD is becoming a vital component in the design of industrial products and processes.

The variable cost of an experiment, in terms of facility hire and/or person – hour costs, is proportional to the number of data points and the number of configurations tested. In contrast, CFD codes can produce extremely large volumes of results at no added expense, and it is very cheap to perform parametric studies, for instance, to optimise equipment performance.

3.2. Working of CFD Codes

There are three distinct streams of numerical solution techniques. They are finite difference, finite element and spectral methods. Finite volume method, a special finite difference formulation, is central to the most well established CFD codes. The numerical algorithms include integration of the governing equations of fluid flow over all the control volumes of the domain, discretisation or conversion of the resulting integral equations into a system of algebraic equations and the solution of these equations by an iterative method.

CFD codes are structured around the numerical algorithms that can tackle fluid flow problems. In order to provide easy access to their solving power, all commercial CFD packages include sophisticated user interfaces to input problem parameters and to examine the results. Hence, all codes contain three main elements. These are:

- Pre – Processor
- Solver Execution
- Post – Processor

Pre – processing consists of the input of the flow problem to a CFD programme by means of an operator – friendly interface and the subsequent transformation of this input into a form suitable for use by the solver. The user activities at the pre – processing stage includes definition of the geometry of the region of interest. It is called the computational domain. Grid generation is the sub – division of the domain into a number of smaller, non –

overlapping sub – domains. It is also called Mesh. Selection of the physical or chemical phenomena that needs to be modelled, definition of fluid properties and the specification of appropriate boundary conditions at cells, which coincide with or touch the domain boundary, are also included in pre – processing [53].

The solver primarily consists of setting up the numerical model and the computation/monitoring of the solution. The setting up of the numerical model includes the following:

- Selection of appropriate physical models. These included turbulence, combustion, multiphase etc.
- Defining material properties like the fluid, solid, mixture etc.
- Prescribing operating conditions
- Prescribing boundary conditions
- Prescribing solver settings
- Prescribing initial solution
- Setting up convergence monitors

The computation of the solution includes:

- The discretised conservation equations are solved iteratively. A number of iterations are required to reach a converged solution.
- Convergence is reached when change in solution variables from one iteration to the next is negligible. Residuals provide a mechanism to help monitor this trend.
- The accuracy of the converged solution is dependent upon problem setup, grid resolution, grid independence, appropriateness and accuracy of the physical model.

Figure 3.1 describes the working of the solver.

Post processing comprises the examination of the results obtained and revision of the model based on these results. These can be further elaborated into:

- Examine the results to view solution and extract useful data.
- Visualization tools can be used to extract the overall flow pattern, separation, shocks, shear layers etc.
- Numerical reporting tools are used to calculate quantitative results like forces, moments, and average heat transfer coefficient, flux balances, surface and volume integrated quantities.
- Are physical models appropriate?

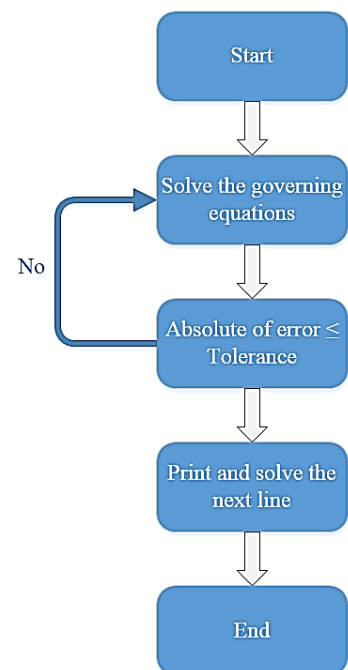


Figure 3.1 CFD Solver

- Are boundary conditions correct?
- Is the grid adequate?
- Can grid be adapted to improve results?
- Does boundary resolution need to be improved?
- Is the computational domain large enough?

Due to the increased popularity of engineering workstations, many of which have outstanding graphic capabilities, the leading CFD packages are now equipped with versatile data visualisation tools. These include domain geometry, grid display, vector plots, line and shaded contour plots, 2D and 3D surface plots, particle tracking, view manipulations, colour post – script output etc. more recently these facilities may also include animation for dynamic result display, and in addition to graphics, all codes produce trustworthy alphanumeric output and have data export facilities for further manipulation external to the codes. As in many other branches of CAE, the graphics output capabilities of CFD codes have revolutionised the communication of ideas to the non – specialists. An overview of CFD modelling is presented in figure 3.2.

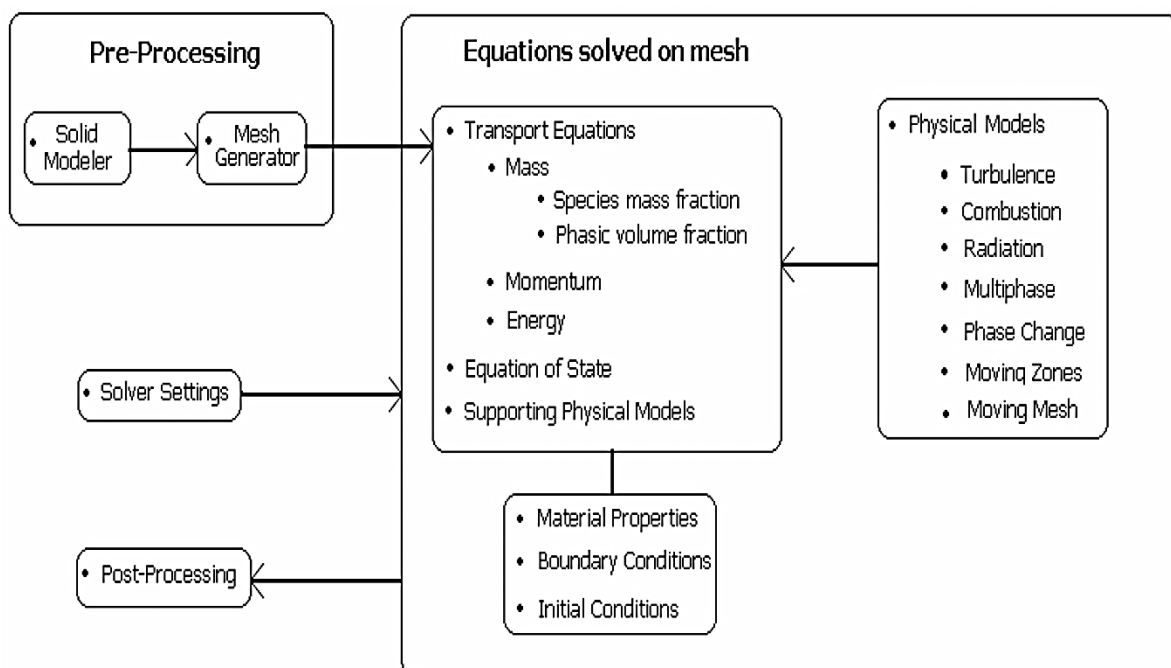


Figure 3.2 Overview of CFD Modelling [54]

3.3. Numerical Formulation of the Fluid Flow

The governing equation of fluid flow represents mathematical statements of the conservation laws of Physics:

- The mass of a fluid is conserved.

- The rate of change of momentum equals the sum of the forces on a fluid particle. (Newton's second law)
- The rate of change of energy is equal to the sum of the rate of heat addition to and the rate of work done on a fluid particle. (First law of thermodynamics)

The fluid is regarded as a continuum. For the flow diagnostics at macroscopic length scales, the molecular structure of matter and molecular motions may be ignored. The behaviour of the fluid is described in terms of macroscopic properties such as velocity, pressure, density and temperature etc. These are averages over suitably large numbers of molecules. A fluid particle or point in a fluid is then the smallest possible element of fluid whose macroscopic properties are not influenced by individual molecules.

3.3.1. Conservation of Mass

The mass balance equation for the fluid element can be written as [55]:

$$\text{Rate of increase of mass in fluid element} = \text{Net rate of flow of mass into fluid element} \quad (3.1)$$

For liquids, as the density is constant, the mass conservation equation is:

$$\text{Div } V = 0 \quad (3.2)$$

This equation describes the net flow of mass out of the element across its boundaries. The above equation in longhand notation can be written as:

$$\frac{\partial u}{\partial x} + \frac{\partial v}{\partial y} + \frac{\partial w}{\partial z} = 0 \quad (3.3)$$

This equation represents the steady, three dimensional mass conservation of the fluid or continuity at a point in an incompressible fluid.

3.3.2. Conservation of Momentum

Newton's second law states that the rate of change of momentum of a fluid particle equals the sum of the forces on the particle [56]:

$$\text{Rate of increase of momentum of the fluid element} = \text{Sum of forces acting on the fluid particle} \quad (3.4)$$

There are two types of forces on fluid particles. These are surface forces and the body forces. Surface forces include pressure, viscous and gravity forces while body forces include centrifugal, coriolis and electromagnetic forces. It is a common practice to highlight the

contributions due to the surface forces as separate terms in the momentum equations and to include the effects of body forces as source terms.

The x – component of the momentum equation is found by setting the rate of change of x – momentum of the fluid particle equal to the total force in the x – direction on the element due to surface stresses, plus the rate of increase of x – momentum due to sources. The equation is as follows:

$$\rho f_x + \frac{\partial \sigma_{xx}}{\partial x} + \frac{\partial \tau_{yx}}{\partial y} + \frac{\partial \tau_{zx}}{\partial z} = \rho \left(\frac{\partial u}{\partial t} + u \frac{\partial u}{\partial x} + v \frac{\partial u}{\partial y} + w \frac{\partial u}{\partial z} \right) \quad (3.5)$$

The y and z – component of momentum equation are given by:

$$\rho f_y + \frac{\partial \tau_{xy}}{\partial x} + \frac{\partial \sigma_{yy}}{\partial y} + \frac{\partial \tau_{zy}}{\partial z} = \rho \left(\frac{\partial v}{\partial t} + u \frac{\partial v}{\partial x} + v \frac{\partial v}{\partial y} + w \frac{\partial v}{\partial z} \right) \quad (3.6)$$

$$\rho f_z + \frac{\partial \tau_{xz}}{\partial x} + \frac{\partial \tau_{yz}}{\partial y} + \frac{\partial \sigma_{zz}}{\partial z} = \rho \left(\frac{\partial w}{\partial t} + u \frac{\partial w}{\partial x} + v \frac{\partial w}{\partial y} + w \frac{\partial w}{\partial z} \right) \quad (3.7)$$

3.3.3. Navier – Stokes Equation

In a Newtonian fluid, the viscous stresses are proportional to the rates of deformation. Liquids are incompressible; the viscous stresses are twice the local rate of linear deformation times the dynamic viscosity. The Navier – Stokes equations are [57]:

$$\rho g_x - \frac{\partial p}{\partial x} + \mu \left(\frac{\partial^2 u}{\partial x^2} + \frac{\partial^2 u}{\partial y^2} + \frac{\partial^2 u}{\partial z^2} \right) = \rho \left(\frac{\partial u}{\partial t} + u \frac{\partial u}{\partial x} + v \frac{\partial u}{\partial y} + w \frac{\partial u}{\partial z} \right) \quad (3.8)$$

$$\rho g_y - \frac{\partial p}{\partial y} + \mu \left(\frac{\partial^2 v}{\partial x^2} + \frac{\partial^2 v}{\partial y^2} + \frac{\partial^2 v}{\partial z^2} \right) = \rho \left(\frac{\partial v}{\partial t} + u \frac{\partial v}{\partial x} + v \frac{\partial v}{\partial y} + w \frac{\partial v}{\partial z} \right) \quad (3.9)$$

$$\rho g_z - \frac{\partial p}{\partial z} + \mu \left(\frac{\partial^2 w}{\partial x^2} + \frac{\partial^2 w}{\partial y^2} + \frac{\partial^2 w}{\partial z^2} \right) = \rho \left(\frac{\partial w}{\partial t} + u \frac{\partial w}{\partial x} + v \frac{\partial w}{\partial y} + w \frac{\partial w}{\partial z} \right) \quad (3.10)$$

3.4. Pre-Processing

Further details about computational fluid dynamics and difference turbulence models can be found in any good CFD book. For reader's interest, some books regarding CFD are recommended here [58-63]. The following sections provide details of the numerical modelling that has been used in the present study. The CFD package that has been used to achieve this is known as Ansys [64]. The pre-processing in CFD is subdivided into two main categories, i.e. creation of the geometry and the meshing of the flow domain. This section provides details of the geometric modelling of the vertical axis wind turbine and meshing of the flow domain.

3.4.1. Geometry of VAWT

A three dimensional vertical axis wind turbine model, similar to Colley [33], has been numerically created as shown in figure 3.3. The model has 12 rotor blades and 12 stator blades. The radius of the core region $r_c=0.5\text{m}$ whereas the radii of the rotor and the stator regions i.e. r_r and r_s are 0.7m and 1m respectively. The height of the VAWT, $h=1\text{m}$.

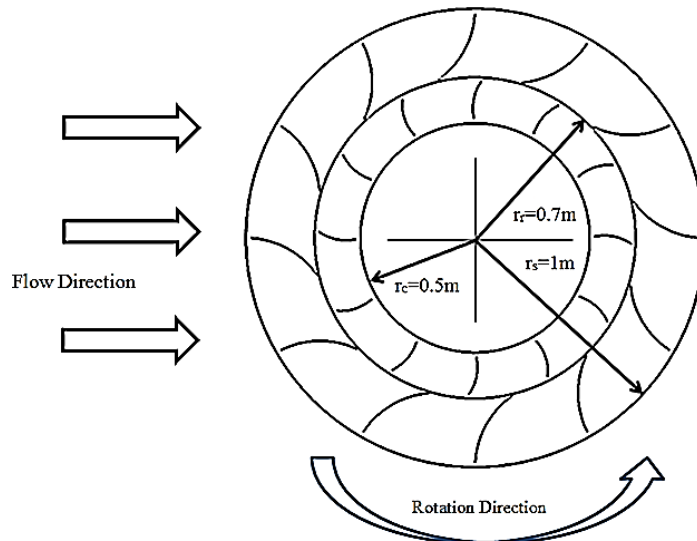


Figure 3.3 Geometry of the VAWT

Figure 3.4 shows the flow domain of the VAWT. The length, width and the height of the flow domain are 13m , 9m and 3m respectively. These dimensions have been taken from Colley and have been used here because the validation of the CFD results, presented in Chapter 4, will be carried out against the published results of Colley in the next chapter.

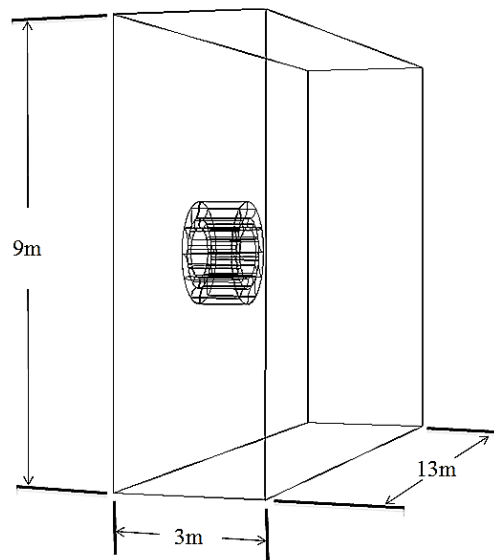
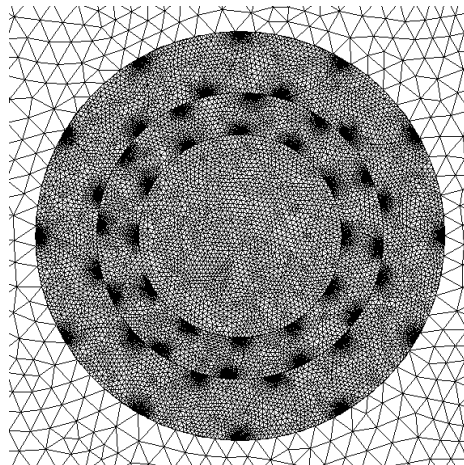


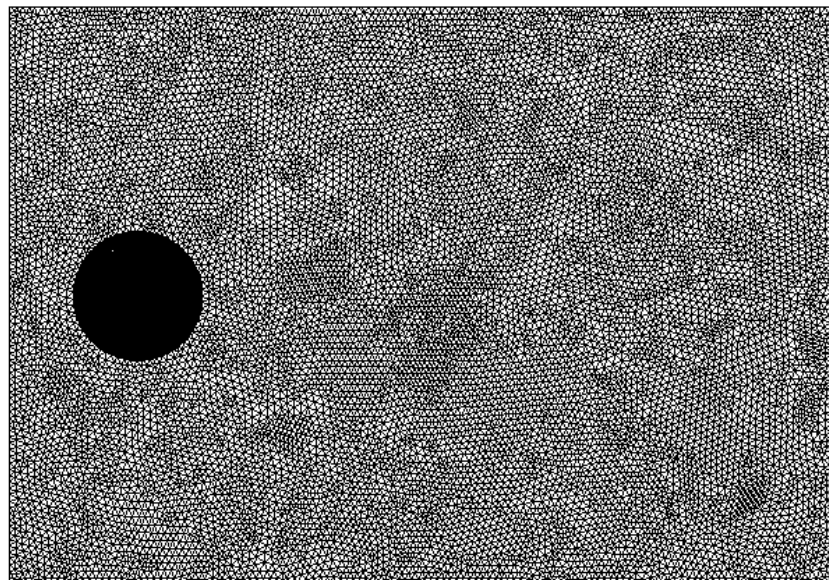
Figure 3.4 Flow Domain of the VAWT

3.4.2. Meshing of the Flow Domain

The mesh has been created in two different steps. Domain mesh has been controlled by global sizing function i.e. maximum size of 100mm and minimum size of 0.1mm. Stator, rotor and the core zones have been meshed for 30mm mesh sizing, whereas the rest of the flow domain has been meshed for 100mm mesh sizing. Figure 3.5 shows mesh in the VAWT and in the flow domain. Mesh independence testing has been carried out, and is discussed in Chapter 4.



(a)



(b)

Figure 3.5 Mesh in (a) VAWT (b) Flow Domain

3.5. Solver Execution

As the flow of air in the present study is at low speeds (4m/s) which is the annual mean wind velocity in Huddersfield (UK), pressure based solver has been chosen for the flow diagnostics of VAWT. In this solver, the density of the fluid remains constant and the primary fluid flow parameter, that is being computed iteratively, is the pressure within the flow domain.

As the interaction between the stationary (stator) and rotating (rotor) frames of references is highly transient, an unsteady solver has been designed to simulate the flow of air. In addition to the aforementioned solver settings, there is a need to model the turbulence in the flow as well. This is because the investigations carried out in the present study focuses on the turbulent flow of air. The criteria for external flows (such as VAWT) to be turbulent is that the Reynolds number of the flow should be higher than 500,000. Furthermore, in practical applications of VAWTs, the velocity of the flow normally ranges from 2m/s to 6m/s. These velocities correspond to Reynolds number of 136,917 to 410,752 for the VAWT under consideration. Hence, the flow is turbulent and a turbulence model is required to predict the parameters of turbulence in the vicinity of the VAWT with reasonable accuracy.

There are many turbulence models available in the commercial CFD package that has been used in this study. Each one of these turbulence models has got its own advantages and disadvantages, which can be found out in any CFD text book. As far as VAWTs are concerned, due to the formation of a wake region downstream the VAWT, k- ω model has been chosen for the modelling of turbulence. The primary reason behind choosing k- ω model is its superiority in accurately modelling the wake regions and extreme pressure gradients. Most recent studies also show that k- ω turbulence model predicts the changes in the flow parameters in VAWTs with reasonable accuracy.

The k- ω is a two equation model that is further divided into two types. The first type is called Standard k- ω model whereas the second type is called Shear-Stress Transport (SST) k- ω model. In the present study, SST k- ω model has been chosen because it includes the following refinements:

- The standard k- ω model and the transformed k- ϵ model are both multiplied by a blending function, and both models are added together. The blending function is designed to be one in the near-wall region, which activates the standard k- ω model, and zero away from the surface, which activates the transformed k- ϵ model.
- The definition of the turbulent viscosity is modified to account for the transport of the turbulent shear stress.

These features make the SST $k-\omega$ model more accurate and reliable for a wider class of flows (e.g., adverse pressure gradient flows, aerofoils, transonic shock waves) than the standard $k-\omega$ model. Other modifications include the addition of a cross-diffusion term in the ω equation and a blending function to ensure that the model equations behave appropriately in both the near-wall and far-field zones. Further details of SST $k-\omega$ model can be found in any turbulence modelling text book and hence have not been included here [65].

3.5.1. Boundary Conditions

The boundary types that have been specified are listed in the table 3.1. The inlet of the flow domain has been specified with velocity inlet boundary type, where the inlet flow velocity is variable. Chapter 3 is based on a constant inlet velocity of 4m/s, which is the average annual wind speed in Huddersfield, UK. However, chapter 4 is based on the transient behaviour of wind gusts, and hence both accelerating and decelerating inlet velocity conditions have been specified. The details of this are presented in section 3.8. Atmospheric conditions at pressure outlet boundary means that zero gauge static pressure has been prescribed, which again is expected in real world conditions. Furthermore, all the walls in the flow domain have been modelled as no-slip boundaries which mean that the flow does not slip on the surface of the walls. This is because, in real world, zero velocity gradient is observed between the walls and the flow layer adjacent to the wall.

Table 3.1 Boundary types and conditions

Boundary Name	Boundary Type	Boundary Condition
Inlet	Velocity Inlet	Variable
Outlet	Pressure Outlet	Atmospheric Conditions
Surrounding Sides	Stationary Walls	No-Slip
Rotor Blades	Rotating Walls	No-Slip
Stator Blades	Stationary Walls	No-Slip

As the interactions between the rotor and the stator blades are highly transient, and hence Sliding Mesh technique has been used to rotate the rotor blades corresponding to the stationary stator blades. The details of this technique are presented in the next section.

3.5.2. Sliding Mesh

When a time-accurate solution for rotor-stator interaction (rather than a time-averaged solution) is desired, sliding mesh model should be used to compute the unsteady flow field. The sliding mesh model is the most accurate method for simulating flows in multiple moving reference frames, but also the most computationally demanding. In the sliding mesh technique two or more cell zones are used. Each cell zone is bounded by at least one interface zone where it meets the opposing cell zone, as shown in figure 3.6 for VAWTs.

The interface zones of adjacent cell zones are associated with one another to form a mesh interface. The two cell zones will move relative to each other along the mesh interface. During the calculation, the cell zones slide (i.e. rotate) relative to one another along the mesh interface in discrete steps. As the rotation takes place, node alignment along the mesh interface is not required. Since the flow is inherently unsteady, a time-dependent solution procedure is required. The sliding mesh model allows adjacent meshes to slide relative to one another. In doing so, the mesh faces do not need to be aligned on the mesh interface. This situation requires a means of computing the flux across the two non-conformal interface zones of each mesh interface.

The flow domain is divided into sub-domains, each of which may be rotating and/or translating with respect to the inertial frame. The governing equations in each sub-domain are written with respect to that sub-domain's reference frame. At the boundary between two sub-domains, the diffusion and other terms in the governing equations in one sub-domain require values for the velocities in the adjacent sub-domain. The solver used in the present study enforces the continuity of the absolute velocity to provide the correct neighbour values of velocity for the sub-domain under consideration. When the relative velocity formulation is used, velocities in each sub-domain are computed relative to the motion of the sub-domain.

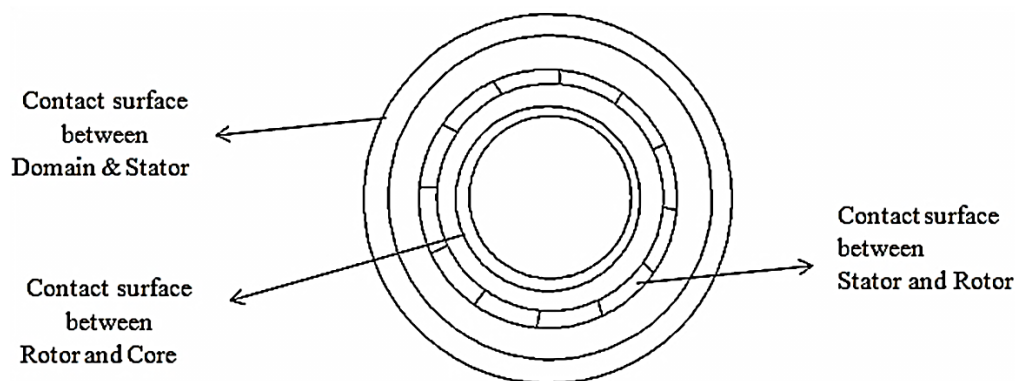


Figure 3.6 Interfaces between different zones

3.6. Solver Settings

Application based solver settings are required to accurately predict the fluid flow behaviour in the flow domain. These settings comprise:

- Pressure – Velocity Coupling
- Gradient, and
- Spatial Discretisation

The Navier-Stokes equations are solved in discretised form. This refers to the linear dependency of velocity on pressure and vice versa. Hence, a pressure – velocity is required to predict the pressure distribution in the flow domain with reasonable accuracy. In the

present study, SIMPLE algorithm for pressure – velocity coupling has been incorporated because it converges the solution faster and is often quite accurate for flows in and around simple geometries such as spheres, cylinders etc. In SIMPLE algorithm, an approximation of the velocity field is obtained by solving the momentum equation. The pressure gradient term is calculated using the pressure distribution from the previous iteration or an initial guess. The pressure equation is formulated and solved in order to obtain the new pressure distribution. Velocities are corrected and a new set of conservative fluxes is calculated [66].

Gradients are needed for constructing values of a scalar at the cell faces, for computing secondary diffusion terms and velocity derivatives. Green – Gauss Node – based gradient evaluation has been used in the present study. This scheme reconstructs exact values of a linear function at a node from surrounding cell – centred values on arbitrary unstructured meshes by solving a constrained minimization problem, preserving a second-order spatial accuracy.

The CFD solver stores discrete values of the scalars at the cell centres. However, face values are required for the convection terms and must be interpolated from the cell centre values. This is accomplished using an upwind spatial discretisation scheme. Upwinding means that the face value is derived from quantities in the cell upstream, or upwind relative to the direction of the normal velocity. In the present study, 2nd order upwind schemes have been chosen for pressure, momentum, turbulent kinetic energy and turbulent dissipation rate. The use of 2nd order upwind scheme results in increased accuracy of the results obtained.

3.7. Convergence Criteria

Getting to a converged solution is often necessary. A converged solution indicates that the solution has reached a stable state and the variations in the flow parameters, w.r.t. the iterative process of the solver, have died out. Hence, only a converged solution can be treated as one which predicts the solution of the flow problem with reasonable accuracy.

The default convergence criterion for the continuity, velocities in three dimensions and the turbulence parameters in Ansys 16 is 0.001. This means that when the change in the continuity, velocities and turbulence parameters drops down to the fourth place after decimal, the solution is treated as a converged solution. However, in many practical applications, the default criterion does not necessarily indicate that the changes in the solution parameters have died out. Hence, it is often better to monitor the convergence rather than relying on the default convergence criteria.

In the present study, torque output of the blades of the VAWT has been monitored throughout the iterative process. The solution has been considered converged once it has become statistically steady i.e. the variations in the torque output become negligibly small between two consecutive rotations of the VAWT.

After numerically simulating the flow of air in the vicinity of VAWT, various results have been gathered from CFD. Detailed discussions on these results are presented in the proceeding chapters, where the next chapter deals with the optimisation of VAWT based on blade angles.

3.8. Scope of Work

Based on the aims and objectives of this study, the scope of the work has been defined, and is presented in table 3.2. Chapter 4 corresponds to the steady flow conditions where the inlet flow velocity remains constant at 4m/s. Three different practical Tip Speed Ratios (TSR, λ) of 0.1, 0.2 and 0.4 have been considered for this purpose, with corresponding rotor blade's rotational speeds of 0.571, 1.143 and 2.286rad/s.

The first part of chapter 5 correspond to accelerating and decelerating inlet flow velocity keeping the rotational speed of the rotor blades (and hence the TSR) constant. This analysis has been carried out at $\lambda=0.2$ only as it being the most practical case in the real world, as mentioned by Colley [33], and this corresponds to the rotor blade's rotational speed of 1.143rad/s. Furthermore, the accelerating part comprises of inlet velocity change from 4m/s to 10m/s in one revolution of the VAWT, whereas the decelerating part comprises of inlet velocity change from 10m/s to 4m/s in one revolution of the VAWT.

The second part of chapter 5 deals with the cases where the rotor's rotational speed varies with the inlet flow velocity, keeping the TSR constant at 0.2. The acceleration in this section is from 4m/s to 10m/s, and deceleration from 10m/s to 4m/s in one revolution of the VAWT. The corresponding rotational speeds of the rotor blades are 1.143 to 2.857rad/s (for acceleration part) and 2.857 to 1.143rad/s (for deceleration part) respectively. Both these parts of chapter 5 together cover a wide range of practical scenarios for VAWTs operating in a variety of flow conditions.

Table 3.2 Scope of Work

Chapter	Flow Condition	λ	v (m/s)	ω (rad/s)
4	Steady	0.1	4	0.571
		0.2		1.143
		0.4		2.286
5	Transient-Accelerating	0.2	4 to 10	1.143
	Transient-Decelerating		10 to 4	
	Transient-Accelerating		4 to 10	1.143 to 2.857
	Transient-Decelerating		10 to 4	2.857 to 1.143

The next chapter presents the numerical results on the performance characteristics of the VAWT operating under a steady/constant inlet flow condition.

CHAPTER 4

PERFORMANCE ANALYSIS OF A VERTICAL AXIS WIND TURBINE OPERATING UNDER CONSTANT WIND VELOCITY

The vertical axis wind turbine design, as discussed in chapter 3, has been analysed, and its performance recorded, in this chapter. Transient analysis of the VAWT has been carried out in order to understand the complex flow phenomena in its vicinity. Detailed qualitative and quantitative analyses, making use of local flow parameters such as static gauge pressure and wind velocity magnitude, have been carried out. Furthermore, three different practical tip speed ratios have been considered in order to quantify their effect on the performance characteristics of the VAWT.

4.1. Grid Sensitivity Analysis

Grid sensitivity study has been carried out in order to establish that the CFD predictions are independent of the spatial resolution of the grid. Three different meshes of 2.5, 3.6 and 4.5 million mesh elements have been numerically generated. Table 4.1 shows the results obtained from the grid sensitivity testing, which depicts that the difference in the average torque output of the VAWT is 2.5% when the number of mesh elements increases from 2.5 and 3.6 million. Moreover, 0.56% difference in the average torque output has been recorded when mesh density increases from 3.6 to 4.5 million elements. These results indicates that the predicted flow phenomena are independent of the mesh density after 3.6 million mesh elements in the flow domain considered here, and hence this particular mesh has been chosen for further analysis.

Table 4.1 Grid sensitivity testing of the VAWT

Number of Cells (Millions)	Average Torque Output (N-m)	Difference w.r.t. 2.5 million elements (%)
2.5	7.80	N/A
3.6	8.00	2.50
4.5	7.96	0.56

4.2. Time Step Independence Testing

Time step independence testing has been carried out in order to establish that the CFD predictions are independent of the temporal discretisation of the case considered. Three different time step sizes corresponding to 1°, 2° and 3° rotation of the rotor blades have been considered in this study. Figure 4.1 depicts reduction in the variations of the instantaneous torque output of the VAWT with increase in time step size. Furthermore, table 4.2 summarises the results obtained from the time step independence testing, which depict that the difference in the average torque output of the VAWT is 3.14% when the time step size increases from 1° to 2°. Moreover, 1.88% difference in the average torque output has been observed when time step size increases from 2° to 3°. Hence, it can be concluded that the time step size of 3° is capable of predicting the fast changing flow phenomena in the vicinity of the VAWT with reasonable accuracy, and hence has been chosen for further analysis.

Table 4.2 Time step independence testing of the VAWT

Time Step Size (°)	Average Torque Output (N-m)	Difference w.r.t. 1° (%)
1	7.71	N/A
2	7.96	3.14
3	7.81	1.88

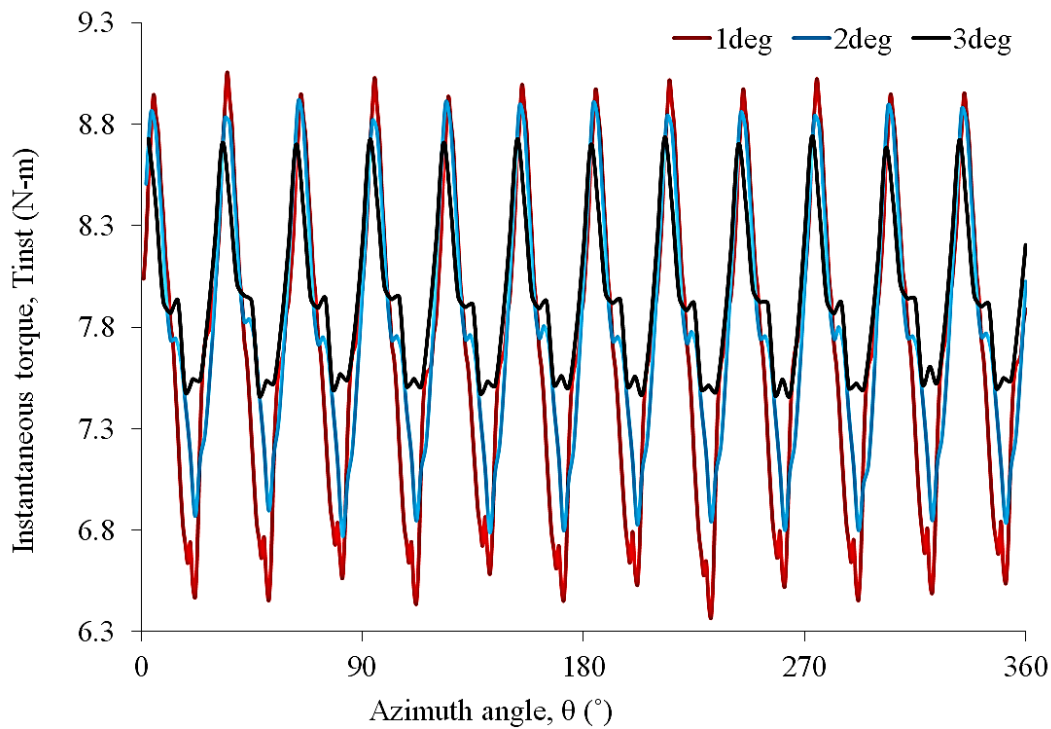


Figure 4.1 Time step independence testing of the VAWT

4.3. Verification of Numerical Results

This section provides the verification approach used to establish the accuracy of the numerical model considered in the present study. The predicted results obtained from the numerical simulations have been compared against the experimental data in order to establish that the numerical model represents the physical model of the real world. Hence, all the geometric, flow and solver-related parameters/variables become important in verification studies.

The numerical results have been verified against the experimental data recorded by Colley [33] for the average torque output of the VAWT. The dimensions of the VAWT, including blade angles, from Colley's work, have been noted to correctly model the VAWT. The dimensions of the model are presented in table 4.3:

Table 4.3 Geometric dimensions of the VAWT

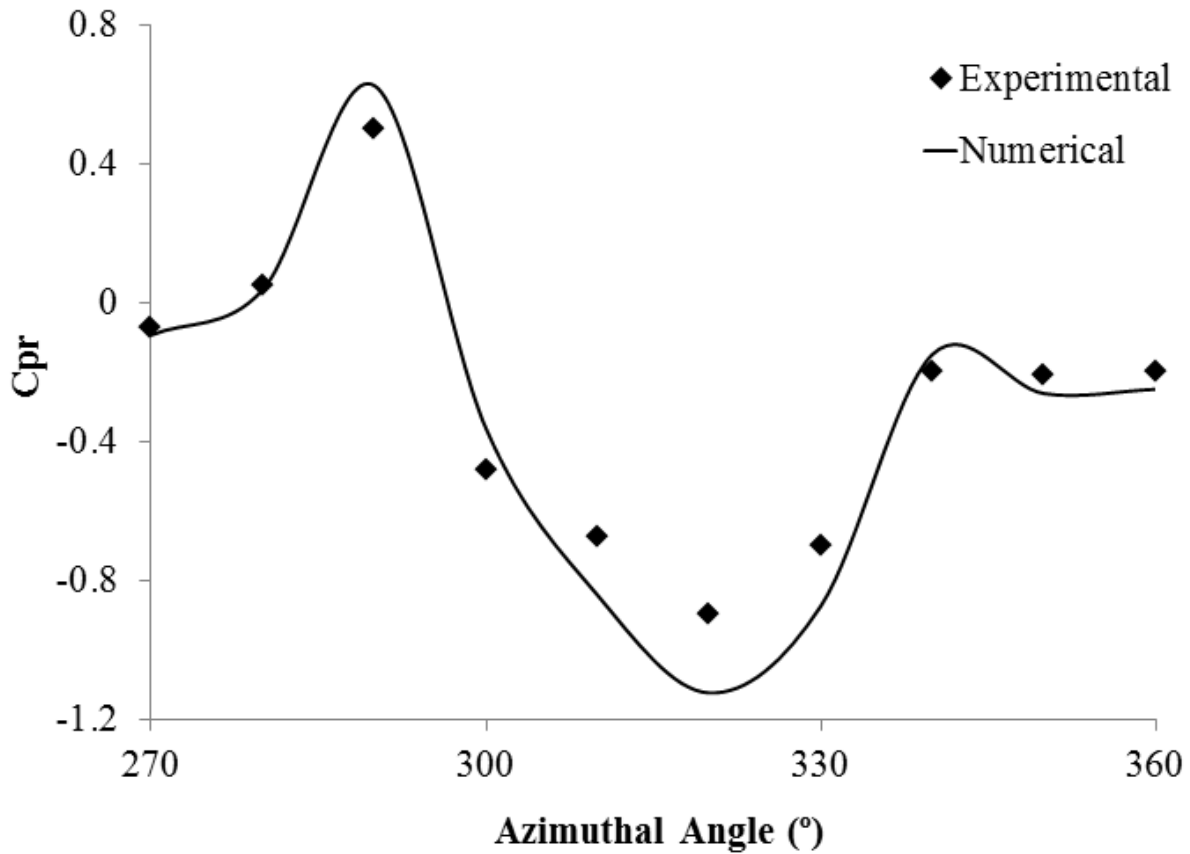
Geometric Entity	Symbol	Dimension
Height of the VAWT	h	1m
Radius of Stator	rs	1m
Radius of Rotor	rr	0.7m
Radius of Core	rc	0.5m

In the present study, the flow conditions i.e. $\lambda=0.5$ and $v=4\text{m/s}$ have been specified similar to Colley's [33] and Park's [67] studies to correctly verify the numerical results. Figure

4.2(a) depicts the variations in the pressure coefficient (C_{pr}) between angular positions of 270° and 360° of the VAWT at a radius of 1.025m, where C_{pr} is defined as follows:

$$C_{pr} = \frac{P - P_\infty}{\frac{1}{2}\rho v_\infty^2} \quad (4.1)$$

where P is the local static gauge pressure, P_∞ is the free stream static gauge pressure, ρ is the density of air and v_∞ is the free stream flow wind velocity. It can be seen in figure 4.2(a) that the numerical model considered in the present study predicts the performance characteristics of the VAWT with reasonable accuracy. The average difference between the experimental and numerical results has been calculated to be less than 10%. Furthermore, figure 4.2(b) depicts the variations in the normalised flow velocity, where the velocity has been normalised with average inlet flow velocity. It can be seen that the velocity variations predicted by the CFD model closely match with that measured experimentally.



(a)

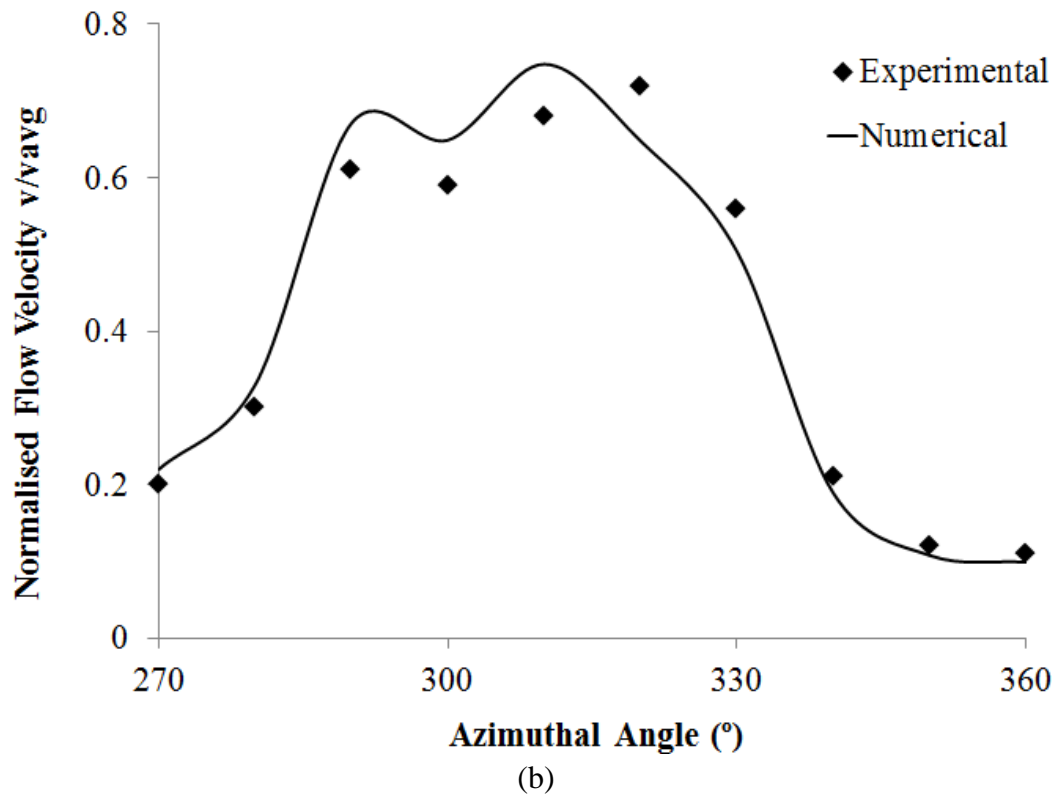


Figure 4.2 Verification of the numerical results (a) variations in pressure coefficient (b) variations in normalised flow velocity

4.4. Performance Analysis of the VAWT

The present numerical study uses the sliding mesh technique, as mentioned in chapter 3, to analyse the transient behaviour of the VAWT. In this approach, the rotor blades are rotating along their central axis; changing their position with respect to the stator blades, which act as the inlet guide vanes for the rotor blades. Therefore, VAWT's geometrical configuration varies constantly. Furthermore, as stated earlier, the VAWT consists of 12 rotor and 12 stator blades, each 30° apart, corresponding to cyclic flow behaviour after periods of 30°. Hence, the current study investigates the flow phenomenon in only one of such periods. In order to cover a wide range of investigations, four different geometrical orientations of the VAWT have been chosen for analysis, as shown in figure 4.3. Figure 4.3(a) refers to the first VAWT configuration, where both the stator and rotor blades are perfectly aligned with each other. In the second configuration, the rotor blades have moved away by 3° (or one time step) from its adjacent stator blade, as shown in figure 4.3(b). The third configuration of the VAWT represents the occasion when the rotor blade is in the middle of two stator blades (corresponding to 15° from the first configuration). Finally, the fourth configuration defines the situation when the rotor blade is approaching the next stator blade, and is 3° apart from it (corresponding to 27° from the first configuration).

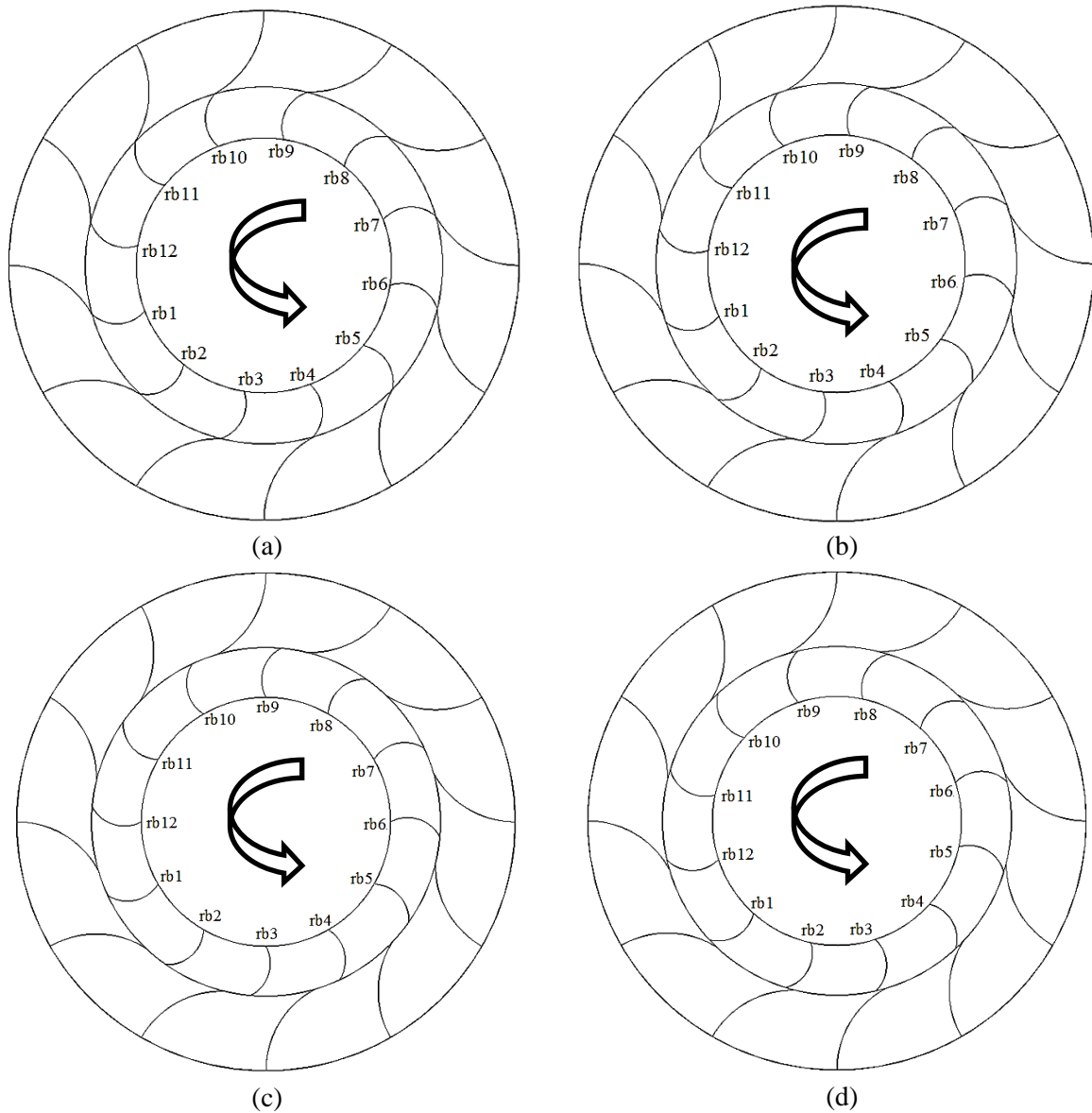


Figure 4.3 Instantaneous evaluation of the VAWT's performance at (a) 0° (b) 3° (c) 15° (d) 27°

In the present study, an effective performance analysis of the wind turbine has been conducted, whereby the following flow and performance parameters have been analysed critically:

- i. Static gauge pressure distribution in the vicinity of the VAWT at a constant wind velocity.
- ii. Flow velocity magnitude in the vicinity of the VAWT at a constant wind velocity.
- iii. Instantaneous torque coefficient of the VAWT
- iv. Instantaneous power coefficient of the VAWT

The first section hereafter comprises of the general flow field description in the vicinity of the VAWT for a given operating condition, whereas the second section deals with the effects of TSR on the performance characteristics of the VAWT.

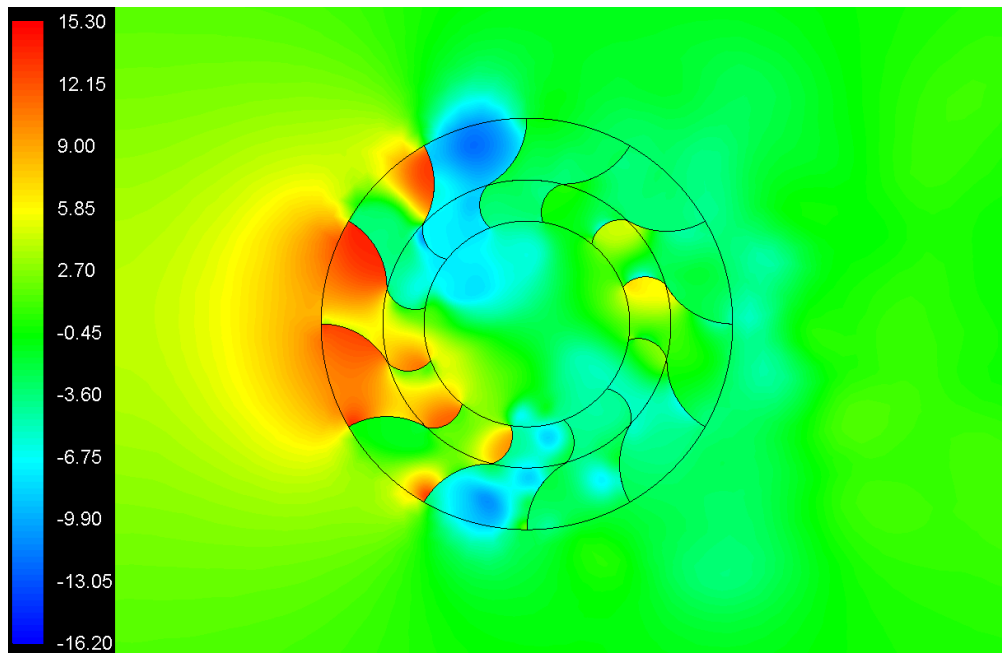
4.4.1. General Performance Characteristics of the VAWT

This section includes analysis on the local flow phenomena in the vicinity of the VAWT at four different geometrical orientations of the rotor blades discussed above. Furthermore, the performance characteristics of the VAWT have also been quantitatively analysed, at a constant wind velocity of 4m/s and a tip speed ratio of 0.1. Figure 4.4 depicts the variations of the static gauge pressure in the vicinity of the VAWT for the four different geometric configurations. The scale of the figures has been kept same throughout the analysis in order to have an effective comparison. It can be seen in figure 4.4(a) that very high pressure is pronounced either on the windward side of the VAWT or in the vicinity of the rotor blades 7 and 8 i.e. rb7 and rb8 (in figure 4.3). Similarly, low pressure regions are observed on the upper and lower side of the VAWT. The overall flow phenomena within the VAWT show similar trends for all the different geometrical configurations considered here. However, substantial local variations in the static gauge pressure have been noticed for different geometrical orientations of the rotor blades.

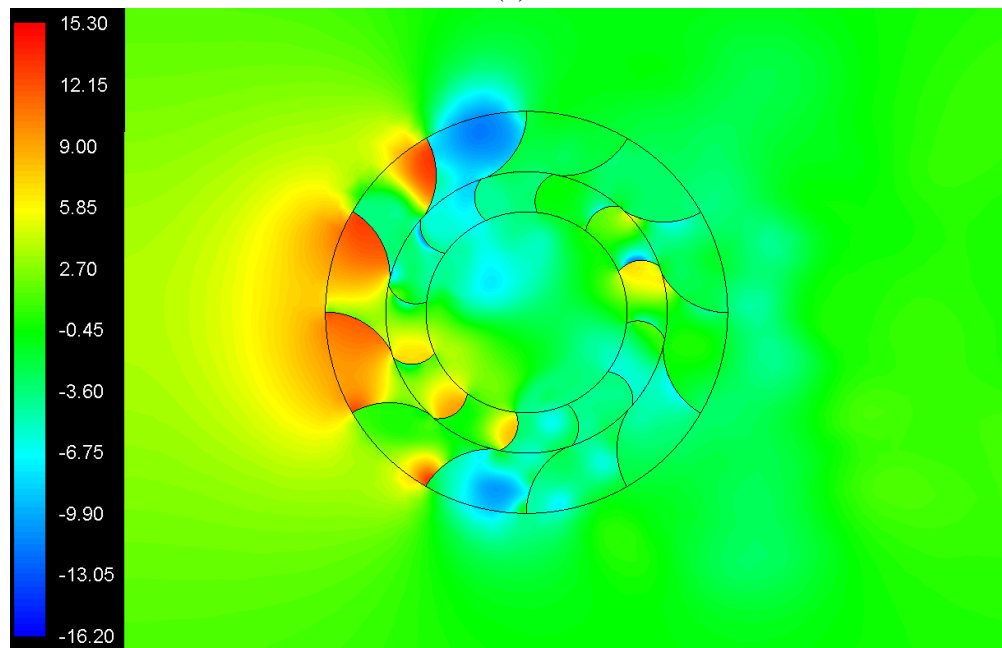
When a rotor blade crosses a stator blade (figure 4.4(b)), the windward section of the VAWT depicts lower pressure. The high pressure regions in the vicinity of the rotor blades also shrink. Hence, it is expected that the performance (torque production capability) of the VAWT reduces when there is some degree of misalignment between rotor and stator blades. When a rotor blade comes exactly in-between two stator blades, it has been noticed (in figure 4.4(c)) that more number of rotor blades exhibit higher pressure zones, whereas the low pressure zones shrink. This behaviour of the VAWT hints towards a possible increase in the performance (as compared to slight misalignment between rotor and stator blades). Possible reasons for this behaviour of the VAWT can be attributed to the fact that in this particular geometrical configuration of the VAWT, there exist two equal passages between a rotor and two stator blades, as compared to two unequal passages formed when the rotor blades are only slightly misaligned with the stator blades.

It can be further observed in next geometric configuration, figure 4.4(d), that the higher pressure regions grow significantly when the rotor blade approaches a stator blade with a small degree of misalignment between the two. This VAWT's characteristic is of great interest as it portrays different behaviour of the VAWT from figure 4.4(b), where the blade leaves the stator blade. Henceforth, the VAWT performs differently when the rotor blade either leaves the stator blade or approaches the stator blade. One of the possible reasons behind this fact is that the stator blade acts as an inlet guide vane, which directs the flow into the rotor blade to increase the power output of the VAWT. The inlet guide vane (stator blade) is concave shaped where maximum flow is introduced on the rotor blade when it is

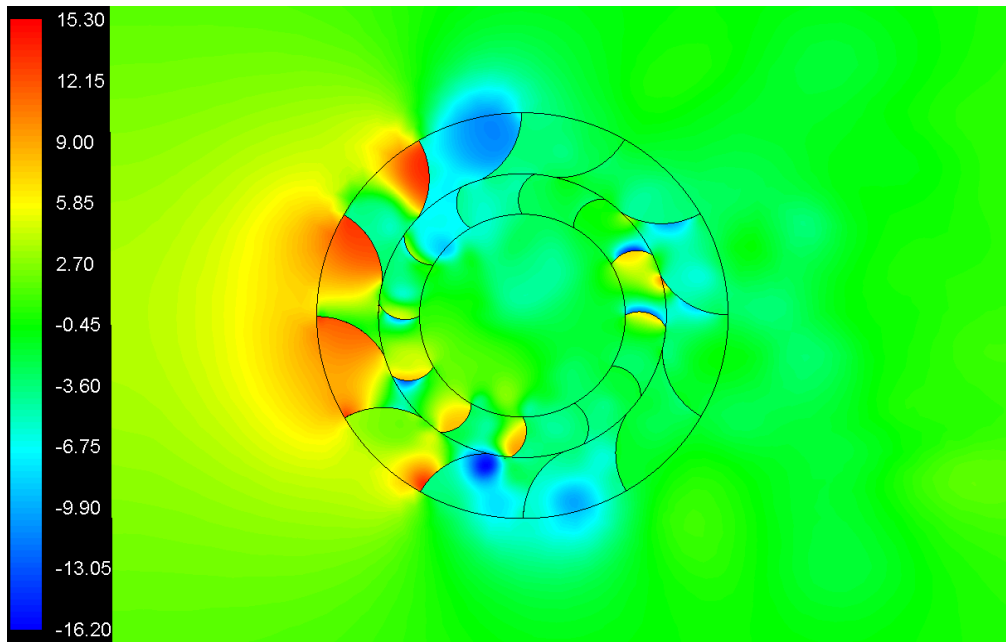
approaching the stator blade, hence maximising the power output at that instant. Therefore, the effects of a rotor blade leaving, and a rotor blade approaching a stator blade would be completely different, as observed here.



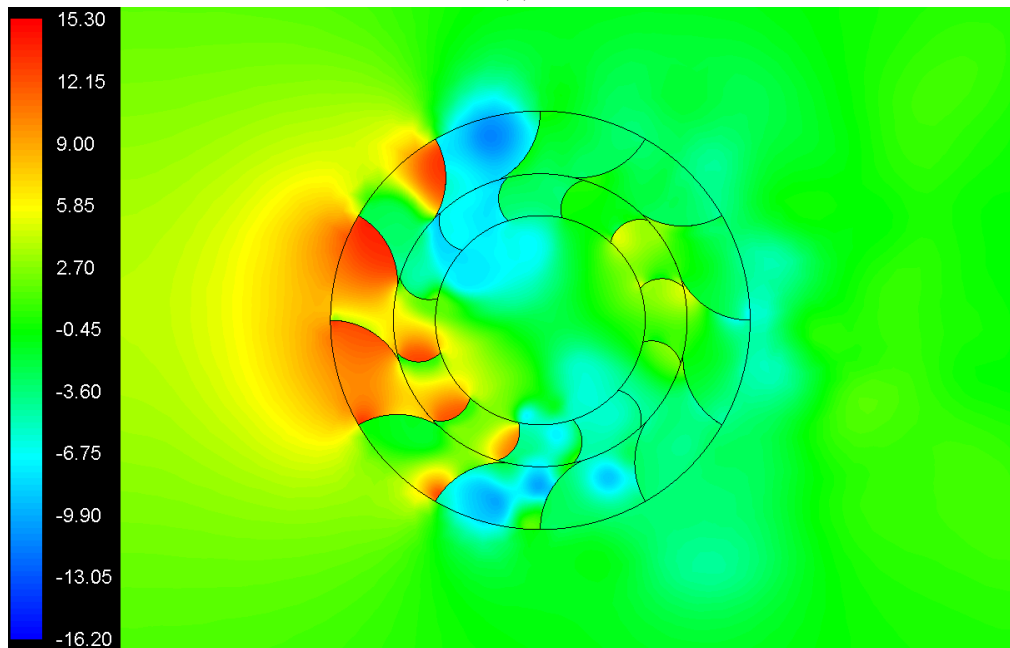
(a)



(b)



(c)



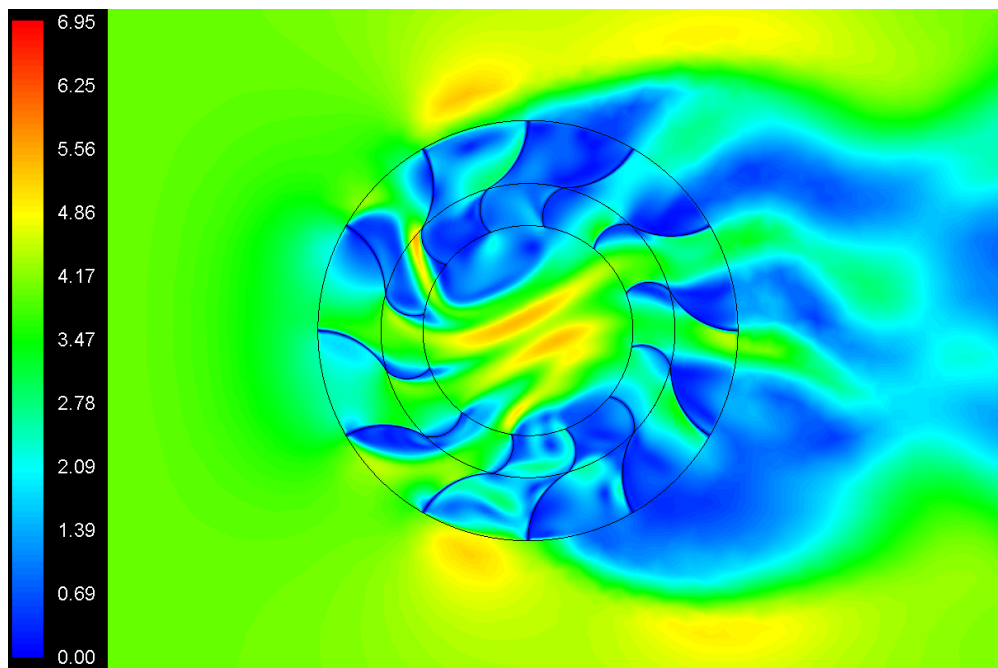
(d)

Figure 4.4 Static gauge pressure (Pa) variations in the vicinity of the VAWT at (a) 0° (b) 3° (c) 15° (d) 27°

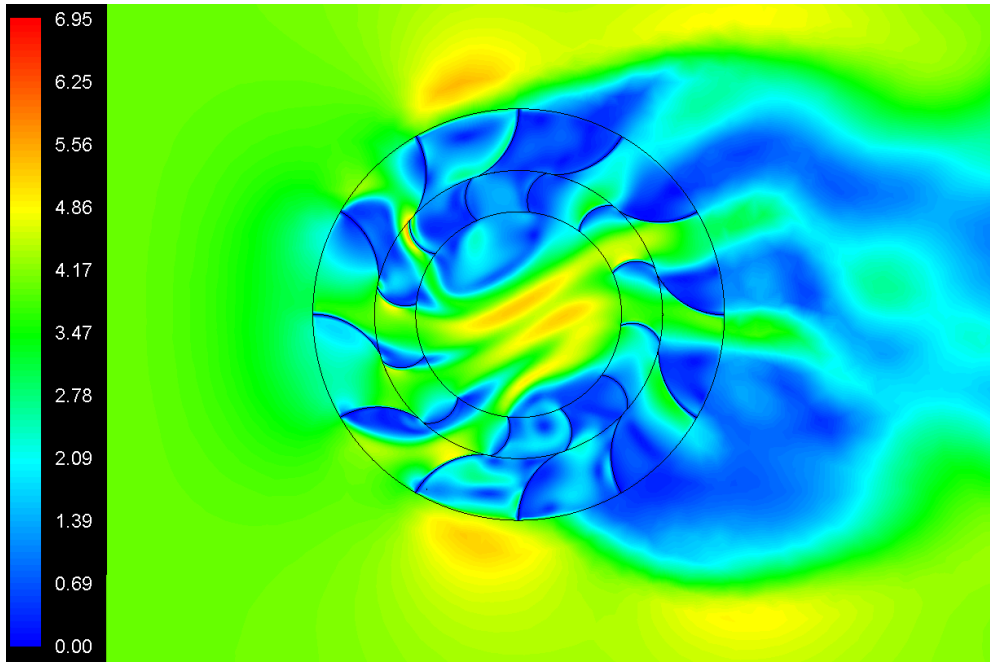
Figure 4.5 depicts the local flow variations of the velocity magnitude in the vicinity of the VAWT for four different geometric configurations. The scale of the figures has again been kept same throughout this analysis in order to compare more effectively. It can be seen from the figure 4.4(a) that although the inlet wind velocity is 4m/sec, it has increased to 6.95m/s within the wind turbine due to constant rotating speed of the rotor blades. The flow velocity is high in the passages between the stator and rotor blades and it is significantly lower in the

sections where separation is taking place (upper and lower section of the wind turbine). Furthermore, the jets are formed in the stator and rotor passages which are even pronounced in the core section of the VAWT.

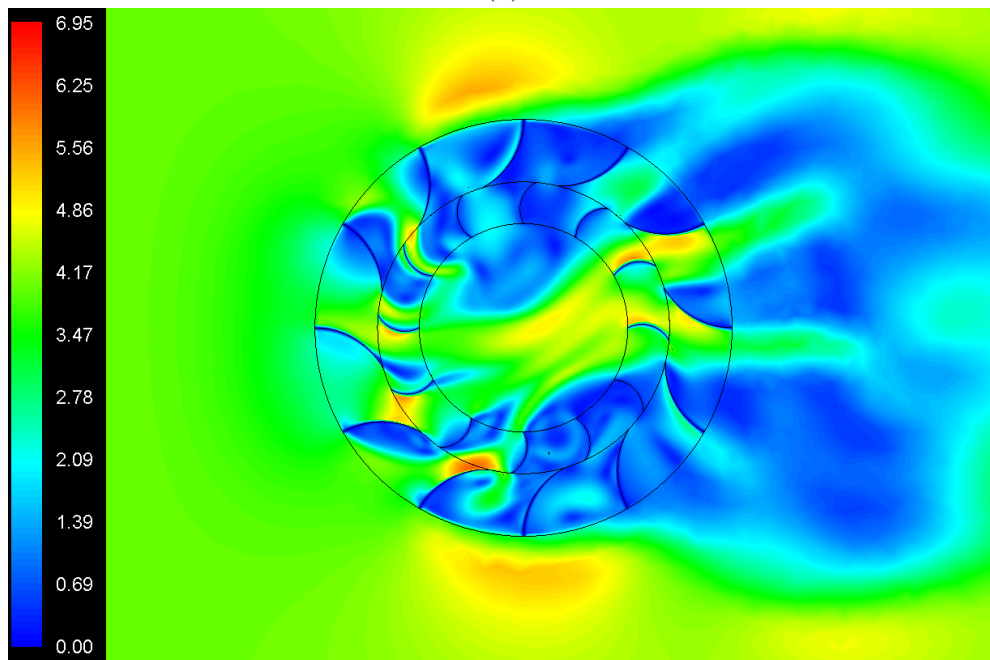
As the rotor blades cross the stator blade there is some degree of misalignment found between them, and it has been noticed (figure 4.5(b)) that more jets appear in the core section of the VAWT. This behaviour of the flow is due to the unequal passages formed between the rotor and stator blades whereby smaller passage accelerates the flow and forms jets. Moreover, with the further rotation of the rotor (figure 4.5(c)) brings the blade in the middle of the two neighbour stator blades. This causes equal passages between the rotor and stator blade whereby the flow accelerates almost equally, hence jets have been moved towards the leeward side of the VAWT from the core region. Furthermore, the figure 4.5(d) depicts the rotor blade approaching the stator blade and it can be observed that same trend of flow velocity is obtained as found in the figure 4.5(b) where the rotor blade is leaving the stator blade.



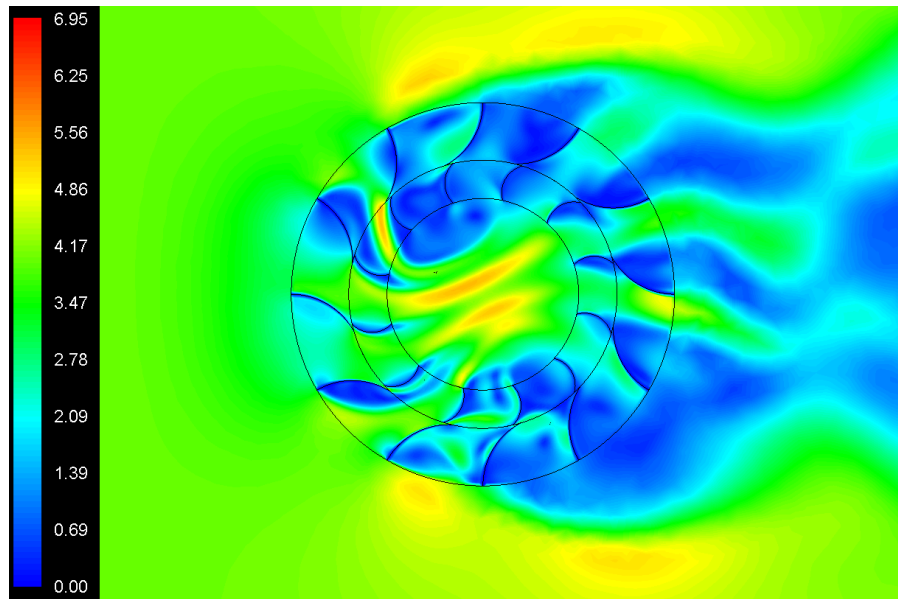
(a)



(b)



(c)



(d)

Figure 4.5 Velocity magnitude (m/s) variations in the vicinity of the VAWT at (a) 0° (b) 3° (c) 15° (d) 27°

After carrying out detailed flow feature analysis in the vicinity of the VAWT, figure 4.6 depicts the variations in the instantaneous torque coefficient generated by the VAWT in one revolution of its operation. The cyclic variations in the torque coefficient has been observed by other researchers as well [34, 35], where the total number of peaks and valleys are equal to the number of rotor blades within the VAWT. Each cyclic variation represents 30° rotation of the rotor in counter-clockwise direction. It can be seen that the highest and lowest torque coefficients recorded are 0.81 and 0.53 respectively.

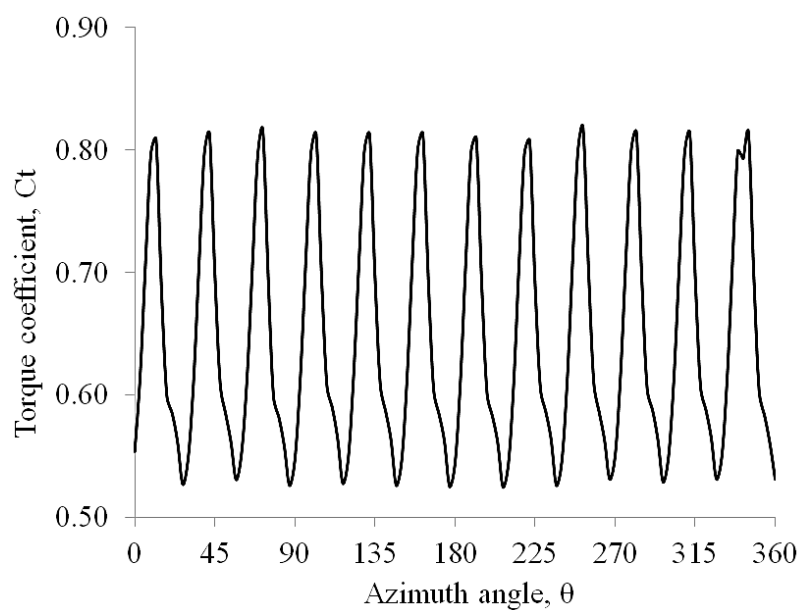


Figure 4.6 Instantaneous torque coefficient of the VAWT at $\lambda = 0.1$

Figure 4.7 depicts the instantaneous power coefficient, which is based on the instantaneous wind velocity of the wind turbine. Similar to torque coefficient, the power coefficient is also cyclic in nature, with the number of peaks and valleys equalling the number of rotor blades of the VAWT. Furthermore, it can be seen that the highest and lowest power coefficients recorded are 0.163 and 0.106 respectively.

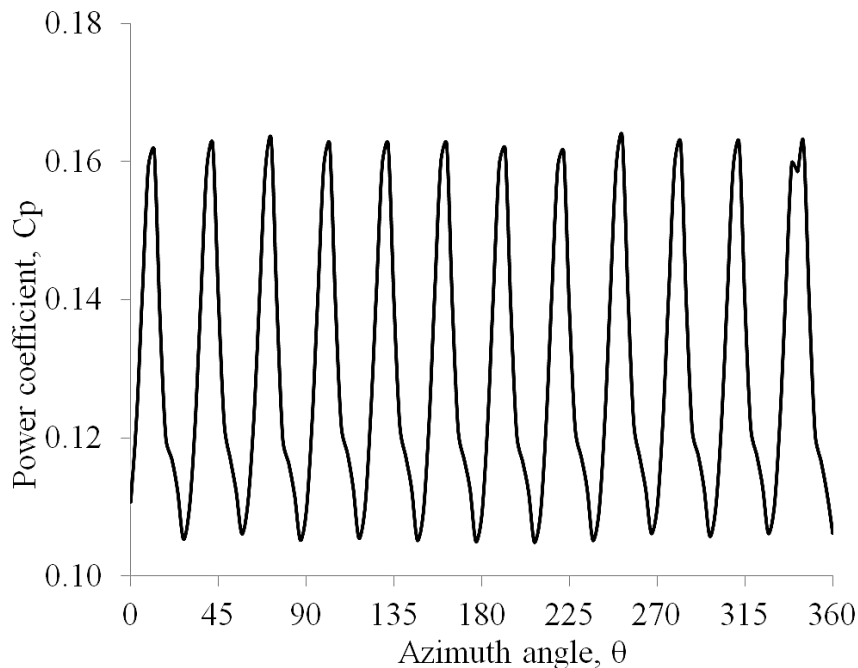


Figure 4.7 Instantaneous power coefficient of the VAWT at $\lambda = 0.1$

It has been noticed that the peaks in the torque and power coefficient's signals occur when a rotor blades is positioned perfectly in-between two stator blades (corresponding to figures 4.4(c) and 4.5(c)). Hence, this particular geometrical configuration of the VAWT has been chosen for further analysis in the next section of this chapter, which quantifies the effects of TSR on the performance characteristics of the VAWT.

4.4.2. Effect of Tip Speed Ratio on the Performance Characteristics of the VAWT

This section investigates the flow characteristics in the vicinity of the VAWT at a constant inlet wind speed of 4m/s at two different tip speed ratios of 0.2 and 0.4. The predicted results have been compared against the results at TSR of 0.1 in order to understand the effects of TSR on the performance characteristics of the VAWT. Qualitative differences in the flow related parameters have been shown in a novel way here, making use of difference contours, where difference contours show only the difference between two flow fields.

Figure 4.8 depicts the static gauge pressure based difference contour between TSRs of 0.2 and 0.1. The scale of the contour suggests that while the static gauge pressure in most of the

flow domain away from the VAWT remains the same as TSR increases from 0.1 to 0.2, there are significant local variations in it, especially at the lower and leeward sections of the VAWT. The concave sides of rb7 and rb8 show reduction in static gauge pressure, as TSR increases from 0.1 to 0.2, whereas the convex sides of these rotor blades depict significantly higher pressures (upto 17.4Pa,g higher). Hence, as TSR increases, the static gauge pressure increases on the lower and leeward sections of the VAWT.

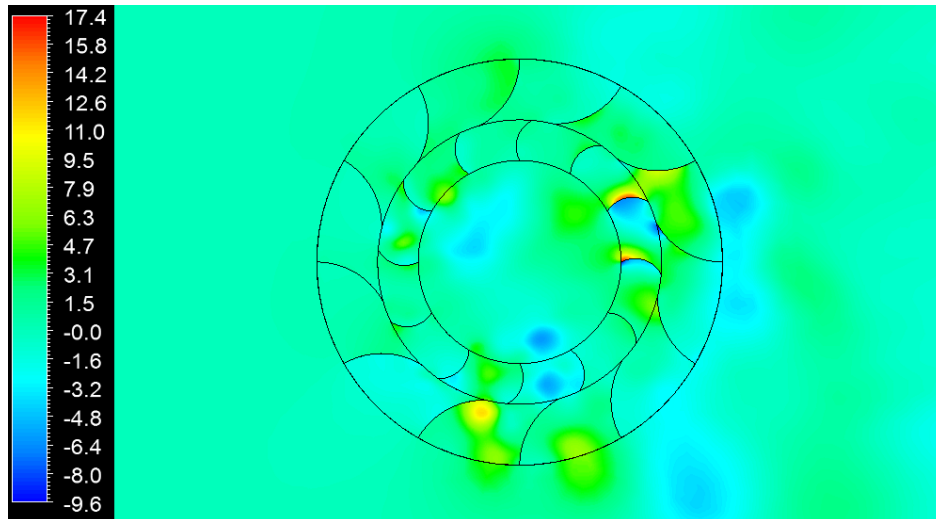


Figure 4.8 Difference contour of static gauge pressure between TSRs of 0.1 and 0.2

Similarly, figure 4.9 depicts the flow velocity magnitude based difference contour between TSRs of 0.2 and 0.1. It can be clearly seen that there are significant local variations in the flow velocity everywhere within the VAWT except in the vicinity of the windward side stator blades. The convex side of rb8 shows a flow velocity difference of upto 5m/s. The scale of the contour suggests that as TSR increases, the flow velocity magnitude in the vicinity of the VAWT also increases.

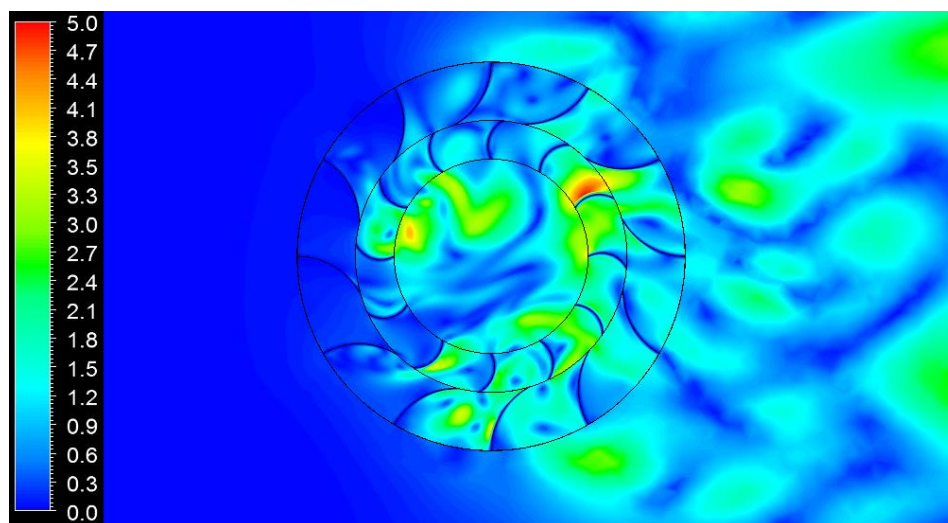


Figure 4.9 Difference contour of velocity magnitude between TSRs of 0.1 and 0.2

Figure 4.10 depicts the static gauge pressure based difference contour between TSRs of 0.4 and 0.1. In comparison with figure 4.8, it can be seen that as TSR increases further, more areas of higher static gauge pressure appear. Moreover, the convex side of rb8 depict a higher static gauge pressure of upto 14.7Pa. However, there are more areas of lower pressure as well, especially on the concave sides of rb8 and rb4.

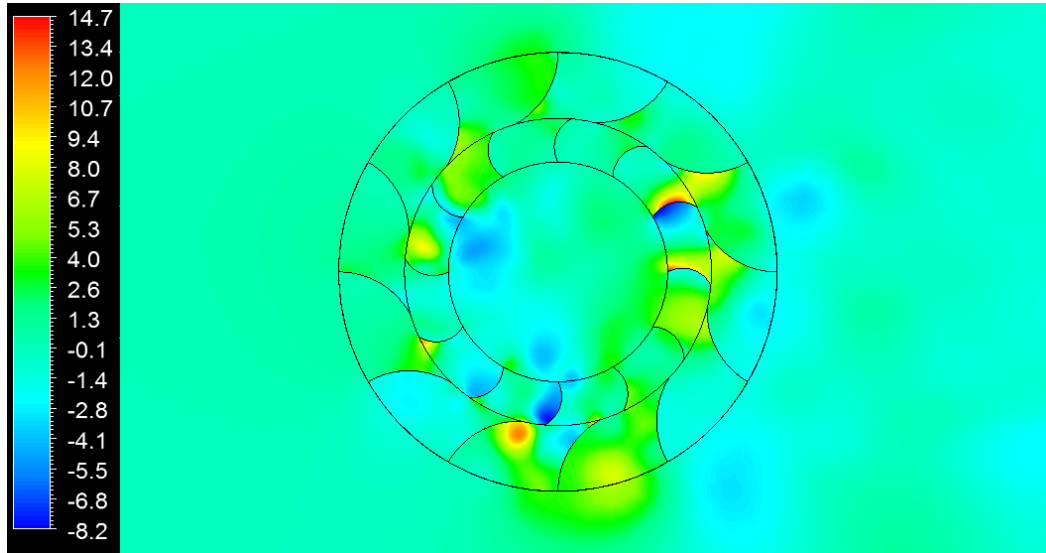


Figure 4.10 Difference contour of static gauge pressure between TSRs of 0.1 and 0.4

Figure 4.11 depicts the flow velocity magnitude based difference contour between TSRs of 0.4 and 0.1. It can be clearly seen that there are significant local variations in the flow velocity everywhere within the VAWT, also in the vicinity of the windward side stator blades. Hence, as TSR increases further, more areas in the vicinity of the VAWT get affected. It has been observed that flow velocity can increase upto 4.7m/s near the stator blades on the lower section of the VAWT.

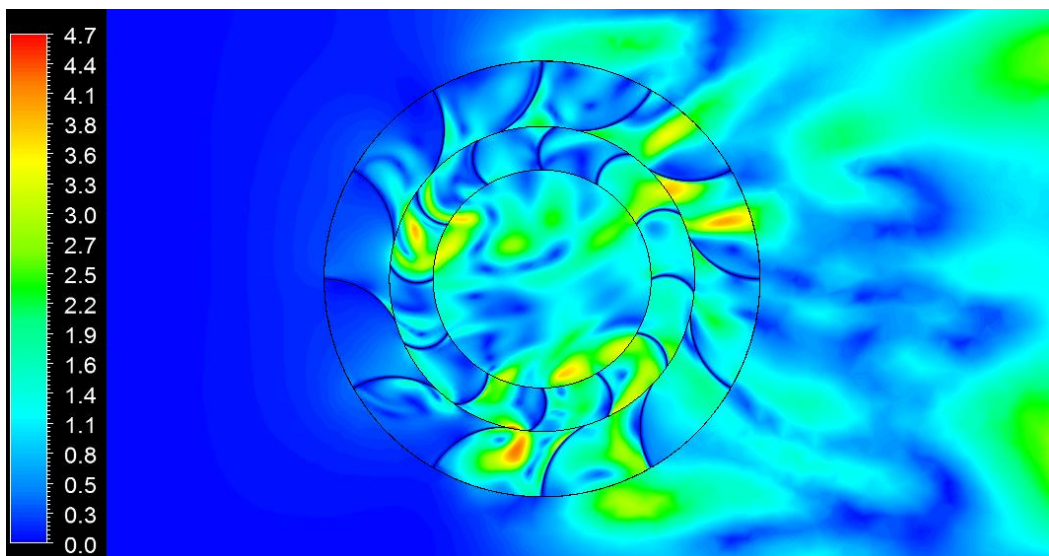


Figure 4.11 Difference contour of velocity magnitude between TSRs of 0.1 and 0.4

After carrying out qualitative analysis on the effects of TSR on the flow fields in the vicinity of the VAWT, the next step is to carry out an instantaneous quantitative analysis of the performance characteristics of the VAWT. Yet again, difference in the C_t and C_p values has been plotted here. Figure 4.12(a) depicts the difference in C_t between TSRs of 0.1 and 0.2, whereas figure 4.12(b) depicts the difference in C_t between TSRs of 0.1 and 0.4. It can be seen in figure 4.12(a) that the difference in C_t , with respect to C_t at TSR=0.1, is mostly negative, indicating that average C_t decreases as TSR increases from 0.1 to 0.2. Furthermore, figure 4.12(b) depicts further decrease in C_t values (upto -0.45 as compared to -0.25 in case of TSR=0.2). Hence, it can be concluded that as TSR increases, C_t decreases.

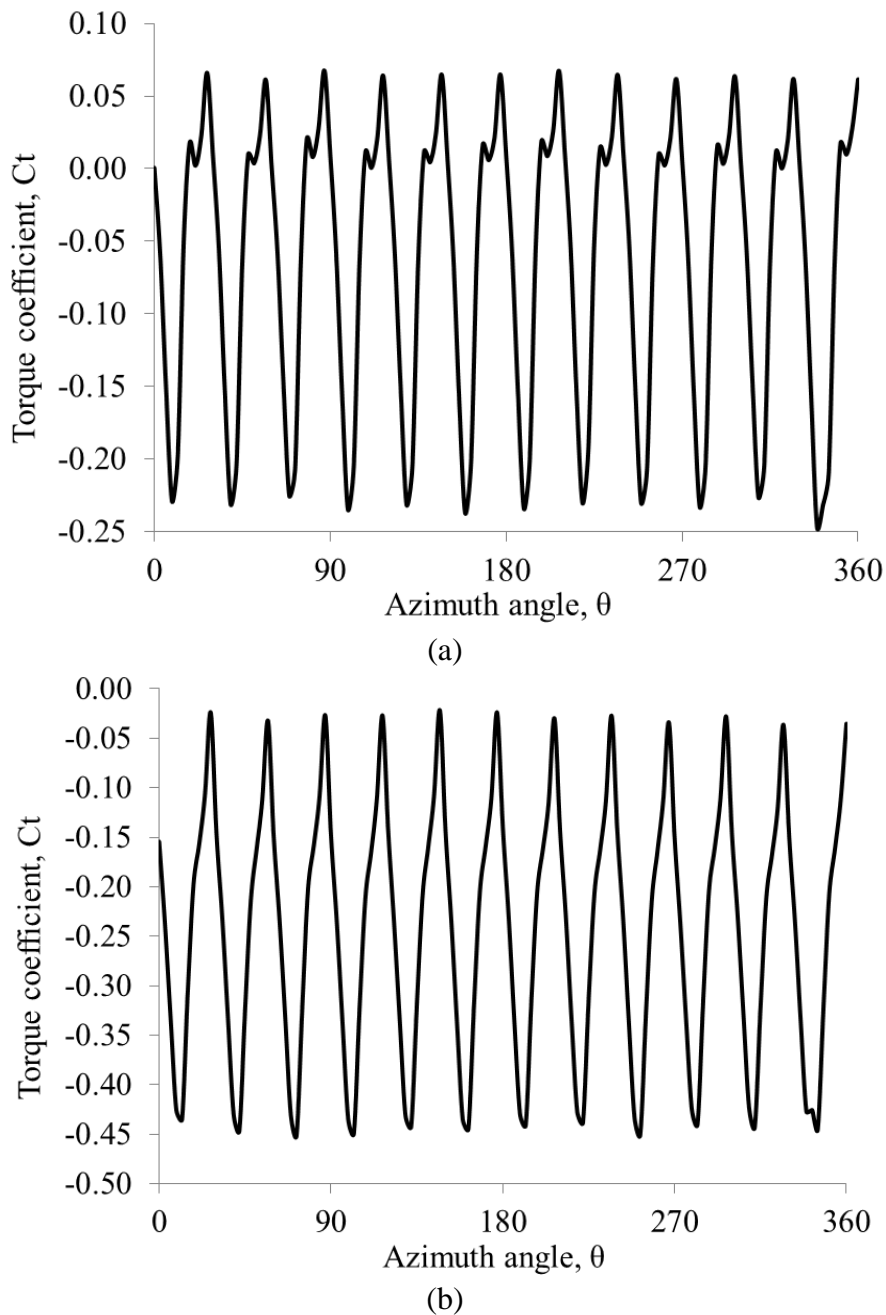
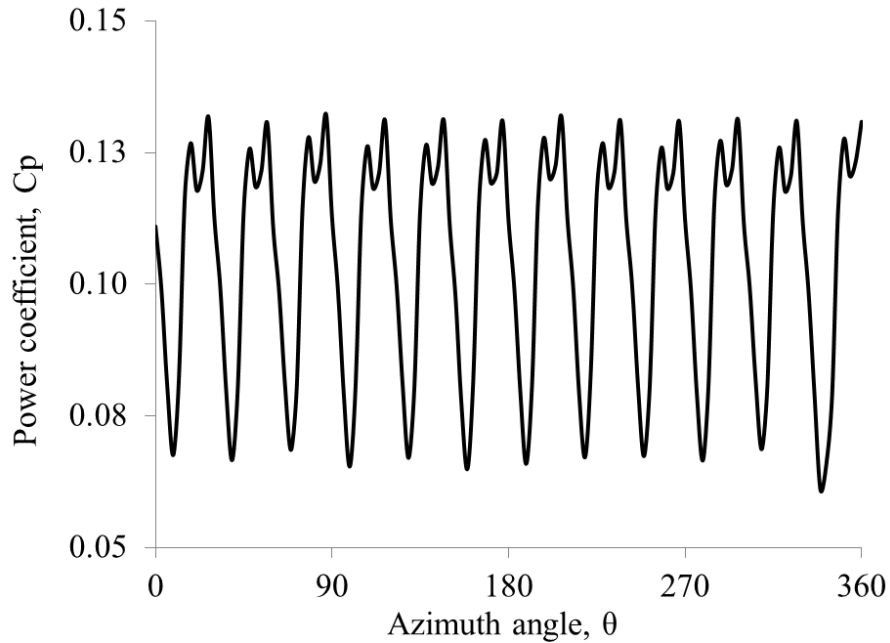
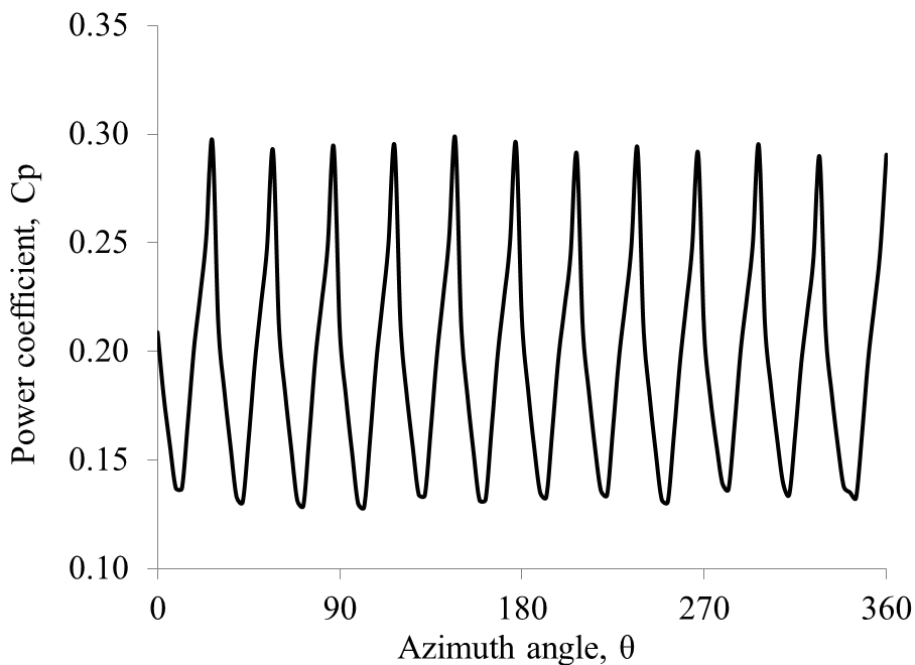


Figure 4.12 Difference in instantaneous C_t between TSRs of (a) 0.1 and 0.2 (b) 0.1 and 0.4

Figure 4.13(a) depicts the difference in C_p between TSRs of 0.1 and 0.2, whereas figure 4.13(b) depicts the difference in C_p between TSRs of 0.1 and 0.4. It can be seen in figure 4.13(a) that the difference in C_p , with respect to C_p at TSR=0.1, is positive, indicating that average C_p increases as TSR increases from 0.1 to 0.2. Furthermore, figure 4.13(b) depicts further increase in C_p values (upto 0.3 as compared to 0.135 in case of TSR=0.2). Hence, it can be concluded that as TSR increases, C_p increases.



(a)



(b)

Figure 4.13 Difference in instantaneous C_p between TSRs of (a) 0.1 and 0.2 (b) 0.1 and 0.4

An overall comparison of instantaneous C_t and C_p values for the three TSRs considered here is presented in figures 4.14 and 4.15. It can be seen in figure 4.14(a) that as TSR increases, average C_t decreases. However, the amplitude of the cyclic variations are significantly different for these three TSRs. Figure 4.14(b) shows the mean instantaneous C_t generated by the VAWT with the error bars indicating the maximum and minimum variations in C_t amplitude. Based on this information, a novel semi-empirical prediction model has been developed, where average C_t has been shown as a function of TSR. This prediction model is presented in equation (4.2), with an average percentage accuracy of more than 98%.

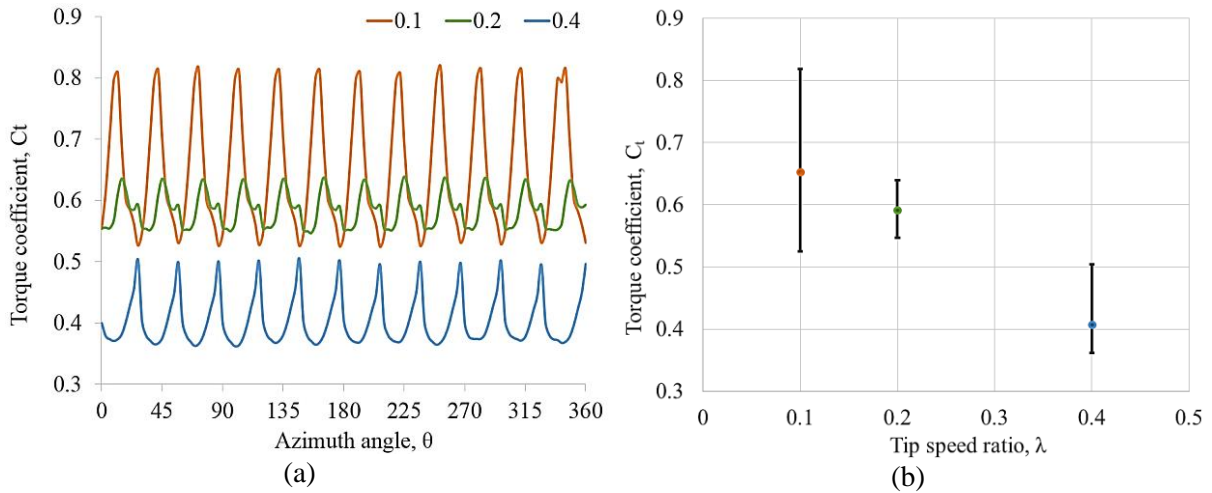


Figure 4.14 Variation of (a) instantaneous torque coefficient, and (b) the mean instantaneous torque coefficient for the VAWT during one revolution

$$C_t = -1.0061\lambda^2 - 0.3133\lambda + 0.6932 \quad (4.2)$$

Similarly, figure 4.15(a) depicts comparison of instantaneous C_p values for the three TSRs considered here. It can be seen in figure 4.15(a) that as TSR increases, average C_p increases. However, the amplitude of the cyclic variations are significantly different for these three TSRs. Figure 4.15(b) shows the mean instantaneous C_p of the VAWT with the error bars indicating the maximum and minimum variations in C_p . Based on this information, a novel semi-empirical prediction model has been developed, where average C_p has been shown as a function of TSR. This prediction model is presented in equation (4.3), with an average percentage accuracy of more than 97%.

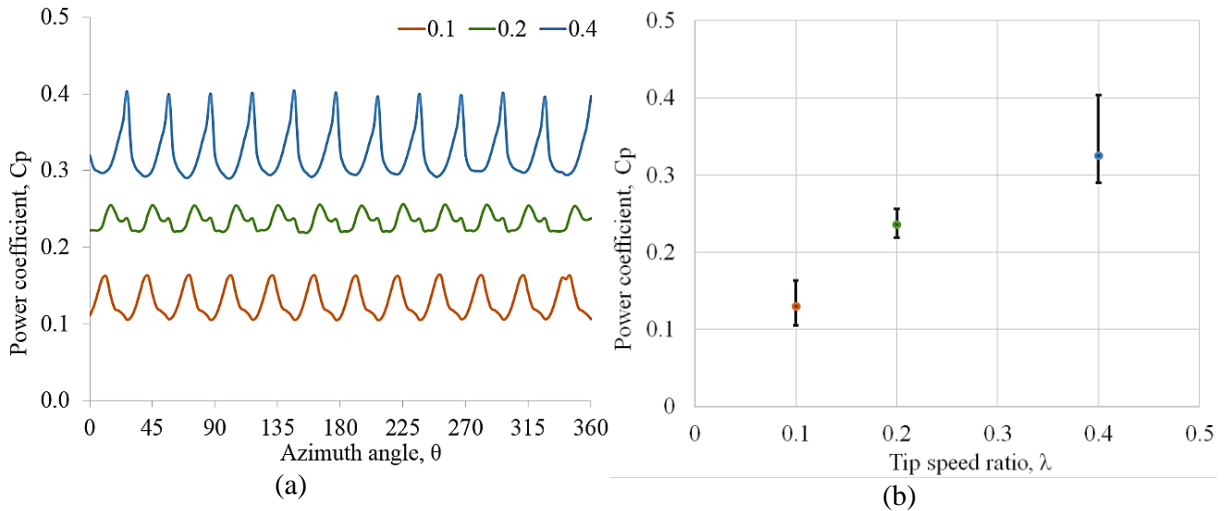


Figure 4.15 Variation of (a) instantaneous torque coefficient, and (b) the mean instantaneous torque coefficient for the VAWT during one revolution

$$C_p = -1.7791\lambda^2 + 1.5298\lambda \quad (4.3)$$

The prediction models developed here are based on multiple regression analysis, where these models are valid from $\lambda=0.1$ to $\lambda=0.4$.

4.4.3. Summary

The main conclusions obtained from the analysis are that the pressure distribution changes significantly with changing rotor position with respect to the stator. The pressure distributions are highly non-uniform and peak pressure value changes both in position and magnitude with the rotation of the rotor blade. Similarly, the flow velocity distribution changes with changing rotor position with respect to the stator. The velocity distributions are highly non-uniform and peak velocity value changes both in position and magnitude with the rotation of the rotor blade. Furthermore, there is a distinct jet and wake effect noticed within the VAWT.

It has been noticed that increase in the tip speed ratio significantly affects both the pressure and velocity fields, where more areas in the vicinity of the VAWT get influenced under increased TSR. Furthermore, detailed comparative study has shown that as the TSR increases, C_t decreases while C_p increases. Furthermore, novel semi-empirical prediction models have been developed for both these performance parameters of the VAWT, as a function of TSR.

The next chapter will discuss in detail the dynamics of VAWT's performance under a variety of transient flow conditions.

CHAPTER 5

PERFORMANCE ANALYSIS OF A VERTICAL AXIS WIND TURBINE OPERATING UNDER VARYING WIND VELOCITY

The performance analysis of a vertical axis wind turbine operating under accelerated and decelerated flow has been carried out in the present chapter. According to the current research, advanced Computational Fluid Dynamics based tools have been employed to predict the variable flow velocity in the vicinity of the VAWT and the complex flow phenomena associated with it. Hence, a thorough qualitative and quantitative investigation has been carried out on variable wind velocity characteristics of the VAWT. Furthermore, the effects of varying rotational speed of the rotor blades under unsteady flow conditions on the performance parameters have been analysed in detail.

5.1. Introduction

The first part of this chapter correspond to accelerating and decelerating inlet flow velocity keeping the rotational speed of the rotor blades (and hence the TSR) constant. This analysis has been carried out at $\lambda=0.2$ only as it being the most practical case in the real world, as mentioned by Colley [33], where the corresponding rotor blade's rotational speed is 1.143rad/s. Furthermore, the accelerating part comprises of inlet velocity change from 4m/s to 10m/s in one revolution of the VAWT, whereas the decelerating part comprises of inlet velocity change from 10m/s to 4m/s in one revolution of the VAWT.

The second part of this chapter deals with the cases where the rotor's rotational speed varies with the inlet flow velocity, keeping the TSR constant at 0.2. The acceleration in this section is from 4m/s to 10m/s, and deceleration from 10m/s to 4m/s in one revolution of the VAWT. The corresponding rotational speeds of the rotor blades are 1.143 to 2.857rad/s (for acceleration part) and 2.857 to 1.143rad/s (for deceleration part) respectively. Both these parts of together cover a wide range of practical scenarios for VAWTs operating in a variety of flow conditions.

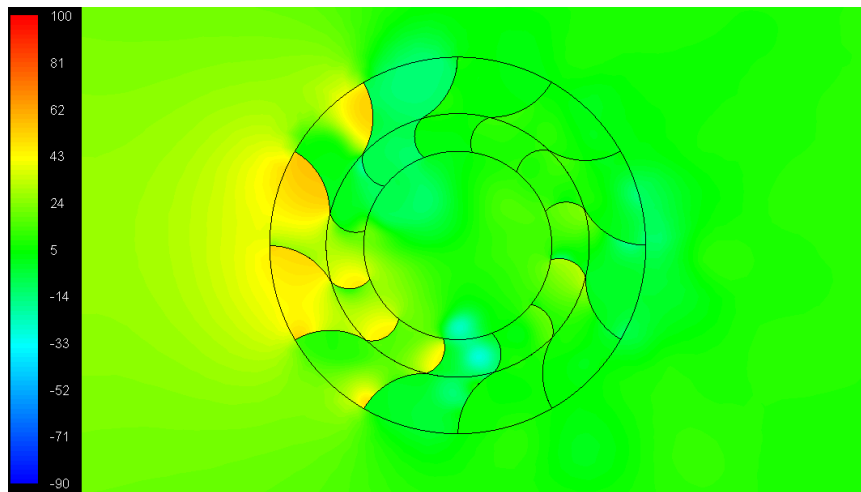
5.2. Performance Evaluation of the VAWT operating under Transient Flow Conditions with constant Rotating Speed

This section of the chapter includes the performance analysis of the VAWT operating under accelerating and decelerating inlet flow conditions and at a constant rotating speed of the rotor blades. The acceleration and deceleration sections comprises of inlet flow velocity variations from 4m/s to 10m/s and from 10m/s to 4m/s respectively, where the rotational speed of the rotor is kept constant at 1.143rad/s. The first part of this section corresponds to local flow field analysis at the four different geometrical configurations of the VAWT shown in figure 4.3. This analysis has been carried out at:

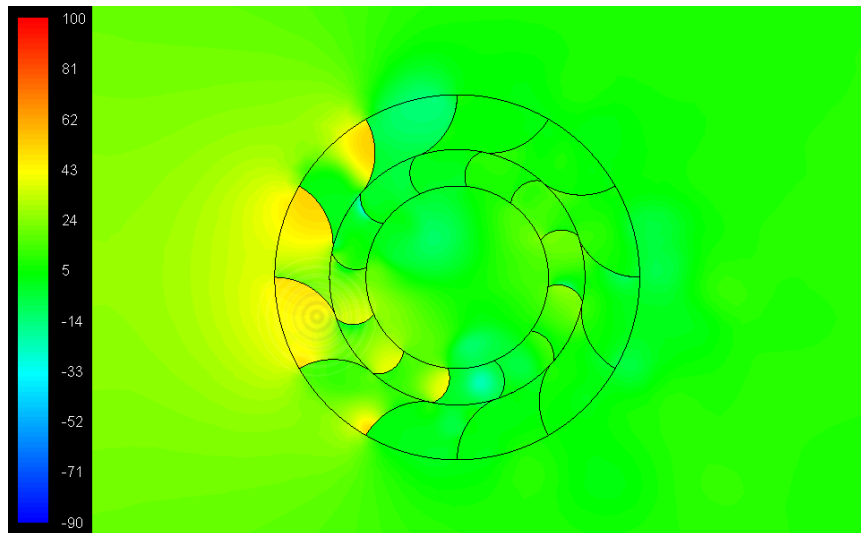
- Around 7m/s inlet flow velocity
- Around 10m/s inlet flow velocity while accelerating from 4m/s to 10m/s
- Around 7m/s inlet flow velocity while decelerating from 10m/s to 4m/s

Figure 5.1 depicts the variations in static gauge pressure in the vicinity of the VAWT for the four different geometric configurations of the VAWT, at inlet flow velocity of around 7m/s. The scale of the contours has been kept same for effective comparison purposes. It can be seen in figure 5.1(a) that the regions with higher pressure are located at the windward side of VAWT. Similarly, regions with lower pressure are pronounced at the upper and lower sections of the VAWT. The overall trend observed is similar to the steady flow cases discussed in chapter 4. However, due to higher wind velocity, the static gauge pressure variations are higher as well.

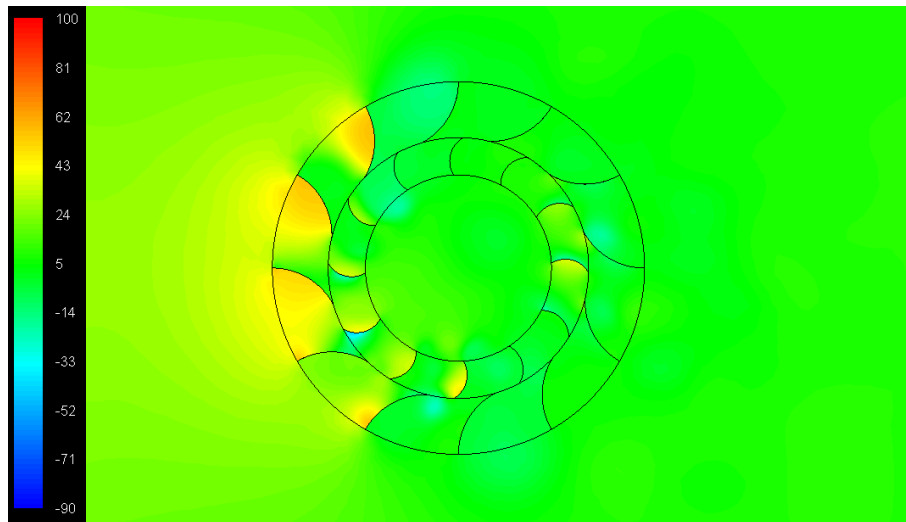
When a rotor blade crosses a stator blade with a small misalignment as depicted in the figure 5.1(b), the windward section of the VAWT depicts lower pressure in comparison to perfectly aligned rotor blades scenario. The high pressure regions in the vicinity of the rotor blades are also reduced. Furthermore, it has been noticed from figure 5.1(c) that more number of rotor blades exhibit high pressure zones when the rotor blade is precisely aligned in-between two neighbouring stator blades. It can be further observed in the last geometric configuration (figure 5.1(d)) that the higher pressure regions grow significantly when the rotor blade approaches a stator blade with a small degree of misalignment between the two. The trends shown here are inline with the one observed in case of VAWT operating in steady flow conditions. However, the scale of the two is different, where increased inlet flow velocity corresponds to higher static gauge pressures in the flow domain.



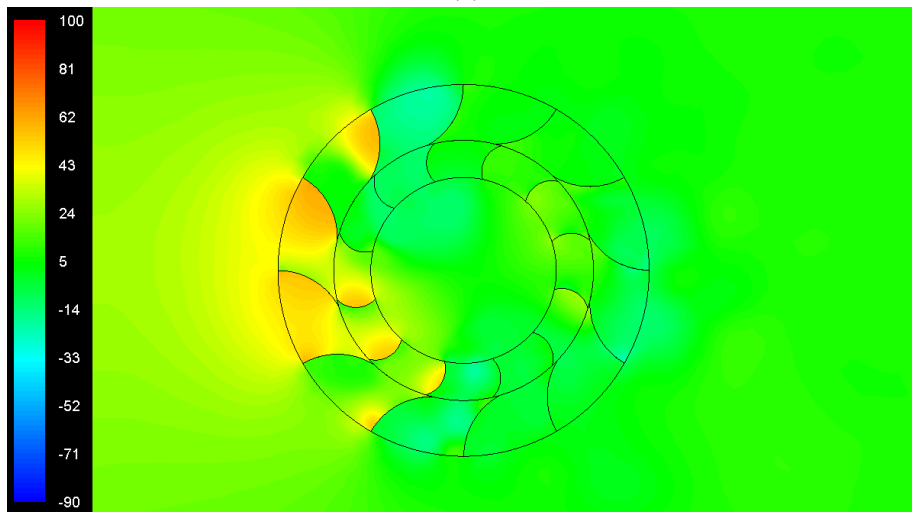
(a)



(b)



(c)

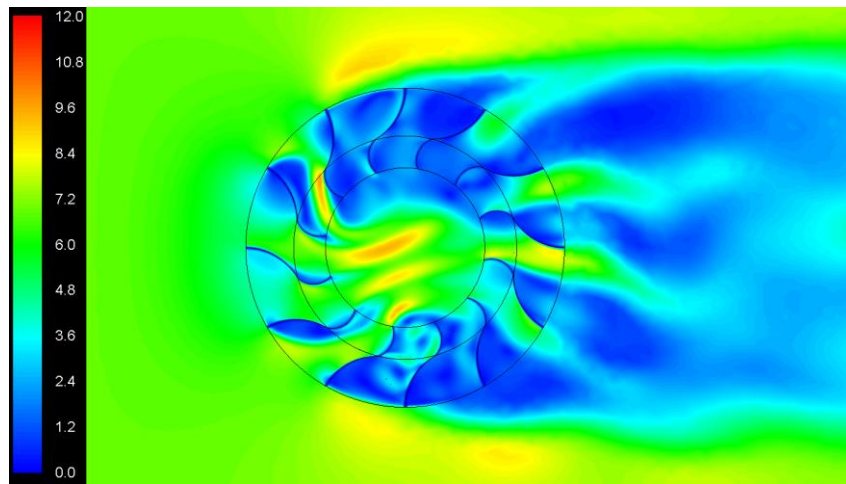


(d)

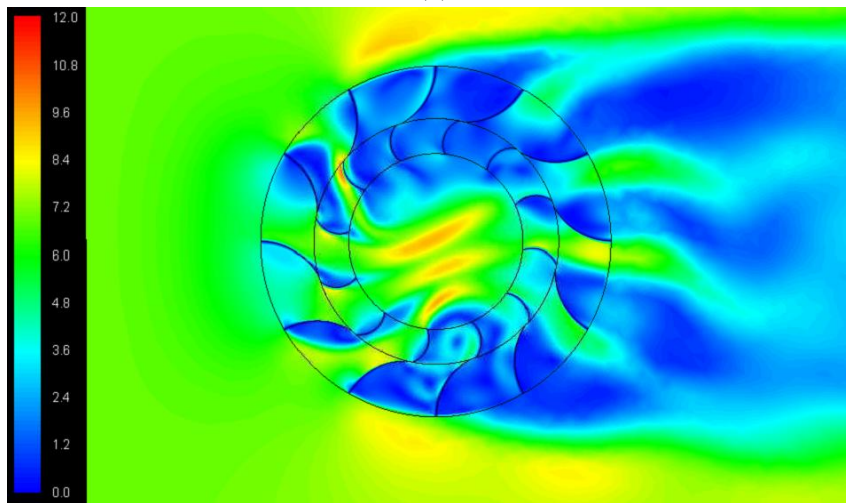
Figure 5.1 Static gauge pressure (Pa) variations in the vicinity of the VAWT at (a) 0° (b) 3° (c) 15° (d) 27° orientation at wind velocities of 6.75m/s, 6.80m/s, 7.00m/s and 7.20m/s respectively and a constant rotating speed of 1.143rad/s

Figure 5.2 depicts the variations in flow velocity magnitude in the vicinity of the VAWT for the four different geometric configurations of the VAWT, at inlet flow velocity of around 7m/s. The scale of the contours has been kept same for effective comparison purposes. It can be seen in figure 5.1(a) that the flow velocity is high in the passages between the stator and rotor blades, and is significantly lower in the sections where the flow separation has taken place (upper and lower section of the wind turbine). Furthermore, jets are formed in the stator and rotor passages, which extend to the core section of the VAWT. The flow behaviour is similar to that observed in case of steady flow conditions. Furthermore, it can be noticed in figure 5.2(b) that extended jets appear in the core section of the VAWT, whereas in figure 5.2(c), when the rotor blades are in-between stator blades, jets have been diminished from the core region. Significantly higher flow velocities are observed in the passages formed between the rotor and the stator blades. Similarly in figure 5.2(d), the trend

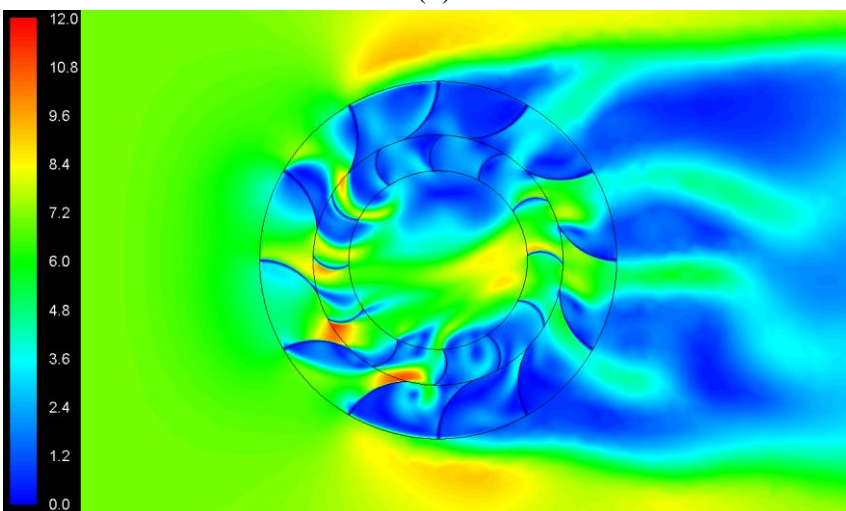
observed is similar to that observed in figures 5.2(a) and 5.2(b), while the jets formed in the core region are further extended.



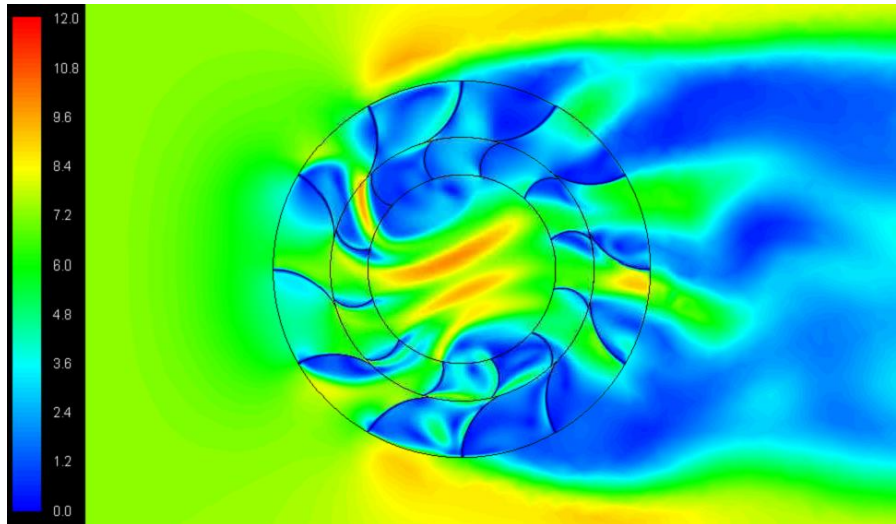
(a)



(b)



(c)

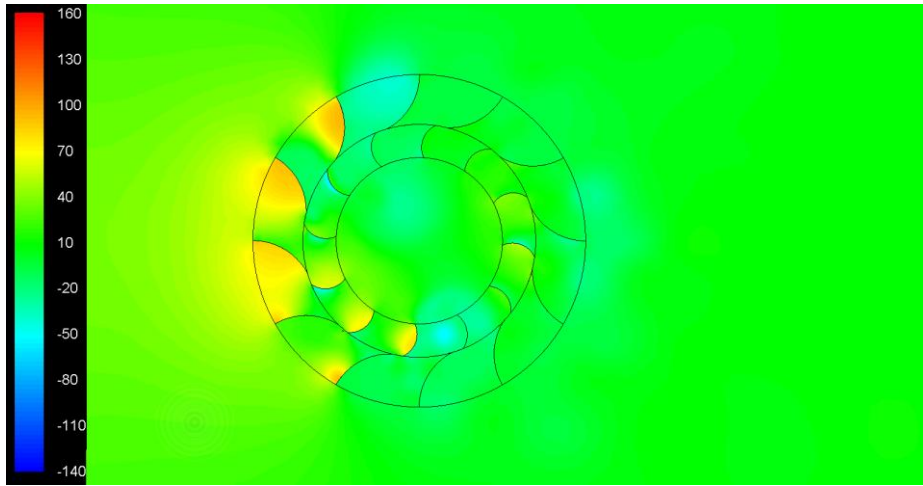


(d)

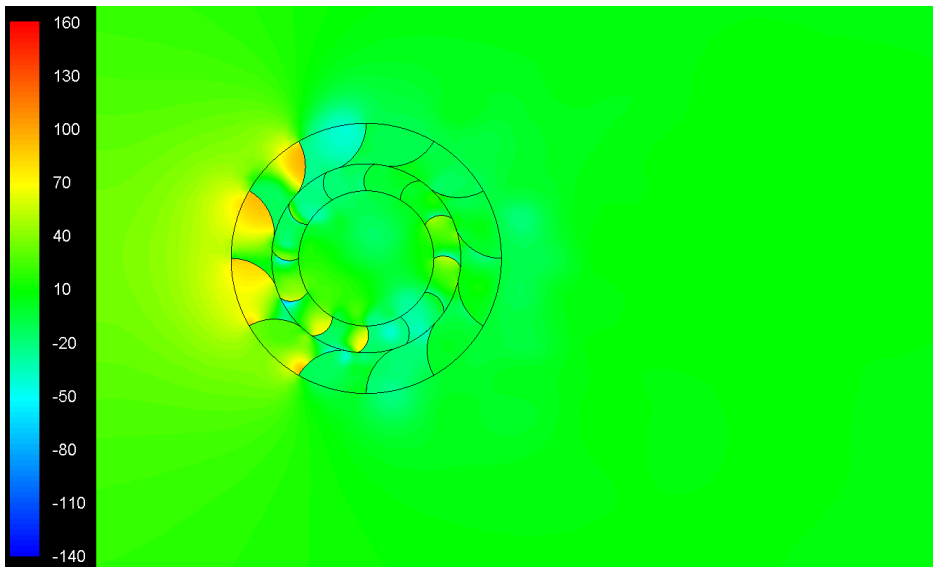
Figure 5.2 Velocity magnitude (m/s) variations in the vicinity of the VAWT at (a) 0° (b) 3° (c) 15° (d) 27° orientation at wind velocities of 6.75m/s, 6.80m/s, 7.00m/s and 7.20m/s respectively and a constant rotating speed of 1.143rad/s

Figure 5.3 corresponds to the scenario where the inlet flow velocity is accelerating, and it is around 10m/s, while the rotational speed of the rotor blades is constant at 1.143rad/s. The scale of the contours has been kept same for effective comparison purposes; however it has increased significantly as compared to the previous case discussed. It can be seen in figure 5.3(a) that the regions with higher pressure are located at the windward side of VAWT. Similarly, regions with lower pressure are pronounced at the upper and lower sections of the VAWT. The overall trend observed is similar to the previous case discussed. However, due to higher wind velocity, the static gauge pressure variations are higher as well.

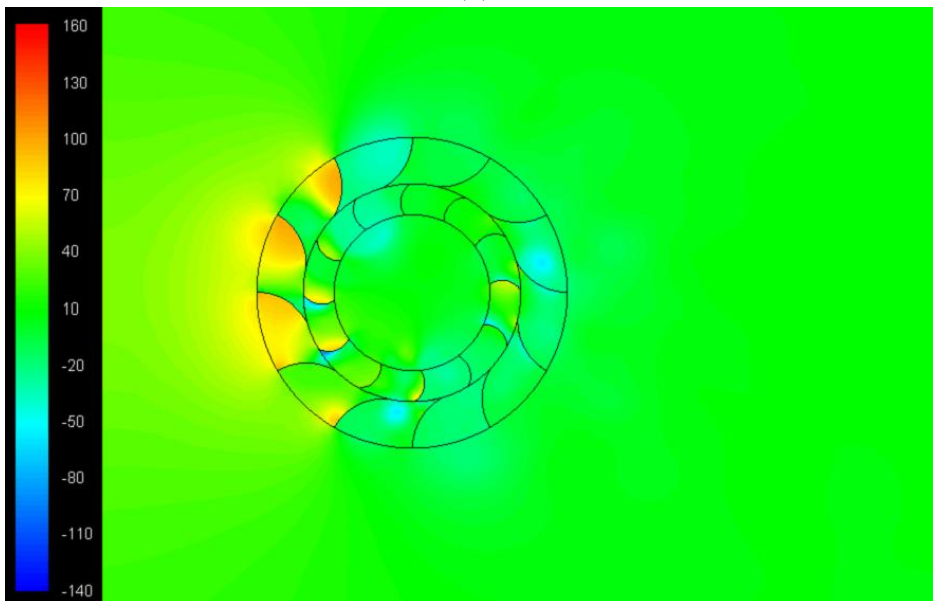
When a rotor blade crosses a stator blade with a small misalignment as depicted in the figure 5.3(b), the windward section of the VAWT depicts lower pressure in comparison to perfectly aligned rotor blades scenario. The high pressure regions in the vicinity of the rotor blades are also reduced. Furthermore, it has been noticed from figure 5.3(c) that more number of rotor blades exhibit high pressure zones when the rotor blades are precisely aligned in-between two neighbouring stator blades. It can be further observed in the last geometric configuration (figure 5.3(d)) that the higher pressure regions grow significantly when the rotor blade approaches a stator blade with a small degree of misalignment between the two. The trends shown here are inline with the one observed in the previous case. However, the scale of the two is different, where increased inlet flow velocity corresponds to higher static gauge pressures in the flow domain.



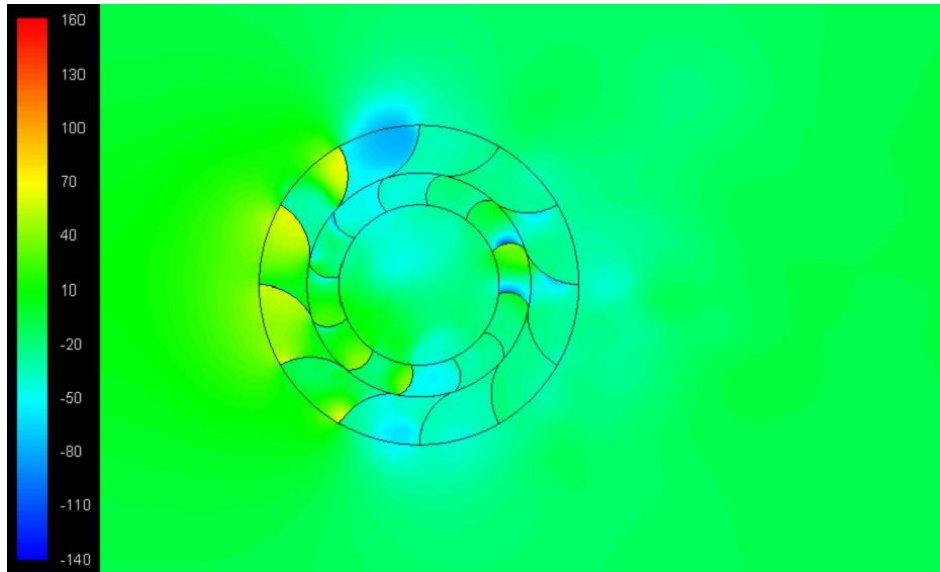
(a)



(b)



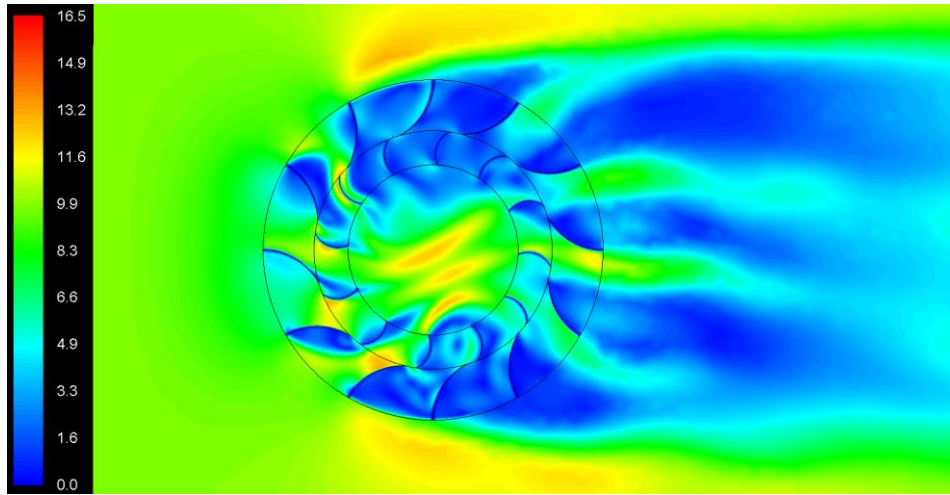
(c)



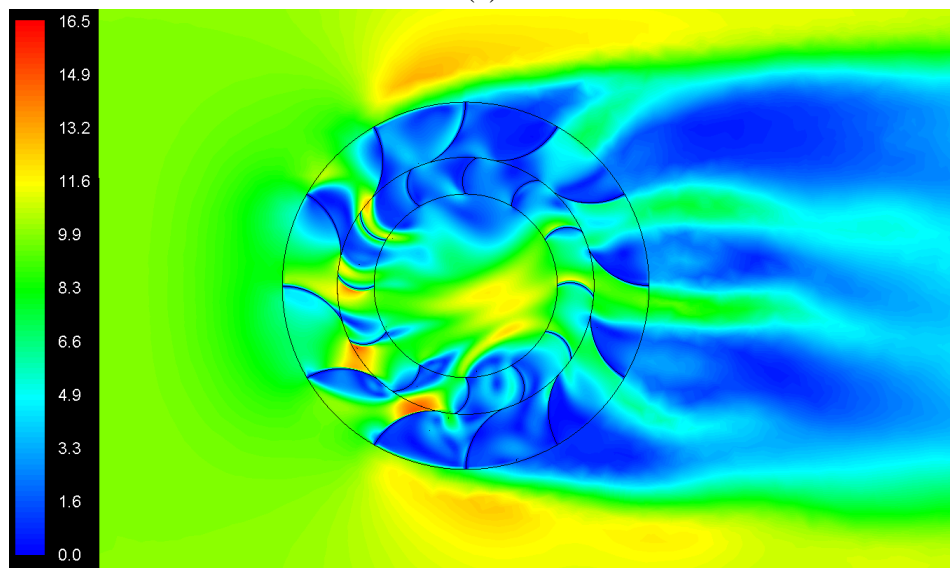
(d)

Figure 5.3 Static gauge pressure (Pa) variations in the vicinity of the VAWT at (a) 0° (b) 3° (c) 15° (d) 27° orientation at wind velocities of 9.75m/s, 9.80m/s, 10.00m/s and 9.20m/s respectively and a constant rotating speed of 1.143rad/s

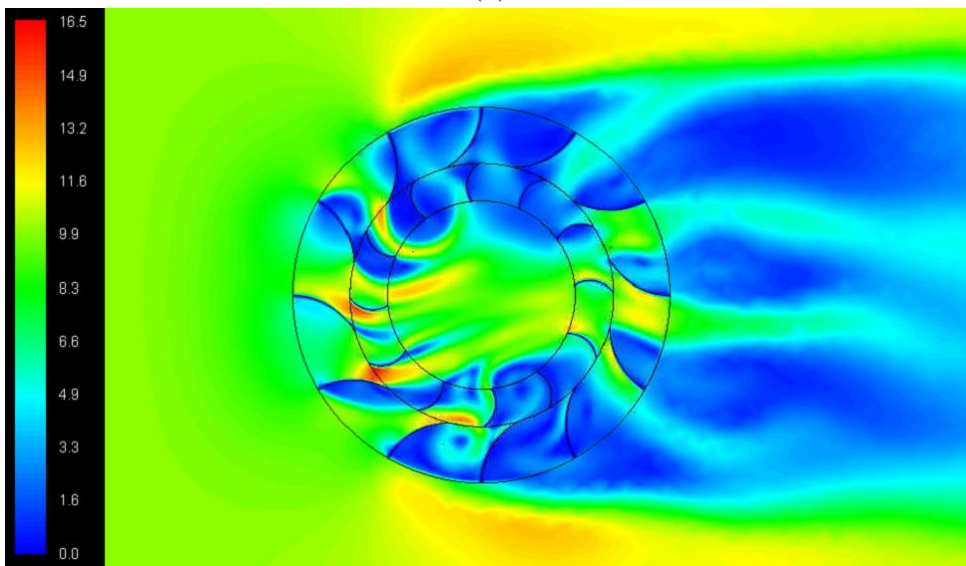
Figure 5.4 depicts the variations in flow velocity magnitude in the vicinity of the VAWT for the four different geometric configurations of the VAWT, at inlet flow velocity of around 10m/s. The scale of the contours has been kept same for effective comparison purposes; however it has increased significantly as compared to the previous case discussed. It can be seen in figure 5.4(a) that the flow velocity is high in the passages formed between the stator and rotor blades, and is significantly lower in the sections where the flow separation has taken place (upper and lower section of the wind turbine). Furthermore, jets are formed in the stator and rotor passages, which extend to the core section of the VAWT. The flow behaviour is similar to that observed in case of steady flow conditions. Furthermore, it can be noticed in figure 5.4(b) that jets appear to merge together in the core section of the VAWT, whereas in figure 5.4(c), when the rotor blades are in-between stator blades, jets are primarily originating from the passages in the rotor region. Significantly higher flow velocities are observed in the passages formed between the rotor and the stator blades. Similarly in figure 5.4(d), the trend observed is similar to that observed in figures 5.4(a) and 5.4(b), while the jets formed in the core region are further extended to the leeward side of the VAWT.



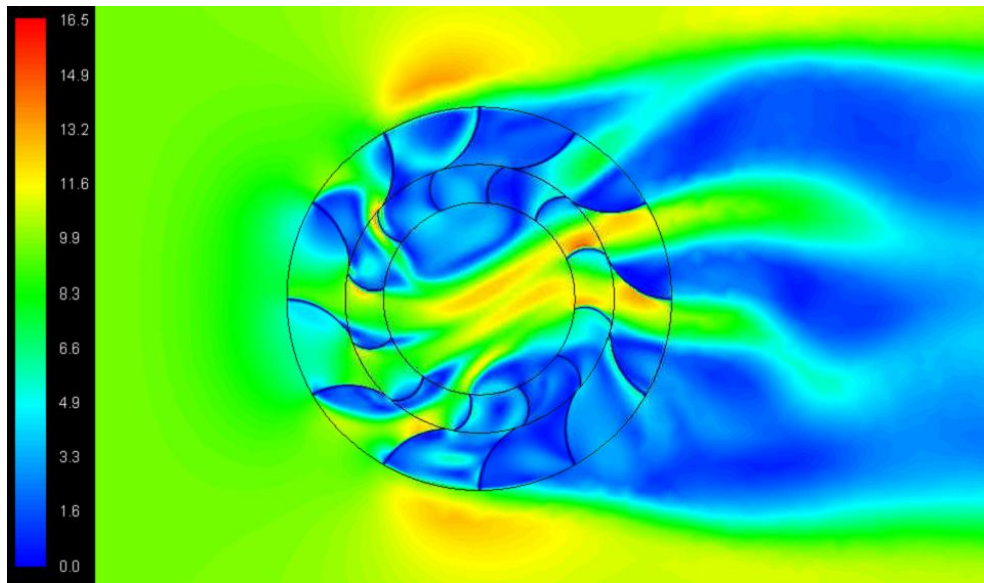
(a)



(b)



(c)

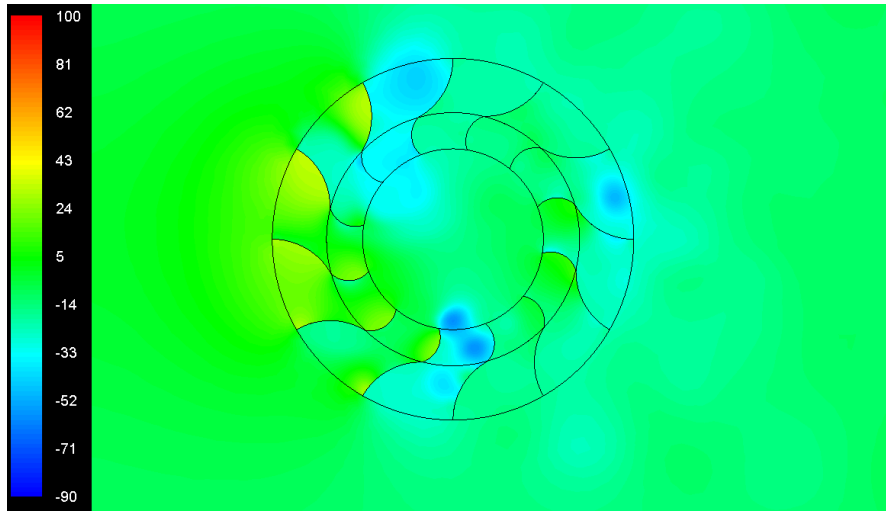


(d)

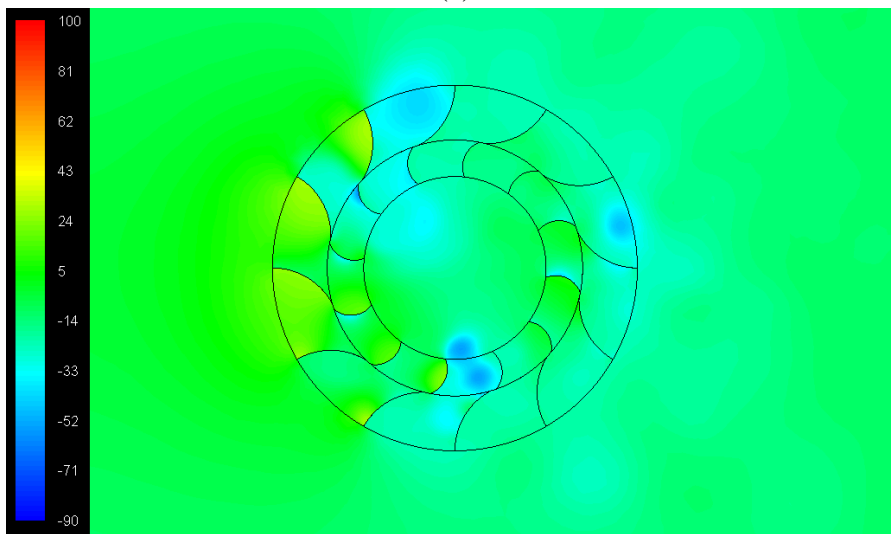
Figure 5.4 Velocity magnitude (m/s) variations in the vicinity of the VAWT at (a) 0° (b) 3° (c) 15° (d) 27° orientation at wind velocities of 9.75m/s, 9.80m/s, 10.00m/s and 9.20m/s respectively and a constant rotating speed of 1.143rad/s

Figure 5.5 corresponds to the scenario where the inlet flow velocity is decelerating, and it is around 7m/s, while the rotational speed of the rotor blades is constant at 1.143rad/s. The scale of the contours has been kept same for effective comparison purposes, and it is same as considered in figure 5.1 in order to establish whether there are any significant variations when the flow conditions become the same while decelerating, as compared to the same flow conditions but while accelerating. It can be seen in comparison between figures 5.1(a) and 5.5(a) that there are significant variations in the pressure field within the flow domain. Although the general trend is the same, however, the areas of higher pressure observed in figure 5.1(a) have reduced, while the areas of lower pressure have become bigger. Furthermore, both the highest and the lowest pressures are lower in case of decelerating flow conditions.

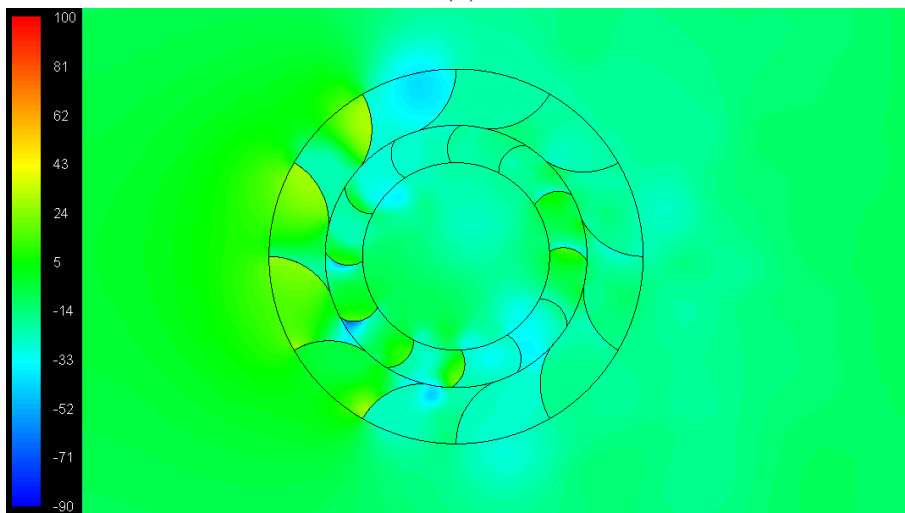
When a rotor blade crosses a stator blade with a small misalignment as depicted in the figure 5.3(b), in comparison with figure 5.1(b), the windward section of the VAWT depicts lower pressure. The high pressure regions in the vicinity of the rotor blades are also reduced. The same trend extends to other geometrical configurations of the VAWT as well, as observed in comparison of figures 5.3(c) and 5.1(c), and 5.3(d) and 5.1(d) respectively.



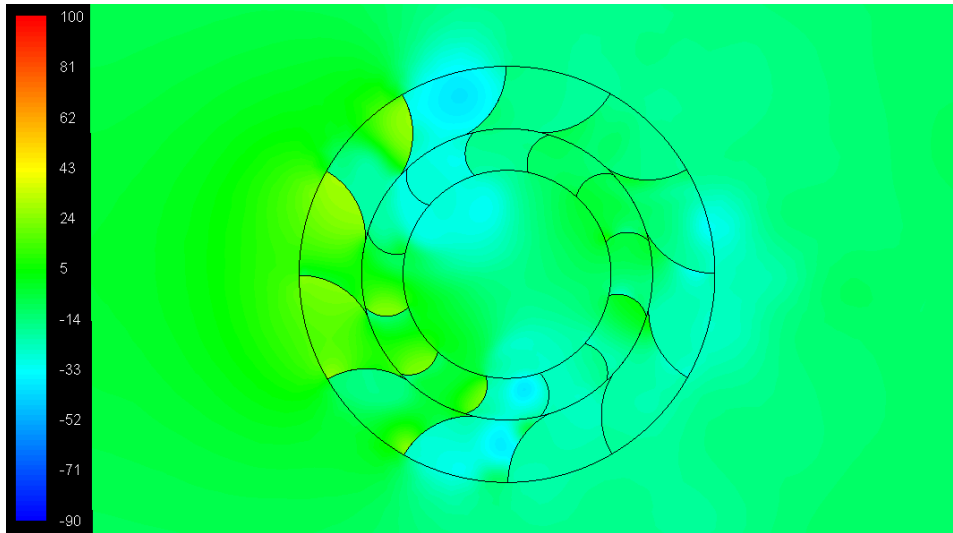
(a)



(b)



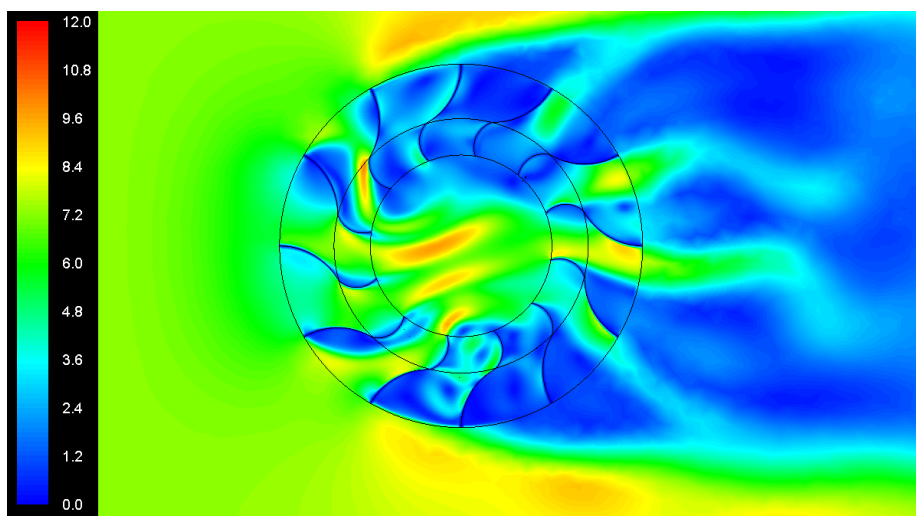
(c)



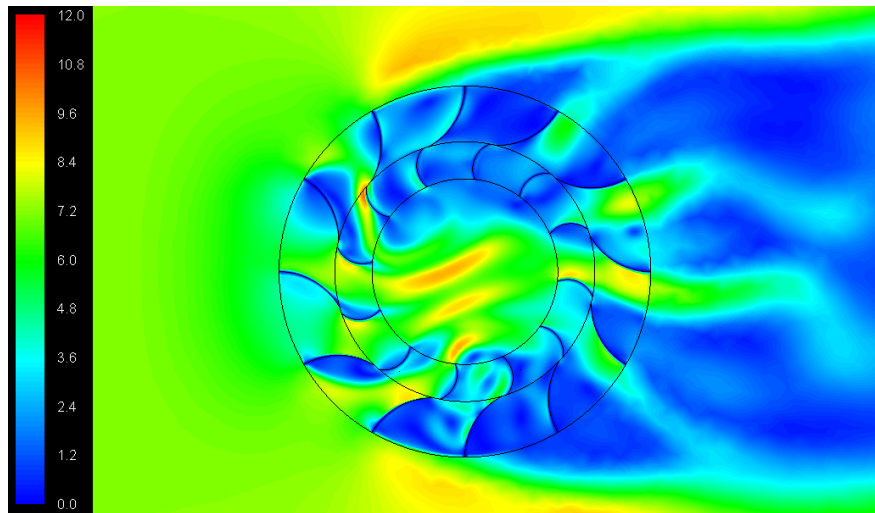
(d)

Figure 5.5 Static gauge pressure (Pa) variations in the vicinity of the VAWT at (a) 0° (b) 3° (c) 15° (d) 27° orientation at wind velocities of 7.25m/s, 7.20m/s, 7.00m/s and 6.80m/s respectively and a constant rotating speed of 1.143rad/sec

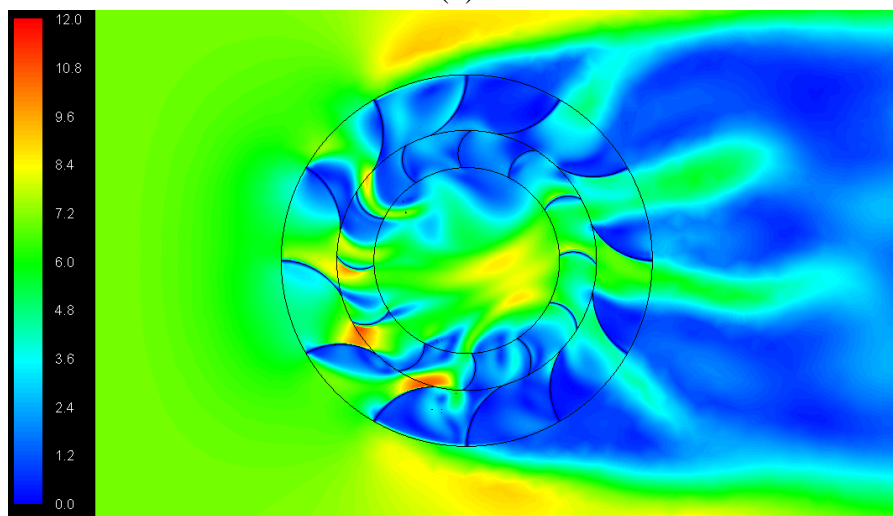
Figure 5.6 corresponds to the scenario where the inlet flow velocity is decelerating, and it is around 7m/s, while the rotational speed of the rotor blades is constant at 1.143rad/s. The scale of the contours has been kept same for effective comparison purposes, and it is same as considered in figure 5.2 in order to establish whether there are any significant variations when the flow conditions become the same while decelerating, as compared to the same flow conditions but while accelerating. It can be seen in comparison between figures 5.2(a) and 5.6(a) that the variations in the velocity field in the vicinity of the VAWT is insignificant. The general trend is the same in all the different geometrical configurations of the VAWT considered here. Similar trends have been in comparison of figures 5.6(b) and 5.2(b), 5.6(c) and 5.2(c), and 5.6(d) and 5.2(d) respectively



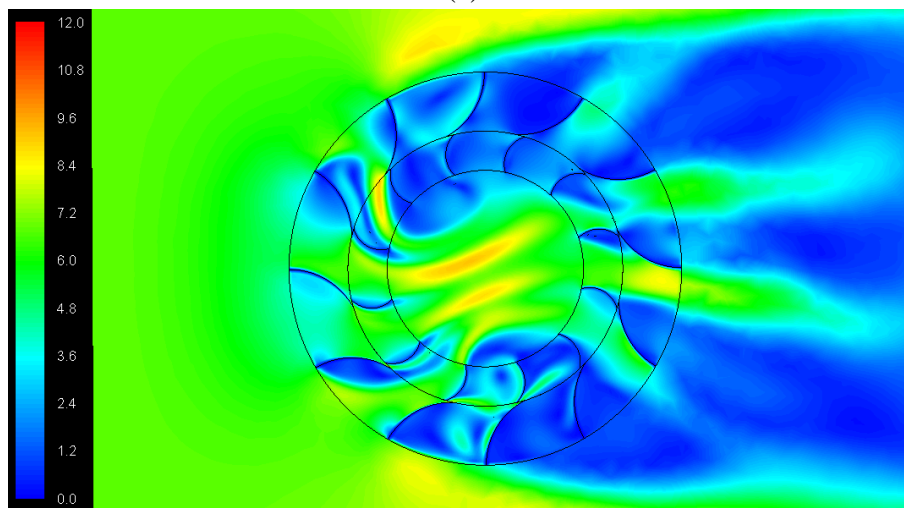
(a)



(b)



(c)



(d)

Figure 5.6 Velocity magnitude (m/s) variations in the vicinity of the VAWT at (a) 0° (b) 3° (c) 15° (d) 27° orientation at wind velocities of 7.25m/s, 7.20m/s, 7.00m/s and 6.80m/s respectively and a constant rotating speed of 1.143rad/s

Figure 5.7 depicts the variations in the instantaneous torque coefficient generated by the VAWT in three revolutions of its operation i.e. steady flow condition at 4m/s, accelerated flow condition from 4m/s to 10m/s and decelerated flow condition from 10m/s to 4m/s, all at a constant rotational speed of the rotor blades i.e. 1.143rad/s. The cyclic variations in the torque coefficients have been observed every 30° of azimuthal angle, and the total number peaks and valleys in one revolution of the VAWT are equal to the number of rotor blades of the VAWT. It can be noticed from figure 5.7 that the fluctuations in the torque coefficient start to increase as the flow is accelerated, and decreases with decelerated flow conditions. Furthermore, it can be clearly seen that as the inlet flow velocity increases, the amplitude of the cyclic variations increases significantly. The overall path followed by the VAWT under accelerating and decelerating flow conditions is the same, despite the observed local variations in the static gauge pressure in the vicinity of the VAWT.

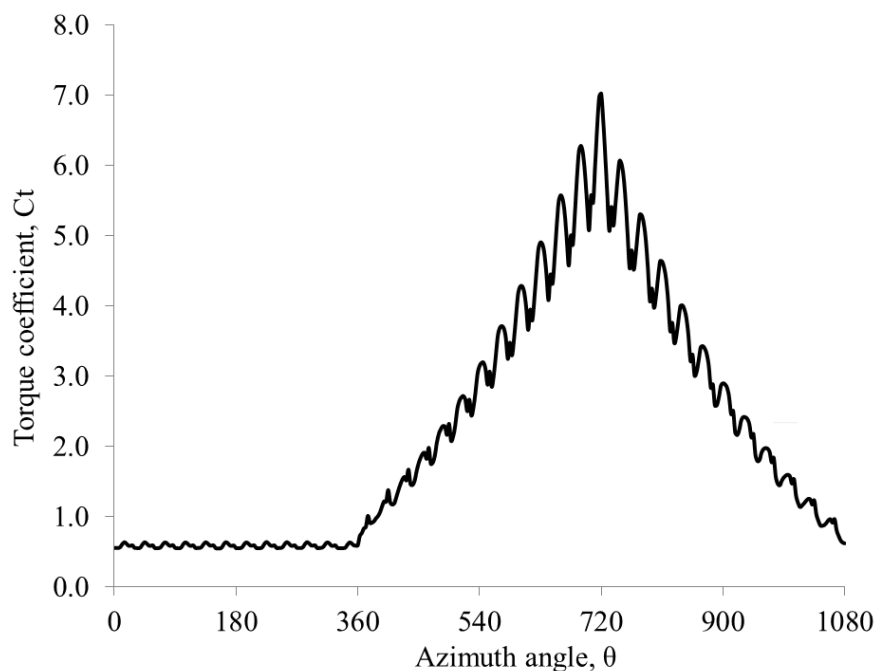


Figure 5.7 Instantaneous torque coefficient of the VAWT under variable wind velocity at a constant rotating speed of 1.143rad/s

Figure 5.8 depicts the variations in the instantaneous power coefficient of the VAWT in three revolutions of its operation i.e. steady flow condition at 4m/s, accelerated flow condition from 4m/s to 10m/s and decelerated flow condition from 10m/s to 4m/s, all at a constant rotational speed of the rotor blades i.e. 1.143rad/s. Similar to figure 5.7, it can be seen in figure 5.8 that the fluctuations in the power coefficient start to increase as the flow is accelerated, and decreases with decelerated flow conditions. Furthermore, it can be clearly seen that as the inlet flow velocity increases, the amplitude of the cyclic variations increases significantly. The overall path followed by the VAWT under accelerating and decelerating flow conditions is the same, despite the observed local variations in the static gauge pressure in the vicinity of the VAWT.

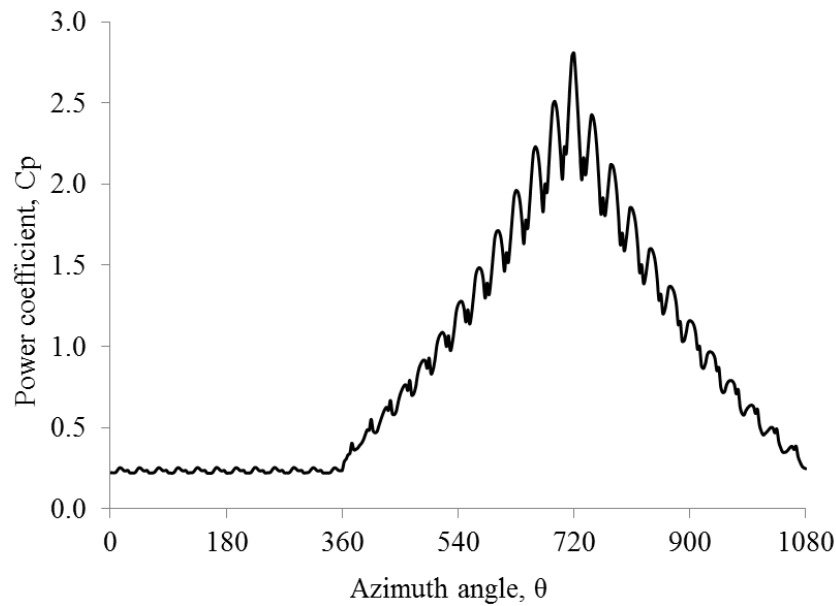


Figure 5.8 Instantaneous power coefficient of the VAWT under variable wind velocity at a constant rotating speed of 1.143rad/s

5.3. Performance Evaluation of the VAWT operating under Transient Flow Conditions with variable Rotating Speed

It has been noticed in the previous chapter that the peaks in the torque and power coefficient's signals occur when rotor blades are positioned perfectly in-between two stator blades. Hence, this particular geometrical configuration of the VAWT has been chosen for further analysis in this section of the chapter, which quantifies the effects of variable rotational speed of the rotor on the performance characteristics of the VAWT. Similar to the previous section, the acceleration and deceleration sections comprises of inlet flow velocity variations from 4m/s to 10m/s and from 10m/s to 4m/s respectively, where the rotational speed of the rotor is variable, which is summarised in table 3.2. Qualitative differences in the flow related parameters have been shown using difference contours, where the following cases have been analysed:

- Static pressure and velocity magnitude difference when the inlet flow velocity changes from steady 4m/s to around 7m/s
- Static pressure and velocity magnitude difference when the inlet flow velocity changes from 7m/s to around 10m/s
- Static pressure and velocity magnitude difference when the inlet flow velocity changes from 10m/s to around 7m/s
- Comparison in the performance outputs of the VAWT for constant and variable rotational speeds of the rotor

Figure 5.9 depicts the static gauge pressure based difference contour between accelerated wind velocity of 7m/s and steady wind velocity of 4m/s. The scale of the contour suggests

that the static gauge pressure increases as the inlet wind velocity increases, from steady flow conditions. Therefore, there are significant global variations in it, especially at the windward and leeward sections of the VAWT. The concave sides of rb1, rb2, rb3 and rb4 show increase in static gauge pressure, as the wind velocity increases from 4m/s to 7m/s, whereas low static gauge pressure is observed at the upper and lower section of the VAWT. Hence, as the wind velocity increases, the static gauge pressure increases on the windward sections of the VAWT.

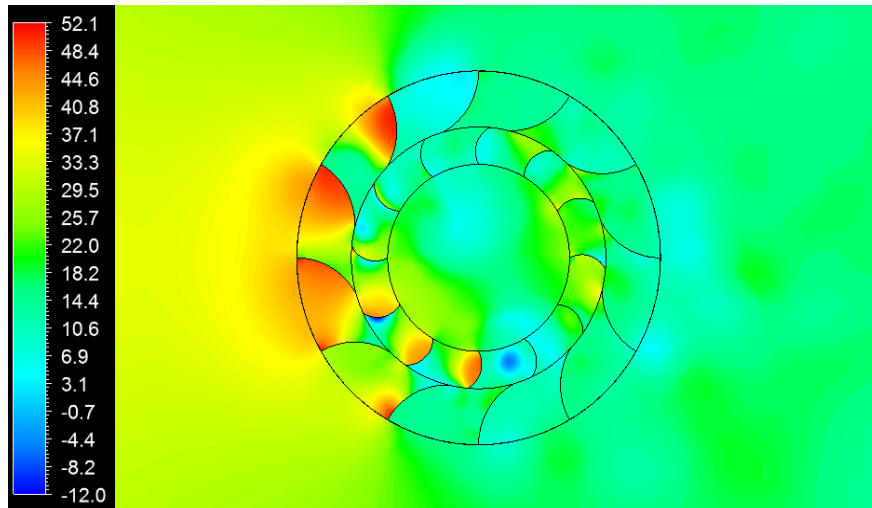


Figure 5.9 Difference contour of static gauge pressure between accelerated wind velocity of 7m/s and steady wind velocity of 4m/s

Similarly, figure 5.10 depicts the flow velocity magnitude based difference contour between accelerated wind velocity of 7m/s and steady wind velocity of 4m/s. It can be clearly seen that there are significant local variations in the flow velocity in the vicinity of the VAWT, especially in the passages between rb2, rb3 and rb4, where the flow velocity difference of upto 8.2m/s has been recorded. The scale of the contour suggests that as the inlet wind velocity increases, the flow velocity magnitude in the vicinity of the VAWT also increases.

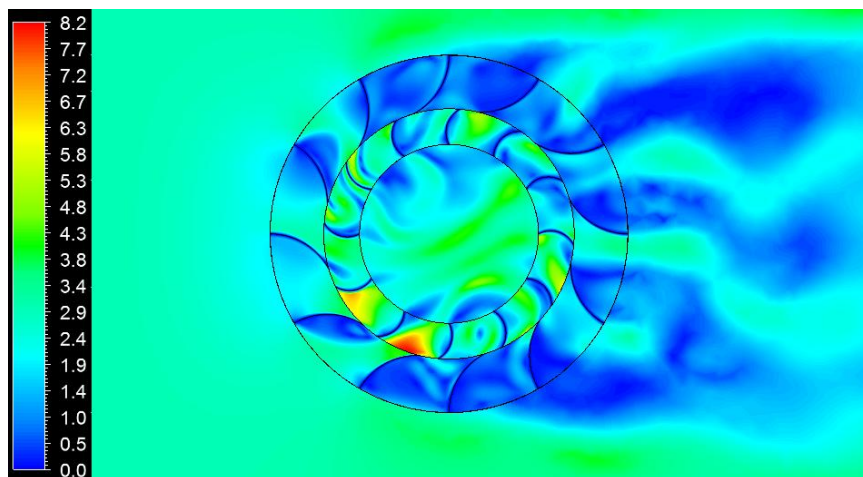


Figure 5.10 Difference contour of velocity magnitude between accelerated wind velocity of 7m/s and steady wind velocity of 4m/s

Figure 5.11 depicts the static gauge pressure based difference contour when the inlet flow velocity accelerates from 7m/s to 10m/s. In comparison with figure 5.9, it can be seen that the overall trend of the static gauge pressure increase/decrease is the same. However, static gauge pressure on the concave side of rb2, rb3 and rb4 has increased significantly. Moreover, it has also increased at concave side of rb7 and convex sides of rb8 upto 72Pa. Hence, as the flow accelerates, the static gauge pressure increases in the rotor of the VAWT.

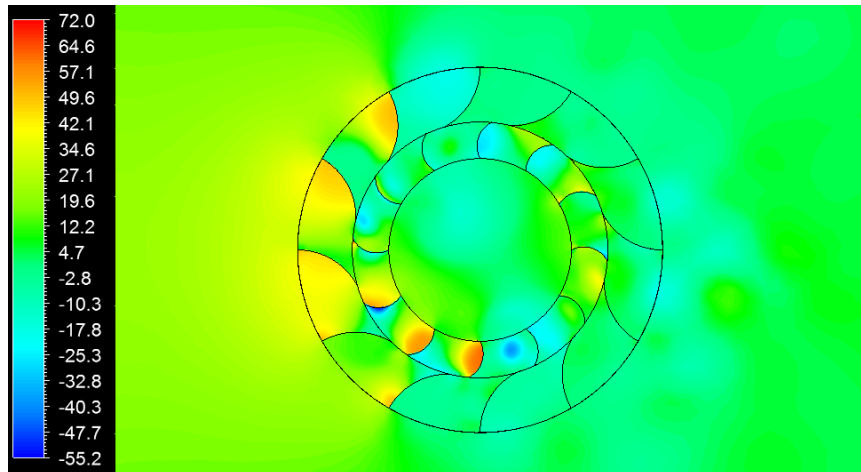


Figure 5.11 Difference contour of static gauge pressure between the wind velocity at the peak of 10m/s and accelerated wind velocity of 7m/s

Figure 5.12 depicts the flow velocity magnitude based difference contour when the inlet flow velocity accelerates from 7m/s to 10m/s. It can be clearly seen that there are significant local variations in the flow velocity in the vicinity of the VAWT especially, in the passages between rb2, rb3 and rb4, where the flow velocity difference of upto 11.3m/s has been recorded. Hence, as the flow accelerates, higher flow velocities are observed in the rotor region of the VAWT.

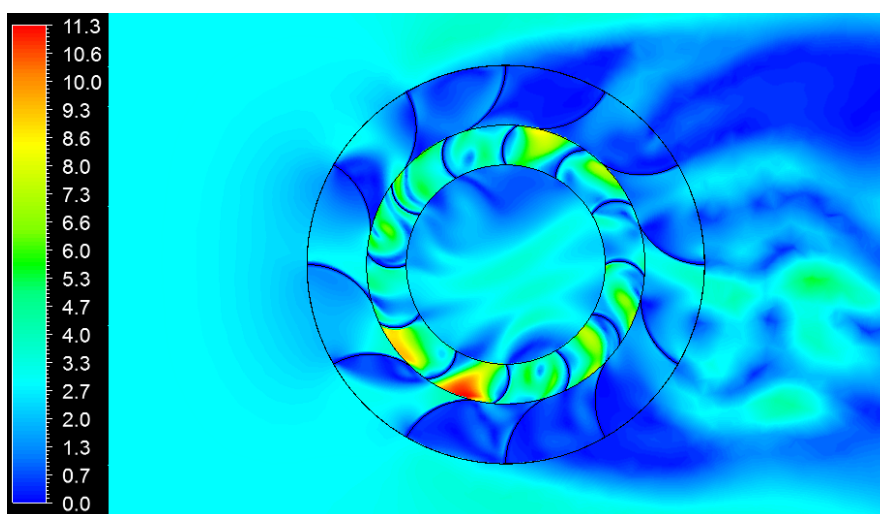


Figure 5.12 Difference contour of velocity magnitude between the wind velocity at the peak of 10m/s and accelerated wind velocity of 7m/s

Figure 5.13 depicts the static gauge pressure based difference contour when the flow decelerates from 10m/s to 7m/s. In comparison with figure 5.11, it can be seen that as the inlet wind velocity decreases, the areas of higher static gauge pressure have shifted to the leeward section of the VAWT, whereas the windward side of the VAWT depicts reduction in static gauge pressure. The maximum static gauge pressure difference of upto 17.6Pa has been observed at the convex side of rb8. Hence, under decelerating flow conditions, the windward side of the VAWT depicts lower, while the leeward side of the VAWT depicts higher static gauge pressures.

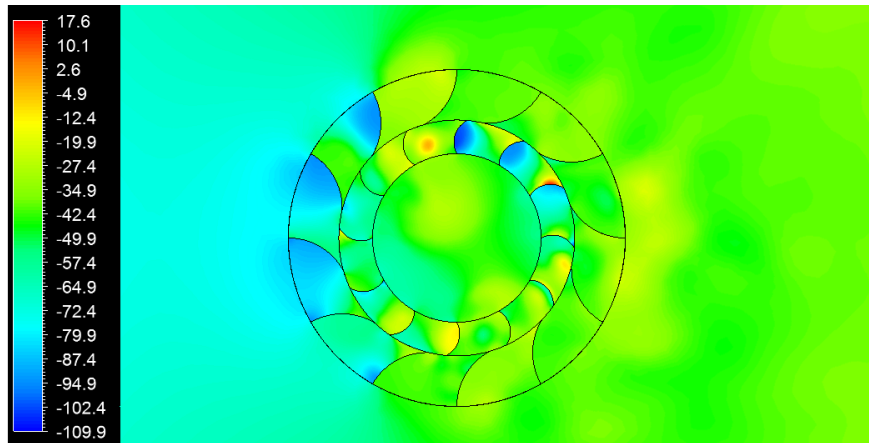


Figure 5.13 Difference contour of static gauge pressure between the decelerated wind velocity of 7m/s and the wind velocity at the peak of 10m/s

Figure 5.14 depicts the flow velocity magnitude based difference contour when the flow velocity decelerates from 10m/s to 7m/s. It can be clearly seen that there are significant local variations in the flow velocity in the vicinity of the VAWT especially, at the upper section of the VAWT, where the flow velocity difference of upto 11.9m/s has been recorded. Hence, as the flow decelerates, more areas in the vicinity of the VAWT get affected.

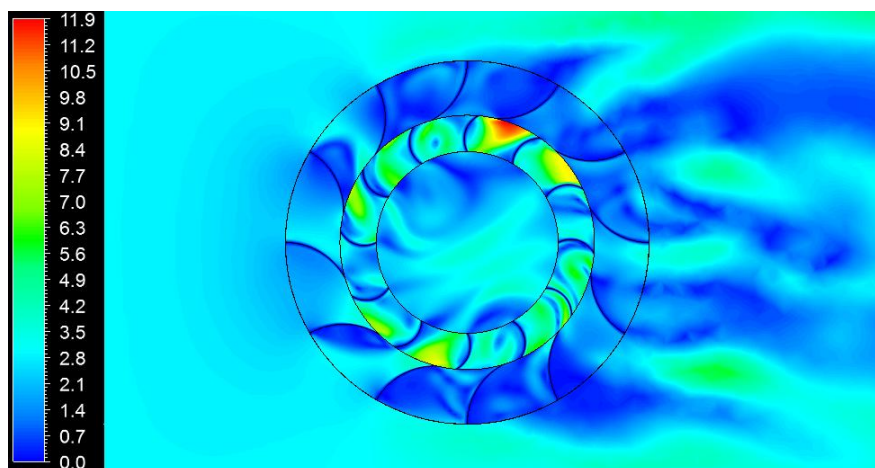


Figure 5.14 Difference contour of velocity magnitude between the decelerated wind velocity of 7m/s and the wind velocity at the peak of 10m/s

Table 5.1 presents the difference in instantaneous torque and power coefficients under accelerated, peak and decelerated wind velocities. It can be seen that the instantaneous torque and power coefficients at the constant rotating speed of the VAWT is 75.1% higher as compared to the variable rotating speed of the VAWT at 7m/s inlet flow velocity, and at the same geometrical configuration of the VAWT. However, in case of decelerated flow, when the inlet flow velocity reaches 7m/s again, the percentage difference in the torque and power coefficients, between constant and variable rotational speeds of the rotor, is reduced to 52.5%. Hence, it can be concluded that the path followed by the VAWT on the torque and power curves, under different flow conditions, is significantly different. Moreover, at the peak inlet wind velocity of 10m/s, the percentage difference in the torque and power coefficients, between constant and variable rotational speeds of the rotor, is 73.8%.

Table 5.1 Difference in instantaneous torque coefficients and instantaneous power coefficients at accelerated, peak and decelerated wind velocities respectively

Flow Condition	v (m/sec)	Constant ω		Variable ω		% Diff. in C_t	% Diff. in C_p
		C_t	C_p	C_t	C_p		
Steady	7	3.142	1.257	1.794	0.718	75.1	75.1
Accelerating	10	7.018	2.807	4.037	1.615	73.8	73.8
Decelerating	7	2.899	1.159	1.900	0.76	52.6	52.5

Apart from the differences in the performance characteristics of the VAWT under a variety of flow conditions, it is important to have a global overview of the findings of this chapter. Figure 5.15 depicts the variations in the instantaneous torque coefficient generated by the VAWT in three revolutions of its operation (steady flow at 4m/s, accelerated flow from 4m/s to 10m/s, and decelerated flow 10m/s to 4m/s) when the rotational speed of the VAWT is both constant (from previous section) and variable (from this section). It can be seen that the torque generating capability of the VAWT is higher when the rotational speed of the VAWT is constant, whereas when it is variable, the torque coefficient is significantly lower. Although the end points (360° and 1080°) are the same for both these cases, torque coefficient is considerably higher for constant rotating speed of the rotor. However, the amplitude of torque variations is also higher in case of constant rotational speed. The possible reason for lower C_t for variable ω is the fact the TSR also keeps on changing, and as it has already been discussed in detail (in chapter 4) that as TSR increases, C_t decreases, that effect is prominent in figure 5.15.

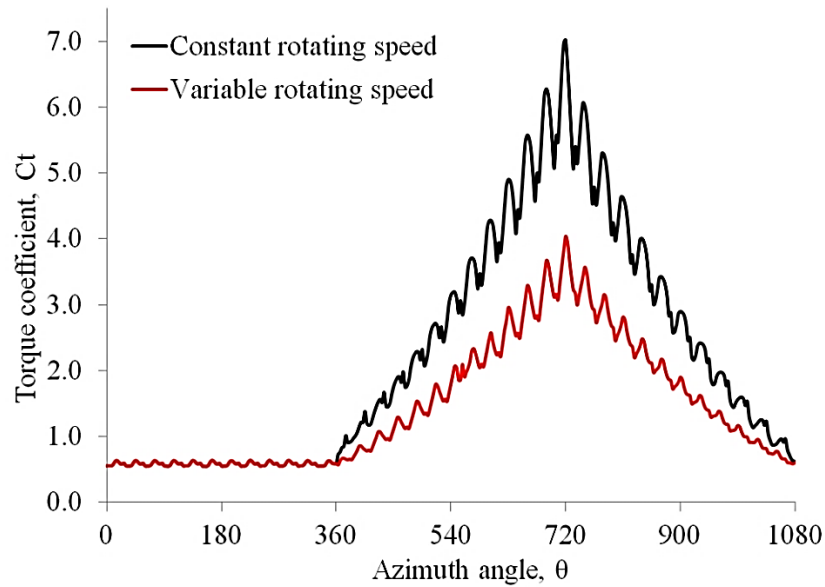


Figure 5.15 Instantaneous torque coefficient of the VAWT under variable flow conditions

Figure 5.16 depicts the variations in the instantaneous power coefficient of the VAWT in three revolutions of its operation (steady flow at 4m/s, accelerated flow from 4m/s to 10m/s, and decelerated flow 10m/s to 4m/s) when the rotational speed of the VAWT is both constant (from previous section) and variable (from this section). It can be seen that the power generating capability of the VAWT is higher when the rotational speed of the VAWT is constant, whereas when it is variable, the power coefficient is significantly lower. Although the end points (360° and 1080°) are the same for both these cases, power coefficient is considerably higher for constant rotating speed of the rotor.

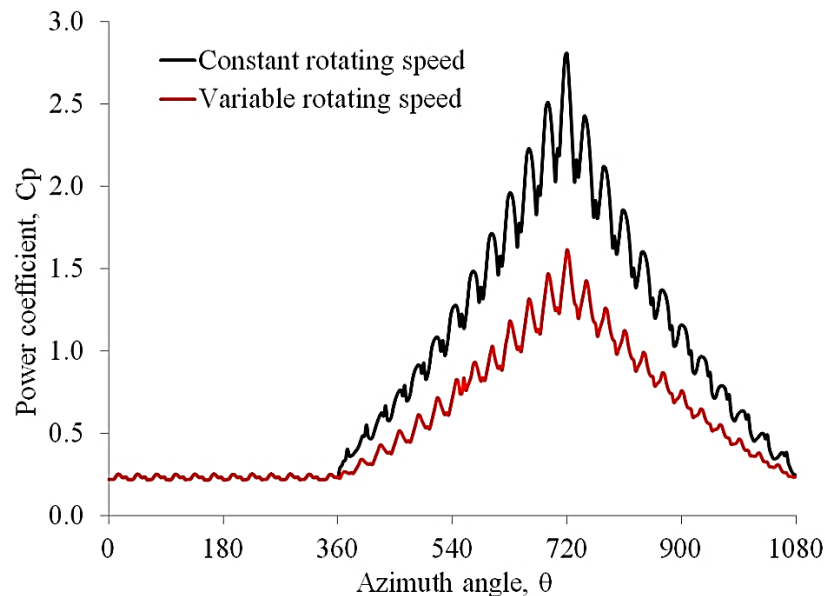


Figure 5.16 Instantaneous power coefficient of the VAWT under variable flow conditions

CHAPTER 6

CONCLUSIONS

The in-depth conclusions have been drawn in this chapter based upon the results obtained from the previous chapters, whereby the performance characteristics of a vertical axis wind turbine operating under steady and unsteady flow conditions have been analysed. The major achievements and contributions to the existing knowledge are summarised, and it has also been referred back to the initial aims of this study wherever possible. Finally, the work carried out in this study is evaluated, and requirements for future work, in the area of VAWT performance evaluation under unsteady flow conditions, are discussed.

6.1. Research Problem Synopsis

To harness the energy from the wind efficiently through a vertical axis wind turbine its performance has to be evaluated under different environmental and operating conditions. Even though, published literature demonstrates that a good amount of research work has been conducted in this area, there is limited information available about the flow features during the transient operating conditions and the effect of the transient flows on the performance characteristics of the VAWT. This is very important to understand as it is very rare to have constant steady wind velocity all the time. VAWT works mostly in unsteady flow conditions and detailed information about the flow field will be very useful in maintaining smooth operation of such installations. This study has adopted a numerical approach to interrelate various performance parameters for the VAWT operating under unsteady flow conditions. This analysis will help understand the implications of current limitations in literature and enhance the knowledge in the flow field around the VAWT under unsteady wind conditions.

The scope of this research study has been defined by formulating a set of aims and objectives to achieve those aims. The aims and objectives were formulated carefully to represent the limitations in the literature and to predict the performance output of VAWT more accurately under transient conditions. Chapter 2 provides a detailed overview of some of the current literature available and the detailed objectives to accomplish these aims. This study has proven that the flow field within and in the vicinity of the vertical axis wind turbine under various operating conditions can be investigated with acceptable range of accuracy.

6.2. Research Aims and Major Achievements

This section enlists the major achievements of this research study:

Research Aim # 1: Analyse the performance characteristics of a Vertical Axis Wind Turbine operating at a constant velocity

Achievement # 1: The performance of the vertical axis wind turbine has been critically analysed numerically for various operating conditions. This investigation focuses on the behaviour of the VAWT operating under steady environmental (constant inlet velocity) condition. The analysis of the flow phenomenon and the performance parameters of the VAWT reveal information about the pressure and velocity variations in the vicinity of the VAWT. Furthermore, the transient analysis of the various geometrical configurations of stator and rotor blade has been carried out. Through this analysis it has been established that the flow fields are strongly dependent on operating conditions and same is true for the performance parameters of the VAWT. It has been seen that both pressure and velocity field are highly non uniform around the wind turbine and these fields continuously change in the

vicinity of the turbine because of complex stator rotor interaction. The tip speed ratio affects these fields considerably as well and this effect has been quantified in this investigation.

Research Aim # 2: Analyse the performance characteristics of a Vertical Axis Wind Turbine with accelerating and decelerating flow

Achievement # 2: The major achievement of this study is the detailed transient analysis of a VAWT operating under various flow conditions, and quantifying the flow fields corresponding to, and the instantaneous torque variations acting on the VAWT. The VAWT's performance has been analysed for different inlet conditions to quantify the gradual change in the pressure and velocity fields during acceleration-deceleration cycle.

6.3. Thesis Conclusions

A comprehensive study has been carried out to support the existing literature regarding the optimisation and performance characteristics of VAWTs. The major conclusions from each facet of this research are summarised here.

Research objective # 1: Investigation of the flow parameters and evaluation of performance characteristics of the VAWT operating under steady flow condition

This study includes a detailed flow field analysis in the vicinity of the VAWT operating in a steady environment. The predictions from the numerical simulations indicate higher level of pressure non-uniformity across the windward and the leeward sections of the VAWT. At the top and lower sections of the VAWT, velocities have been observed to be less, indicating susceptibility of the flow separation. It has also been noticed that the alignment of the rotor and stator blades has significant effect on the flow field, and hence the torque output of the VAWT. The high pressure regions shrink in size with higher degree of misalignment between the rotor and stator blades. The decrease in the size of the pressure regions reduces the torque generating capability of the VAWT.

Research objective # 2: Analysing the effects of Tip Speed Ratio on the performance characteristics of the VAWT under steady flow conditions

It has been seen that the tip speed ratio strongly affects both the pressure and velocity fields, as well as the torque and power outputs of the VAWT. The effect of tip speed ratio is predominant in the near-VAWT regions. These effects are more pronounced on the leeward side as compared to the windward side of the VAWT.

Research objective # 3: Development of novel semi-empirical torque coefficient and power coefficient prediction tools accounting a range of varying flow conditions of the VAWT

The instantaneous torque output from the VAWT has been investigated and quantified for different operating conditions. The findings depict a cyclic variation in the instantaneous torque output. Semi-empirical predictor expressions have been developed for the torque and power coefficients of the VAWT operating in steady environment with different tip speed ratios, considering the transient movement of the rotor blade in the vicinity of the VAWT. The predictor tool has been shown to predict the torque and power outputs of the VAWT with reasonable accuracy.

Research objective # 4: Investigation of the flow parameters and evaluation of performance characteristics of the VAWT operating under unsteady flow conditions with accelerating and decelerating wind velocities at a constant rotational speed

The flow structure in the vicinity of the VAWT and its performance parameters have been critically analysed for the transient flow conditions, where the rotational speed of the VAWT has been kept constant. Accelerating and decelerating inlet flow conditions affects the transient response of the VAWT considerably. The results presented in this study reveal that there are significant variations in the structure of the pressure and velocity fields in the vicinity of the VAWT when it is being operated under accelerated and decelerated flow conditions even when the VAWT is operating at the same flow velocity within acceleration-deceleration cycle.

Research objective # 5: Investigation of the flow parameters and evaluation of performance characteristics of the VAWT operating under unsteady flow conditions with accelerating and decelerating wind velocities at variable rotational speeds

It has been established that change in the rotational speed of the VAWT brings about considerable change in the flow field over and above that noticed in achieving objective 4. The results presented in this study indicate that both the torque and power outputs of the VAWT is less when the rotational speed of the VAWT varies with the inlet wind velocity correspondingly, as compared to a constant rotational speed of the VAWT. This effect is predominantly the Tip Speed Ratio effect.

6.4. Recommendations for Future Work

Performance characteristics of a VAWT operating under various incoming wind velocity conditions have been analysed in the present study, aiming to bridge the gaps identified in the literature. In light of the concluding remarks provided in the previous section, a vast

potential for further research in this potential area has been unlocked. Some of the recommended future works are suggested below to enhance the VAWT design and evaluate the VAWT performance.

Recommendation # 1

More advanced modelling techniques have now become available such as two degree of freedom model, six degree of freedom model etc. Using such models, the impact of flow on rotating bodies can be analysed with much better accuracy. In these techniques, the VAWT is treated as free body, partially or completely, and the rotor blades revolve under the action of aerodynamic forces being generated on the blades. These advanced models do not require any inputs in terms of the rotor blade angular velocity. The aerodynamic forces acting on the blades are enumerated on-the-fly and necessary modifications are carried out for the orientation of the rotor blades. These advanced modelling techniques are indeed computationally very expensive and require massive computational power. Furthermore, these tools require extra computational skills in terms of writing complex scripts to define the changing mesh structure and extraction of the data.

Recommendation # 2

Condition based health monitoring of vertical axis wind turbines is essential for its widespread commercial acceptability. An investigation of the effect of the various wind condition on the health of the VAWT and fault detection system is required that can predict the faults in a VAWT. This type of model can predict the required maintenance and enhance the life cycle of the VAWT. The condition monitoring strategy includes the development of prediction models that links the severity and number of blade faults to the performance outputs of the VAWT. However, this type analysis will require high performance computation facilities capable of handling the required computational load.

Recommendation # 3

Current study adopted numerical approach to investigate the effect of variable wind velocity on the performance characteristics of the VAWT by analysing the pressure and velocity field s as well as and the instantaneous torque output. However the investigation has been conducted only on limited tip speed ratios. Using the wider range of tip speed ratio will provide more in-depth understanding of the VAWT performance under different operating condition.

REFERENCES

- [1] Fleming P. D., Probert S. D. (1984). The evolution of wind-turbines: An historical review. *Applied Energy*; Vol. 18, 163-177.
- [2] Dodge D. M. (2001-2015). The illustrated history of wind power development. Littleton Colorado: US. Federal Wind Energy Program. Available at: <http://www.telosnet.com/wind/> (accessed September 2015).
- [3] Meyer N. I. (1995). Danish wind power development, Article in *Energy for sustainable development*, Vol. 2, 18-25.
- [4] Thomas R. L. and Robbins W. H. (1980). Large wind-turbine projects in the United States wind energy program.
- [5] Islam M. R. et al., (2013). Progress and recent trends of wind energy technology. *Renewable and Sustainable Energy Reviews*, Vol. 21, 456-468.
- [6] IEA, *Energy technology perspectives: scenarios and strategies to 2020*. Available at: <http://www.worldenergyoutlook.org/publications/2008-1994> (accessed September 2015).
- [7] International Energy Agency, IEA (2009). *Technology roadmap: wind energy*. Available at: <https://www.iea.org/roadmaps/> (accessed September 2015).
- [8] Solangi K. H. et al., (2010). A review on global solar energy policy. *Renewable and sustainable Energy Reviews*, Vol. 15, 2149-2163.
- [9] Hameed Z. et al., (2007). Condition monitoring and fault detection of wind turbines and related algorithms: A review. *Renewable and Sustainable Energy Reviews*, Vol. 13, 1-39.
- [10] Eriksson, S.H., Bernhoff, and Leijon, M. (2006) Evaluation of different turbine concepts for wind power, *Renewable and Sustainable Energy Reviews*, McGraw-Hill, New York.
- [11] Hau E. (2000). *Wind turbines: Fundamentals, technologies, application and economics*, Springer.
- [12] Global wind energy council (2015). *Global Wind Report 2014*. Available at: <http://www.gwec.net> (accessed September 2015).
- [13] Manwell J. F., McGowan J. G. and Rogers A. L. (2009). *Wind energy explained: theory, design and application*, Wiley, 2nd Ed.

- [14] Gitano Briggs H. (2012). Advances in wind power: Low speed wind turbine design. Available at: <http://www.intechopen.com/books/export/citation/ReferenceManager/advances-in-wind-power/low-speed-wind-turbine-design> (accessed September 2015).
- [15] Sayigh A (1999). Renewable energy: the way forward. *Applied Energy* Vol. 64, 15–30.
- [16] Mathew S., Philip G. S. (2012). Wind turbines: evolution, basic principles and classifications. *Comprehensive Renewable Energy*, pg.93–111.
- [17] Schaffarczyk A. P. (2014). *Introduction of Wind Turbine Aerodynamics*. Green Energy and Technology, Springer.
- [18] WETF, (2012). Growth of wind turbine size: modern wind technology. Available at: <http://www.wind-energy-the-facts.org/en/part-i-technology/chapter-3-wind-turbine-technology/evolution-of-commercial-wind-turbine-technology/growth-of-wind-turbine-size.html> (accessed September 2015).
- [19] Mittal, N. (2001) Investigation of Performance Characteristics of a Novel VAWT, Thesis submitted for the M.Sc. degree, Department of Mechanical Engineering, University of Strathclyde, Glasgow, UK.
- [20] Snel, H. (1998). Review of the present status of rotor aerodynamics. *Wind Energy Systems*. Vol. 1, 46–69.
- [21] Roynarin W. (2004). Optimisation of vertical axis wind turbines. PhD thesis, Northumbria University.
- [22] Bos R. (2012). Self-starting of a small urban Darrieus rotor: Strategies to boost performance in low Reynolds-number flows. Master Thesis, Delft University of Technology.
- [23] Hameed, M. S., Afaq, S. K. and Shahid, F. (2013) Finite Element Analysis of a Composite VAWT Blade, *Ocean Engineering*, 109, 669-676.
- [24] Castelli, M. R. Englaro, A. and Benini, E. (2011). The Darrieus wind turbine, *Energy*, 36, 4919-4934.
- [25] Modi, V. and Fernando, M. (1989). On the Performance of the Savonius Wind Turbine, *Journal of Solar Energy Engineering*, 111/71.
- [26] D'Ambrosio, M. and Medaglia, M. (2010). Vertical Axis Wind Turbines, Master Thesis in Energy Engineering, Hogskolan, Halmstad.

- [27] Sheldahl, R. (1978). Wind Tunnel performance data for two and three bucket Savonius rotors, *Energy*, 2, 160-164.
- [28] Sivasegaram, S. (1978). Secondary parameters affecting the performance of resistance-type vertical-axis wind rotors, available at <http://adsabs.harvard.edu/abs/1978WiEng...2...49S>.
- [29] Clayton, B. (1978). Observations of the flow in and around Savonius and Darrieus rotors, *Proceedings of the First British Wind Energy Association Conference*, Cranfield, 24-31.
- [30] Fujisawa, N. Shirai, H. and Mizuno, Y. (1987). Hot wire anemometer measurements of flow fields around Savonius rotors in open circuit wind tunnel, *Laser and hot wire/film velocimetry and their applications*, 109-122.
- [31] Walker, S. L. (2011). Building mounted wind turbines and their suitability for the urban scale: A review of methods of estimating urban wind resource, *Energy and Buildings*, 43, 1852-1862.
- [32] Ajith, H. V. (2012). Design and performance analysis of pitched-plate vertical axis wind turbine for domestic power generation. Master thesis, KTH Industrial Engineering and Management.
- [33] Colley, G. (2012) Design, Operation, and Diagnostics of a Vertical Axis Wind Turbine, Ph.D. Thesis, School of Computing & Engineering, University of Huddersfield, UK.
- [34] Chong, W. T., A. Fazlizan, et al. (2013). "The design, simulation and testing of an urban vertical axis wind turbine with the omni-direction-guide-vane." *Applied Energy* 112: 601-609.
- [35] Mohammed, G. and M. Aboelyazied (2007). "Effect of dust on the performance of wind turbines." *Desalination* 209(1-3): 209-220.
- [36] Vries, O. d. (1979). Fluid dynamic aspects of wind energy conversion, DTIC Document.
- [37] Hameed, M. S. and S. K. Afaq (2013). "Design and analysis of a straight bladed vertical axis wind turbine blade using analytical and numerical techniques." *Ocean Engineering* 57: 248-255.
- [38] Hau, E. (2003). "Wind Turbines-Fundamentals, Technologies, Application, Economics." *IEEE Electrical Insulation Magazine* 19(2): 48.
- [39] Park, K., Asim, T., Mishra, R., Shahzad, A., & Marangwanda, G. (2012). Computational Fluid Dynamics based Performance Optimisation of Vertical Axis Marine Current Turbines.

- [40] Colley, G. Mishra, R. Rao, V. and Woolhead, R. (2009) Performance evaluation of three cross flow vertical wind axis turbine configurations, Computing and Engineering Annual Researchers' Conference, Huddersfield, UK.
- [41] Sabaeifard, P., H. Razzaghi, et al. (2012). "Determination of vertical axis wind turbines optimal configuration through CFD simulations." IPCBEE 28: 109-113.
- [42] Asim, T., R. Mishra, et al. (2013). "Effect of the Shape of Stator Blades on the Performance Output of a Vertical Axis Marine Current Turbine."
- [43] Colley, G., Mishra, R., Rao, H. V., & Woolhead, R. (2010). Effect of rotor blade position on Vertical Axis Wind Turbine performance. In proceedings of the International Conference on Renewable Energies and Power Quality (ICREPQ'10) Granada, Spain.
- [44] Takao, M., H. Kuma, et al. (2009). "A straight-bladed vertical axis wind turbine with a directed guide vane row—Effect of guide vane geometry on the performance—." Journal of thermal Science 18(1): 54-57.
- [45] Howell, R., N. Qin, et al. (2010). "Wind tunnel and numerical study of a small vertical axis wind turbine." Renewable energy 35(2): 412-422.
- [46] Mcintosh, S., H. Babinsky, et al. (2007). Optimizing the energy output of vertical axis wind turbines for fluctuating wind conditions. 45th AIAA aerospace sciences meeting and exhibit, Reno, Nevada.
- [47] Kooiman, S. and S. Tullis (2010). "Response of a vertical axis wind turbine to time varying wind conditions found within the urban environment." Wind Engineering 34(4): 389-402.
- [48] Hara, Y., K. Hara, et al. (2012). "Moment of inertia dependence of vertical axis wind turbines in pulsating winds." International Journal of Rotating Machinery 2012.
- [49] Scheurich, F. and R. E. Brown (2013). "Modelling the aerodynamics of vertical-axis wind turbines in unsteady wind conditions." Wind Energy 16(1): 91-107.
- [50] Scheurich, F., T. M. Fletcher, et al. (2011). "Simulating the aerodynamic performance and wake dynamics of a vertical-axis wind turbine." Wind Energy 14(2): 159-177.
- [51] Danao, L. A. and R. Howell (2012). Effects on the performance of vertical axis wind turbines with unsteady wind inflow: a numerical study. 50th AIAA aerospace sciences meeting including the new horizons forum and aerospace exposition, Nashville, TN, USA.
- [52] Danao, L. A., O. Eboibi, et al. (2013). "An experimental investigation into the influence of unsteady wind on the performance of a vertical axis wind turbine." Applied Energy 107: 403-411.
- [53] Versteeg, H. K. and Malalasekera, W. (1995) An Introduction to Computational Fluid Dynamics, Longman Scientific and Technical, UK, ISBN: 0131274988.

- [54] Pozrikidis, C. (2001) Fluid Dynamics Theory, Computation and Numerical Simulation, Kluwer Academic Publishers, U.S.A., ISBN: 038795869X.
- [55] Tuncer, C. Jian, P. S. Fassi, K. and Eric, L. (2005) Computational fluid dynamics for engineers.
- [56] Blazek, J. (2001) Computational Fluid Dynamics Principles and Applications, Elsevier, ISBN: 0080430090.
- [57] Lomax, H. Pulliam, T. H. and Zingg, D. W. (2001) Fundamentals of Computational Fluid Dynamics. Springer, ISBN: 3540416072.
- [58] Hoffmann, K. A. and Chiang, S. T. (2000) Computational Fluid Dynamics, Engineering Education System, U.S.A., ISBN: 0962373133.
- [59] Munson, B. R., Young, D. F., and Okiishi, T. H. (2002) Fundamentals of Fluid Mechanics, John Willey and Sons Inc., 4th ed., U.S.A., ISBN: 0471675822.
- [60] Patankar, S. V. and Spalding, D. B. (1972) A Calculation Procedure for Heat, Mass and Momentum Transfer in Three-Dimensional Parabolic Flows, Heat and Mass Transfer, 15, 1787-1806.
- [61] Rauch, R. D. Batira, J. T. and Yang, N. T. Y. (1991) Spatial Adaption Procedures on Unstructured Meshes for Accurate Unsteady Aerodynamic Flow Computations, Technical Report, American Institute of Aeronautics and Astronautics, 91, 1106.
- [62] Barth, T. J. and Jespersen, D. (1989) The Design and Application of Upwind Schemes on Unstructured Meshes, 27th Technical Report, Aerospace Sciences Meeting, Nevada.
- [63] Venkatakrishnan, V. (1993) On the Accuracy of Limiters and Convergence to Steady State Solutions, Technical Report, American Institute of Aeronautics and Astronautics, 93, 880.
- [64] Ansys 13.0.0 User Guide accessible at http://www1.ansys.com/customer/content/documentation/130/wb2_help.pdf.
- [65] Menter, F. R. (1994) Two-Equation Eddy-Viscosity Turbulence Models for Engineering Applications, American Institute of Aeronautics and Astronautics, 32, 1598-1605.
- [66] Patankar, S. V. Spalding, D. B. (1972), "A Calculation Procedure for Heat, Mass and Momentum Transfer in Three-Dimensional Parabolic Flows", Heat and Mass Transfer, vol. 15, pp: 1787-1806.

Park, K. (2013) Optimal Design of a Micro Vertical Axis Wind Turbine For Sustainable Urban Environment, Ph.D. Thesis, University of Huddersfield, U.K.